

Copyright © by
Peter James Lingane
1966

- I. CHRONOAMPEROMETRY AND CHRONOPOTENTIOMETRY WITH
UNSHIELDED, CIRCULAR, PLANAR ELECTRODES
- II. APPLICATIONS OF POTENTIAL STEP CHRONOCOULOMETRY
- III. FARADAIC INTEGRATION OF THE DIFFUSE DOUBLE LAYER

Thesis by
Peter James Lingane

In Partial Fulfillment of the Requirements

For the Degree of
Doctor of Philosophy

California Institute of Technology
Pasadena, California

1966

(Submitted April 27, 1966)

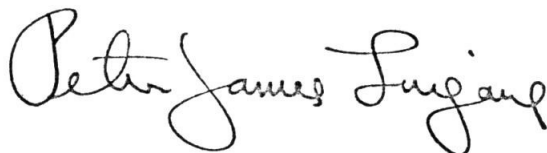
PREFACE

Joseph H. Christie has provided a major contribution to the quality and contents of this dissertation; his guidance, collaboration and comradeship will be remembered with a great deal of pride and satisfaction in the years to come. In addition, I wish to acknowledge the aid, instruction, succor or friendship which I have received from my research supervisor, Fred C. Anson, and from Janet G. Jones, George Lauer, Robert A. Osteryoung, William P. Schaefer, and Zoltán G. Soos.

I am indebted to the people of these United States who financed my graduate education through a U.S. Public Health Service, Division of General Medical Sciences, predoctoral fellowship.

I wish to thank the editors of Analytical Chemistry, the Journal of Electroanalytical Chemistry, and the Journal of Physical Chemistry for permission to quote copywrited material in Chapters 1, 2, 4, 5, and 6.

This dissertation is dedicated to my father, James J. Lingane, the quality of whose scientific research and the clarity of whose writing have been both goals to be equaled and marks to be exceeded.

A handwritten signature in cursive script that reads "Peter James Lingane". The signature is written in black ink and is positioned in the lower right quadrant of the page.

Pasadena, California

April, 1966

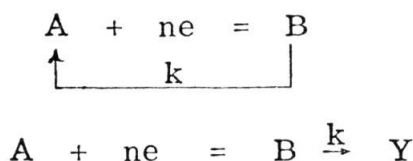
ABSTRACT

The first portion of this dissertation demonstrates both theoretically and experimentally that the chronoamperometric and chronopotentiometric constants obtained with unshielded, circular, planar electrodes are of the form

$$\begin{aligned}
 i t^{\frac{1}{2}}/AC &= nFC \sqrt{\frac{D}{\pi}} \left[1 + 2.1 \left(\frac{Dt}{\rho_0^2} \right)^{\frac{1}{2}} + \dots \right] \\
 i \tau^{\frac{1}{2}}/AC &= \frac{nFC}{2} \sqrt{\pi D} \left[1 + 1.0 \left(\frac{D\tau}{\rho_0^2} \right)^{\frac{1}{2}} + \dots \right]
 \end{aligned}$$

Higher order terms appear to be unimportant under normal experimental conditions (1,2).

The second portion presents the results of detailed calculations of "working tables" for double potential step chronocoulometry applied to the study of first-order chemical reactions of the form



where Y is non-electroactive. The double potential step chronocoulometric technique is applied to the study of the Ti(III)-hydroxylamine reaction (3) and it is shown that the previously determined value of the Arrhenius energy is inexplicably too small by a factor of two. A new technique for the estimation of the electrochemical parameters of electrode reactions from potential step data is developed (4) and it is shown

that this technique eliminates the need for a short- or a long-time approximation.

The final sections discuss the results of chronopotentiometric and chronocoulometric experiments conducted in the presence of "insufficient" supporting electrolyte. It is shown that the observed chronopotentiometric $E-t$ curves should be distorted by the sum of "liquid junction" and " iR_u " voltages. Doublet chronopotentiometric waves are observed for the reduction of certain transition metals. The measured chronopotentiometric constant increases at high current densities and this is interpreted in terms of the reaction of electroactive material in the diffuse layer. It is shown that the residual uncompensated resistance in solutions of low concentrations of supporting electrolyte introduces sufficiently large uncertainties in the potential step chronocoulometric $Q-t^{\frac{1}{2}}$ intercepts as to invalidate this technique under these conditions.

A least-squares analysis of chronopotentiometric data for the estimation of adsorption statistics according to three common models is described and the listing of a suitable Fortran IV computer program is included.

Extensive tables are calculated for the amount of a doubly charged ion in the diffuse double layer as a function of the concentration of the singly charged indifferent electrolyte.

- (1) Anal. Chem., 36, 1723 (1964).
- (2) J. Phys. Chem., 68, 3821 (1964).
- (3) J. Electroanal. Chem., in press (1966).
- (4) J. Electroanal. Chem., 10, 284 (1965).

TABLE OF CONTENTS

<u>Part</u>	<u>Title</u>	<u>Page</u>
I	Chronoamperometry and Chronopotentiometry with Unshielded, Circular, Planar Electrodes	1
Chap. 1	Derivation of the Chronoamperometric Constant	2
	Introduction	2
	Formal Solution	5
	Special Case: One-Component System	9
	Discussion	23
Chap. 2	Evaluation of the Experimental Chronopotentiometric and Chronoamperometric Constants	25
	Introduction	25
	Results	26
	Discussion	34
	Experimental	35
	Acknowledgment	38
II	Applications of Potential Step Chronocoulometry	39
Chap. 3	The Evaluation of Working Curves for the Study of the Rates of Solution Reactions	43
	The Catalytic Reaction	43
	The Following Reaction	46
Chap. 4	Catalytic Reactions: The Ti(III)-Hydroxylamine Reaction	55
	Introduction	55
	Results and Discussion	58
	Conclusion	68
	Experimental	69
	Acknowledgment	72
Chap. 5	Improved Method for the Determination of the Kinetic Parameters of Electrode Reactions	73
	Introduction	73

<u>Part</u>	<u>Title</u>	<u>Page</u>
	Theoretical	74
	The Least Squares Estimation of a and b	78
	Fortran IV Computer Program for the Least Squares Estimation of Electrochemical Parameters According to the A* Technique	86
Chap. 6	Investigation of the Kinetic Parameters of the Zn(II)/Zn(Hg) and Cd(II)/Cd(Hg) Couples	90
	Results and Discussion	90
	Conclusions	101
	Experimental	102
III	Faradaic Integration of the Diffuse Double Layer ...	103
	General Statement of the Problem	103
	Characteristics of the Pilot Ion	108
	Non-Equilibrium Changes in the Composition of the Diffuse Layer	110
Chap. 7	The Relative Population Densities in the Diffuse Layer for Mixtures of Ions	118
Chap. 8	Chronopotentiometric Results	130
	Constancy of V	130
	Morphology of the Chronopotentiometric Wave ..	135
	The Chronopotentiometric Constant as a Function of Current Density	137
	Quantitative Adsorption Estimates	145
	Origin of the "Negative Adsorption"	149
	Experimental	150
	Appendix	155
	Fortran IV Computer Program for the Least Squares Estimation of Adsorption Statistics from Chronopotentiometric Data	158
Chap. 9	Potential Step Chronocoulometric Results	162
	Minimizing the Effects of R_u	163

<u>Part</u>	<u>Title</u>	<u>Page</u>
	Results and Discussion	165
	Experimental	174
	Fortran IV Computer Program for the Least Squares Estimation of Adsorption Statistics from Single Potential Step Chronocoulometric Data	177

<u>Part</u>	<u>Title</u>	<u>Page</u>
Proposition I:	The calculation of Tatwawadi and Bard for the extent of electroactive adsorption of riboflavin on mercury electrodes is incorrect because the particular least squares analysis employed by these authors is not applicable; their observations that mathematical reformulations of the models leads to apparently different values of the parameters D and nFT is a direct consequence of this error	179
Proposition II:	The time-dependent solutions for twin electrode, thin layer electrochemistry are presented for Dirichlet, Neumann, and Cauchy boundary conditions and it is shown that the values of the "time to steady state" parameter obtained for these boundary conditions are in the ratio 1:4:16	183
Proposition III:	It is proposed to use pulse polarography to determine the amount of ruthenium extracted into molten zinc-magnesium solvents from uranium breeder reactor fuels	191
Proposition IV:	It is proposed to verify the shift in the half-wave potential of a polarographic wave distorted by a second order catalytic reaction following the electron-transfer step by pH, ionic strength, and temperature studies of the uranium(V) disproportionation reaction	193
Proposition V:	It is proposed that iron, cobalt, and nickel complexes with dimethylglyoxime and similar oximes should form series of salts interrelated by one-electron transfer reactions	197

TABLE OF FIGURES

<u>Figure</u>		<u>Page</u>
1	Model for the circular disk electrode	4
2	Plot of $g(\rho, t)$ as a function of ρ illustrating the redistribution of the sources of $C^I(\rho, z, t)$	17
3	Typical concentration profiles for $C(\rho, z, t)$ and $C^I(\rho, z, t)$	22
4	Plot of the chronopotentiometric constant as a function of $(D\tau/\rho_0^2)^{1/2}$ for the reduction of ferric chloride and for the oxidation of potassium ferrocyanide	27
5	Plot of the chronoamperometric constant as a function of $(Dt/\rho_0^2)^{1/2}$ for the oxidation and reduction of a variety of substances	28
6	The characteristic potential regions for the application of potential step chronocoulometry superimposed on an idealized polarographic current-potential curve..	40
7	Theoretical plot of $ Q_p/Q_f $ as a function of $\beta^2\tau$ for first-order catalytic and following reactions	45
8	Experimental I-t and Q-t traces for extreme values of $\beta\tau^{1/2}$	60
9	Plot of $\log k_T$ vs. T^{-1}	67
10	Block diagram of the electronic apparatus	71
11	Q , A^* , and B^* plotted vs. $\lambda t^{1/2}$. Theoretical	77
12	The CHI-SQUARE distribution function	83
13	Experimental plot of A^* and Q vs. $t^{1/2}$ for the reduction of Zn(II)	93
14	Plot of $\log K$ vs. $(E - E_{1/2})$ for the reduction of Cd(II). Uncompensated.....	98
15	Schematic representation of an electrochemical cell in the presence of uncompensated resistance	100

<u>Figure</u>		<u>Page</u>
16	Schematic representation of the initial change in the composition of the diffuse layer following an abrupt shift in the potential of the electrode	116
17	$-2FF_1/Q_e$ as a function of Q_e and potential	127
18	Comparison of the distortion of reversible and irreversible chronopotentiograms in the absence of supporting electrolyte	134
19	Experimental chronopotentiograms observed for the reduction of Zn(II) in the absence of supporting electrolyte	136
20	Plot of the chronopotentiometric constant for the reduction of Co(II) in the presence of increasing amounts of $LiNO_3$	139
21	Plot of the chronopotentiometric constant for the reduction of hydrogen ion in the presence of increasing amounts of $LiNO_3$	140
22	Plot of the chronopotentiometric constant for the reduction of Tl(I) in the presence of increasing amounts of $LiNO_3$	141
23	Plot of the chronopotentiometric constant for the reduction of Zn(II) in the presence of increasing amounts of $LiNO_3$	142
24	Plot of the chronopotentiometric constant for the reduction of Zn(II) in the presence of increasing amounts of $HClO_4$	143
25	Block diagram of the apparatus for the chronopotentiometric experiments	151
26	Block diagrams of two possible compensation circuits	164
27	Experimental $Q-t^{1/2}$ intercepts observed for the reduction of Zn(II) in the presence of small amounts of supporting electrolyte	170

I. CHRONOAMPEROMETRY AND CHRONOPOTENTIOMETRY WITH UNSHIELDED, CIRCULAR, PLANAR ELECTRODES

In the following two chapters, it is shown on both theoretical and experimental grounds that the chronoamperometric and chronopotentiometric constants obtained with unshielded, circular, planar electrodes are linear functions of $(Dt/\rho_0^2)^{\frac{1}{2}}$ or $(D\tau/\rho_0^2)^{\frac{1}{2}}$. With this information it is possible to estimate values for the time scale and electrode radius so as to minimize the effects of nonlinear diffusion. In very accurate work, it may be desirable to extrapolate the measured values of these parameters to the $t^{\frac{1}{2}} = 0$ or the $\tau^{\frac{1}{2}} = 0$ intercepts.

It is seen that frequently only negligible errors result if the effects of nonlinear diffusion are completely neglected. Therefore, the use of the experimentally less convenient shielded, planar electrodes or cylindrical electrodes is often unnecessary.

CHAPTER 1.

Derivation of the Chronoamperometric Constant*Introduction

The Cottrell equation

$$\frac{it^{\frac{1}{2}}}{AC} = \frac{nFD^{\frac{1}{2}}}{\pi^{\frac{1}{2}}} \quad (1)$$

does not adequately describe the current-time behavior observed with electrodes of finite size at times longer than a few seconds (1,2,3). Therefore, we have calculated the current-time behavior for a circular electrode of radius ρ_0 and have shown that the chronoamperometric constant can be expanded as a power series in \sqrt{Dt}/ρ_0 ; the coefficient of the term in \sqrt{Dt}/ρ_0 is calculated. We discuss only the mixed boundary condition problem in which the concentration is fixed at the surface of the electrode; the solution to the Neumann problem (chronopotentiometry) may be obtained analogously.

*This work was performed in collaboration with Zoltán G. Soos. A summary appeared in the Journal of Physical Chemistry, 68, 3821 (1964).

(1) H. A. Laitinen, Trans. Electrochem. Soc., 82, 289 (1942).

(2) H. A. Laitinen, I. M. Kolthoff, J. Am. Chem. Soc., 61, 3344 (1939).

(3) D. J. Macero and C. L. Rulfs, J. Am. Chem. Soc., 81, 2942 (1959).

If we neglect the effect of turbulence and of convective stirring, then the current passing through the area \vec{A} is simply

$$\underline{i} = \underline{nF} \frac{d\vec{N}}{dt} \cdot \vec{A} = \frac{\underline{nF}}{RT} \underline{C} D \nabla \bar{\mu} \cdot \vec{A} \quad (2)$$

where \underline{i} is the current in amperes, \underline{n} is the number of equivalents per mole, \underline{D} is the diffusion coefficient in cm^2/sec , $\bar{\mu}$ is the electrochemical potential, and \underline{C} is the concentration of the electroactive species in moles/cc. If the solution contains a large concentration of supporting electrolyte, the transference number of the electroactive species is essentially zero. Under these conditions (4), the diffusion equation reduces to

$$\frac{\partial \underline{C}}{\partial t} = \underline{D} \nabla^2 \underline{C}. \quad (3)$$

In the presence of excess supporting electrolyte, the compact double layer (5,6) can be approximated by a parallel plate condenser whose plates are separated by one or two molecular diameters. Therefore, the charge on the double layer for a circular electrode of radius ρ_0 will be uniform until $\rho - \rho_0$ approaches the thickness of the compact double layer (cf. Fig. 1). Since the metallic electrode is an equipotential surface, the uniformity of the double-layer charge requires

(4) H. L. Kies, J. Electroanal. Chem., 4, 156 (1962).

(5) D. C. Grahame, Chem. Rev., 41, 441 (1947).

(6) R. Parsons, in "Advances in Electrochemistry and Electrochemical Engineering," Vol. 1, P. Delahay, Ed., Interscience Publishers, Inc., New York, N. Y., 1961, Chapter I.

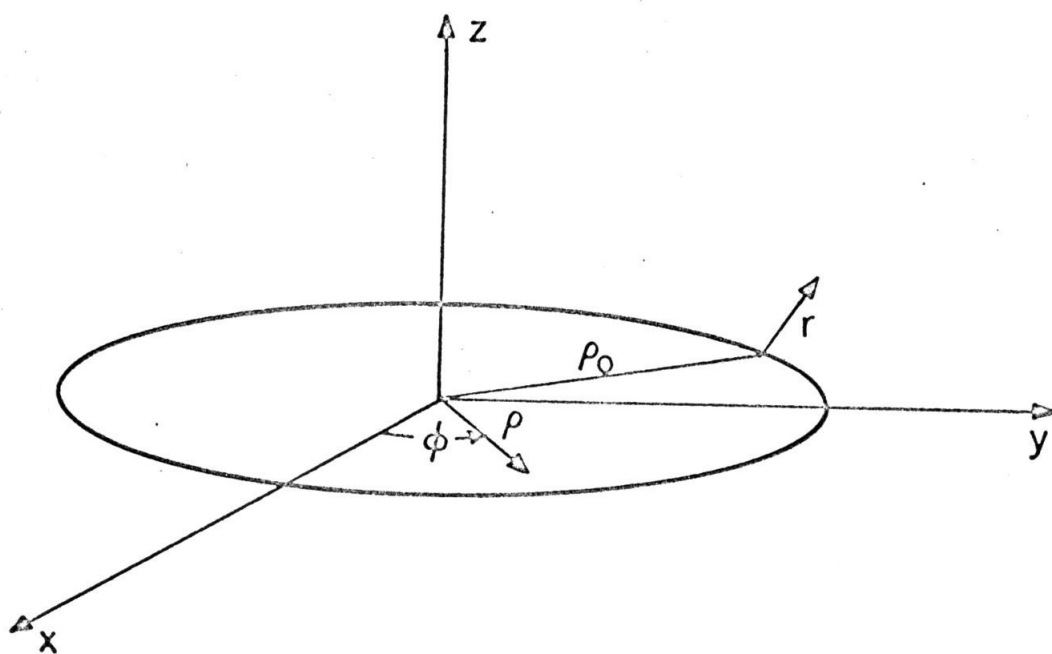


Figure 1. Model for the circular disk electrode.

that the potential at the outer Helmholtz plane also be uniform until $\rho - \rho_0$ approaches the thickness of the compact double layer. Very close to the edge, the potential at the outer Helmholtz plane will decrease with respect to the solution potential.

Therefore, it is very reasonable to assume that the concentration of the electroactive species will be uniform at the outer Helmholtz plane of metallic electrodes of finite size in the presence of excess supporting electrolyte if the concentration is governed by the Nernst equation.

Formal Solution

We will first consider the oxidation of a single insoluble species to give a soluble product, e.g., the generation of silver ion into a solution initially free of silver. Our electrode is a circular planar disk of radius ρ_0 situated in the $z = 0$ plane (cf. Fig. 1). This electrode is potentiostated at a fixed potential \underline{E} , and it is assumed that the Nernst equation is obeyed. This guarantees that diffusion and not the electron-transfer step will control the current. Observe that under these conditions the concentration at the surface of the electrode will continuously increase with potential and no limiting current will be achieved. This approach is purely one of convenience and is taken to achieve greater generality as will become evident in the Discussion section.

The cylindrical symmetry enables us to write the concentration as $\underline{C}(\rho, z, t)$. The boundary conditions for $\underline{C}(\rho, z, t)$ are

$$C(\rho, 0, t) = \begin{cases} C^0(E) & \rho \leq \rho_0 & t \geq 0^+ \\ 0 & \rho > \rho_0 & t = 0^+ \end{cases}$$

$$\frac{\partial C}{\partial z}(\rho, 0, t) = 0 \quad \rho > \rho_0 \quad t \geq 0^+ \quad (4)$$

$$C(\rho, z, 0) = 0 \quad z > 0$$

$$\lim_{\rho \rightarrow \infty} C(\rho, z, t) = \lim_{z \rightarrow \infty} C(\rho, z, t) = 0$$

$$\lim_{t \rightarrow \infty} C(\rho, z, t) = C^0(E) \quad (5)$$

We use the superposition theorem and write

$$C(\rho, z, t) = C^I(\rho, z, t) + C^{II}(\rho, z, t) \quad (6)$$

In general, the surface of an electrode can be represented by a continuum of current sources whose distribution and strengths are time-dependent. The source distribution for an infinite planar electrode is time-independent and is uniform over the surface of the electrode. The time-dependent sources of $\underline{C^I(\rho, z, t)}$ are chosen to be equivalent to such a uniform distribution for $\rho \leq \rho_0$ at $t = 0^+$. Therefore, $\underline{C^I(\rho, z, t)}$ is equivalent, initially, to the concentration distribution at a circular section of an infinite electrode. At later times, radial diffusion causes the sources of $\underline{C^I(\rho, z, t)}$ to decrease near the edge of the electrode and apparent sources to appear at $\rho > \rho_0$. The sources of $\underline{C^{II}(\rho, z, t)}$ could be chosen so that the boundary condition (4) is satisfied at all times. Alternatively, the sources of $\underline{C^{II}(\rho, z, t)}$ might be chosen so that the total flux from the finite electrode into the region $\rho \leq \rho_0$ is the same as from the infinite electrode. We shall adopt the second condition because we wish to approximate the sources for $\underline{C^{II}(\rho, z, t)}$ by a line

source. Such an approximation gives a nonuniform concentration at the surface of the electrode. Obviously, an exact solution would satisfy both conditions simultaneously.

The initial conditions for $C^I(\rho, z, t)$ are

$$C^I(\rho, 0, 0^+) = \begin{cases} C^0(E) & \rho \leq \rho_0 \\ 0 & \rho > \rho_0 \end{cases} \quad (7)$$

Since the diffusion equation contains only a first derivative with respect to time, it is convenient to make the partial separation

$$C^I(\rho, z, t) = C^0 g(\rho, t) f(z, t) \quad (8)$$

where $C^0(E)$ is the concentration at the outer Helmholtz plane and $f(z, t)$ and $g(\rho, t)$ are dimensionless functions to be determined. It is evident that under certain conditions, such as $t \rightarrow 0$ or $\rho \rightarrow 0$, the solution must reduce to the solution for the infinite planar electrode. Hence, $f(z, t)$ is taken to be the well-known solution for the infinite planar electrode (7)

$$f(z, t) = 1 - \operatorname{erf}\left(\frac{z}{2\sqrt{Dt}}\right) \quad (9)$$

and $g(\rho, t)$ represents the effect of diffusion in the radial direction.

Furthermore, the initial condition for $g(\rho, t)$ is

* J. N. Foster has suggested that the identification of $f(z, t)$ with the solution for the infinite planar electrode is not valid since it amounts to setting the separation constant, which could be time dependent, equal to zero. No generality is lost by this procedure, however, since any errors introduced are adjusted for in the calculation of C^{II} .

(7) P. Delahay, "New Instrumental Methods in Electrochemistry," Interscience Publishers, Inc., New York, N. Y., 1954, Chapter 3.

$$g(\rho, 0^+) = \begin{cases} 1 & \rho \leq \rho_0 \\ 0 & \rho > \rho_0 \end{cases} \quad (10)$$

$g(\rho, t)$ must satisfy the radial portion of the diffusion equation.

$g(\rho, t)$ may be obtained via a Hankel transform (8). Only zeroth-order Bessel functions appear because of the cylindrical symmetry.

The integrand is a solution to the diffusion equation for each value of \underline{k} , and hence $g(\rho, t)$ is a solution.

$$g(\rho, t) = \int_0^\infty k dk f(k) e^{-Dk^2 t} J_0(k\rho) \quad (11)$$

$$f(k) = \int_0^\infty \rho d\rho g(\rho, 0^+) J_0(k\rho)$$

As is shown in Fig. 2, $g(\rho, t)$ is a step function at $t = 0^+$; at later times, the time dependence of Eqn. (11) gives different superpositions of the Bessel functions and the step-function decays. This decay expresses the fact that there is radial diffusion.

Since $C^I(\rho, z, t)$ satisfies the boundary conditions only at $t = 0^+$, it is evident that a current source must be added toward the edge of the electrode to maintain a uniform concentration distribution. This current source will produce the concentration $C^{II}(\rho, z, t)$. Once we have calculated $C^I(\rho, z, t)$, we will be able to determine $C^{II}(\rho, z, t)$ and thus the nature of the current sources that produce $C^{II}(\rho, z, t)$.

The current flowing through the electrode is given rigorously by the gradient with respect to \underline{z} of the concentration evaluated at $\underline{z} = 0$, $\rho \leq \rho_0$. Therefore, the current density corresponding to $C^I(\rho, z, t)$

(8) P. M. Morse and H. Feshbach, "Methods of Theoretical Physics," McGraw-Hill Book Co., New York, N. Y., 1953.

is

$$\frac{i}{\pi\rho_0^2} = n\bar{\nu}D \frac{2}{\rho_0^2} \int_0^{\rho_0} \left(\frac{\partial C^I}{\partial z} \right)_{z=0} \rho d\rho = - \frac{n\bar{\nu}DC^0}{\sqrt{\pi Dt}} \int_0^{\rho_0} \rho d\rho g(\rho, t) \quad t > 0 \quad (12)$$

$$g(\rho, t) = \int_0^\infty k dk e^{-Dk^2 t} J_0(k\rho) \times \int_0^\infty \rho' d\rho' g(\rho', 0^+) J_0(k\rho') \quad (13)$$

By reversing the orders of integration freely, it is possible to show that for an arbitrary $g(\rho, 0^+)$ the current density is an expansion in powers of \sqrt{Dt}/ρ_0 .

Special Case: One-Component System

A. Expressions for $g(\rho, t)$. We now consider in detail the properties of $C^I(\rho, z, t)$. The initial conditions are fixed by Eqn. (7); $f(z, t)$ is given by Eqn. (9); $g(\rho, 0^+)$ is the step function defined by Eqn. (11). We integrate Eqn. (11) to obtain

$$f(k) = \int_0^\infty \rho' d\rho' g(\rho', 0^+) J_0(k\rho') = \rho_0 \frac{J_1(k\rho_0)}{k} \quad (14)$$

The exponential in Eqn. (13) is now expanded in a Hankel transform. Only zeroth-order Bessel functions appear because of the symmetry in the \underline{k} -plane. The inverse transformation reduces to a Laplace transform (9).

$$e^{-Dk^2 t} = \int_0^\infty q dq J_0(kq) f(q) \quad (15)$$

(9) W. Magnus and F. Oberhettinger, "Formulas and Theorems for the Functions of Mathematical Physics," Chelsea Publishing Co., New York, N. Y., 1949, p. 132.

$$\begin{aligned}
 f(q) &= \int_0^\infty k dk e^{-Dk^2} J_0(kq) = \\
 &= \frac{1}{2Dt} \int_0^\infty dy e^{-y} J_0\left(\frac{q}{\sqrt{Dt}} \sqrt{y}\right) = \frac{1}{2Dt} e^{-\frac{q^2}{4Dt}}
 \end{aligned} \tag{16}$$

Combining Eqns. (12), (13), (15), and (16), we obtain

$$\begin{aligned}
 g(\rho, t) &= \frac{\rho_0}{2Dt} \int_0^\infty q dq e^{-\frac{q^2}{4Dt}} \times \\
 &= \int_0^\infty J_0(kq) J_0(k\rho) J_1(k\rho_0) dk
 \end{aligned} \tag{17}$$

The integral over the Bessel functions is a special case of the formula of Sonine and Dougall (10).

$$\begin{aligned}
 g(\rho, t) &= \frac{1}{2\pi Dt} \int_0^\infty q dq e^{-q^2/4Dt} A(\rho, \rho_0, q) \\
 A(\rho, \rho_0, q) &= \begin{cases} \pi & \rho_0^2 > (\rho + q)^2 \\ \cos^{-1}\left(\frac{\rho^2 + q^2 - \rho_0^2}{2q\rho}\right) & (\rho + q)^2 > \rho_0^2 > (\rho - q)^2 \\ 0 & (\rho - q)^2 > \rho_0^2 \end{cases}
 \end{aligned} \tag{18}$$

Hence

$$\begin{aligned}
 \rho \leq \rho_0 \quad g(\rho, t) &= 1 + \frac{1}{\pi} \int_{\rho_0 - \rho}^{\rho_0 + \rho} dq e^{-\frac{q^2}{4Dt}} \times \\
 &= \frac{\partial}{\partial q} \left(\cos^{-1} \left(\frac{\rho^2 + q^2 - \rho_0^2}{2q\rho} \right) \right)
 \end{aligned} \tag{20}$$

$$\begin{aligned}
 \rho > \rho_0 \quad g(\rho, t) &= \frac{1}{\pi} \int_{\rho - \rho_0}^{\rho + \rho_0} dq e^{-\frac{q^2}{4Dt}} \times \\
 &= \frac{\partial}{\partial q} \left(\cos^{-1} \left(\frac{\rho^2 + q^2 - \rho_0^2}{2q\rho} \right) \right)
 \end{aligned} \tag{21}$$

(10) W. Magnus and F. Oberhettinger, "Formulas and Theorems for the Functions of Mathematical Physics," Chelsea Publishing Co., New York, N. Y., 1949, p. 37.

In order to evaluate the integrals in Eqns. (20) and (21), we first evaluate $\partial g/\partial \rho(\rho, \underline{t})$. We can easily verify (or observe from the boundary conditions) that $\partial g/\partial \rho(\rho, 0^+)$ is a δ -function of unit strength.

$$\begin{aligned} t = 0^+ \quad \frac{\partial g}{\partial \rho}(\rho, 0^+) &= -\rho_0 \int_0^\infty k dk J_1(k\rho) J_1(k\rho_0) \\ &= -\delta(\rho - \rho_0) \end{aligned} \quad (22)$$

$$\begin{aligned} t > 0^+ \quad \frac{\partial g}{\partial \rho}(\rho, t) &= -\frac{\rho_0}{2} \int_0^\infty dy e^{-Dty} J_1(\rho\sqrt{y}) J_1(\rho_0\sqrt{y}) \\ &= -\frac{\rho_0}{2Dt} I_1\left(\frac{\rho\rho_0}{2Dt}\right) e^{-\frac{\rho^2 + \rho_0^2}{4Dt}} \end{aligned} \quad (23)$$

The Laplace transform (10) in Eqn. (23) gives the modified Bessel function of the first order.

We define $\Delta g(\rho, \underline{t})$ to be the deviation of $g(\rho, \underline{t})$ from the step function $g(\rho, 0^+)$.

$$\begin{aligned} \Delta g(\rho, t) &= g(\rho, t) - 1 & \rho \leq \rho_0 \\ &= g(\rho, t) & \rho > \rho_0 \end{aligned} \quad (24)$$

We now obtain an expression for $\Delta g(\rho, \underline{t})$, $\rho \leq \rho_0$. It is evident from Eqn. (20) that $g(0, \underline{t}) = 1$ for all $\underline{t} > 0$. Equation (23) then gives

$$\begin{aligned} \Delta g(\rho, t) &= g(\rho, t) - g(0, t) = \int_0^\rho \frac{\partial g}{\partial \rho'}(\rho', t) d\rho' \quad \rho \leq \rho_0 \\ &= -\frac{\rho_0}{2Dt} \int_0^\rho I_1\left(\frac{\rho'\rho_0}{2Dt}\right) e^{-\frac{(\rho')^2 + \rho_0^2}{4Dt}} d\rho' \end{aligned} \quad (25)$$

If we set $\chi = \rho\rho_0/2Dt$, $\chi_0 = \rho_0^2/2Dt$, and $\beta = Dt/\rho_0^2 = 1/2\chi_0$, we find

$$\Delta g(\chi, t) = -e^{-\chi_0/2} \int_0^\chi I_1(x) e^{-\beta x^2} dx \quad (26)$$

We use the properties of the modified Bessel functions (11) and integrate Eqn. (26) by parts repeatedly.

$$\begin{aligned} \Delta g(x,t) &= -e^{-x_0/2} \left\{ \sum_{\nu=0}^{\infty} (2\beta x)^{\nu} I_{\nu}(x) e^{-\beta x^2} - 1 \right\} \\ &= e^{-x_0/2} \left\{ 1 - e^{-\rho^2/4Dt} \sum_{\nu=0}^{\infty} \left(\frac{\rho}{\rho_0} \right)^{\nu} I_{\nu} \left(\frac{\rho \rho_0}{2Dt} \right) \right\}, \end{aligned} \quad (27)$$

$\rho \leq \rho_0$

where I_{ν} is the modified Bessel function of order ν .

B. Correction to the Current Density. Expressions (26) and (27) will be used to evaluate $g(\rho, t)$. Before we perform this calculation, which requires a variety of special conditions, we will evaluate the decay in the current density at the electrode due to the apparent motion of the current sources for $C^I(\rho, z, t)$ to $\rho > \rho_0$ in the $z = 0$ plane. We replace $g(\rho, t)$ in Eqn. (12) by $\Delta g(\rho, t)$; except for constants, we have

$$\begin{aligned} \int_0^{\rho_0} \rho d\rho \Delta g(\rho, t) &= \frac{\rho_0^2}{2} e^{-\frac{x_0}{2}} - \\ &\int_0^{\rho_0} \rho d\rho e^{-\frac{\rho^2 + \rho_0^2}{4Dt}} \sum_{\nu=0}^{\infty} \left(\frac{\rho}{\rho_0} \right)^{\nu} I_{\nu} \left(\frac{\rho \rho_0}{2Dt} \right) \\ &= e^{-\frac{x_0}{2}} \left\{ \frac{\rho_0^2}{2} - \left(\frac{2Dt}{\rho_0} \right)^2 \sum_{\nu=0}^{\infty} \int_0^{x_0} (2\beta x)^{\nu} e^{-\beta x^2} I_{\nu}(x) dx \right\} \end{aligned} \quad (28)$$

We integrate by parts repeatedly to obtain

(11) H. B. Dwight, "Tables of Integrals and Other Mathematical Data," The Macmillan Co., New York, N. Y., 1961.

$$\int_0^{x_0} x^{\nu+1} e^{-\beta x^2} I_\nu(x) dx = \sum_{\mu=\nu+1}^{\infty} \frac{(2\beta x_0)^\mu}{2\beta^{\nu+1}} I_\mu(x_0) e^{-\beta x_0^2} \quad (29)$$

Substituting Eqn. (29) in Eqn. (28), we have

$$\int_0^{x_0} \rho d\rho \Delta g(\rho, t) = e^{-\frac{\rho_0^2}{4Dt}} \times \left\{ \frac{\rho_0^2}{2} - 2Dt e^{-\frac{4Dt}{\rho_0^2}} \sum_{\nu=0}^{\infty} \nu I_\nu \left(\frac{\rho_0^2}{2Dt} \right) \right\} \quad (30)$$

Using the recursion relations for the modified Bessel functions, we find

$$\begin{aligned} \frac{1}{2x} \sum_{\nu=1}^{\infty} \nu I_\nu(x) &= \frac{1}{2} \sum_{\nu=1}^{\infty} \{I_{\nu-1}(x) - I_{\nu+1}(x)\} \\ &= \frac{1}{2} \{I_0(x) + I_1(x)\} \end{aligned} \quad (31)$$

Substituting Eqn. (31) in Eqn. (30), we obtain

$$\int_0^{x_0} \Delta g(\rho, t) \rho d\rho = -\frac{\rho_0^2}{2} e^{-\frac{\rho_0^2}{2Dt}} \times \left\{ I_0 \left(\frac{\rho_0^2}{2Dt} \right) + I_1 \left(\frac{\rho_0^2}{2Dt} \right) - e^{+\rho_0^2/4Dt} \right\} \quad (32)$$

Hence

$$\frac{\Delta i}{\pi \rho_0^2} = \frac{n\bar{v}DC^0}{\sqrt{\pi Dt}} e^{-\frac{\rho_0^2}{2Dt}} \left\{ I_0 \left(\frac{\rho_0^2}{2Dt} \right) + I_1 \left(\frac{\rho_0^2}{2Dt} \right) - e^{+\rho_0^2/4Dt} \right\} \quad (33)$$

Equation (33) is an exact expression. The current sources for $\underline{C^I(\rho, z, t)}$ have an initial uniform distribution over the surface of the electrode that is identical with the time-independent distribution of the current sources for the infinite planar electrode. However, the current sources for $\underline{C^I(\rho, z, t)}$ are redistributed in time because of radial diffusion; the

sources near the edge of the electrode decay, and apparent sources are found outside the electrode ($\rho > \rho_0$). $g(\underline{\rho}, \underline{t})$ is identically unity for the infinite planar electrode since there is no radial diffusion in that case.

C. Evaluation of $g(\underline{\rho}, \underline{t})$ for Experimental Conditions. In order to find $g(\underline{\rho}, \underline{t})$, $\rho < \rho_0$, and thus determine the position of the sources that we shall use for $C^{\text{II}}(\underline{\rho}, \underline{z}, \underline{t})$, it is convenient to specialize to the experimental conditions, i. e., $\rho_0 \geq 0.2$ cm, $D \sim 10^{-5}$ cm²/sec, $\underline{t} \lesssim 100$ sec. Under these conditions, $\rho_0^2/4D\underline{t} = \chi_0/2 > 10$. From the definition of I_ν , it is evident that $I_{\nu+1}(\underline{x}) < I_\nu(\underline{x})$ for all ν when $\underline{x} = 0$. Hence, we have from Eqn. (27)

$$|\Delta g(\rho, t)| < e^{-\frac{\rho_0^2 + \rho^2}{4Dt}} I_0\left(\frac{\rho\rho_0}{2Dt}\right) \sum_{\nu=0}^{\infty} \left(\frac{\rho}{\rho_0}\right)^\nu = e^{-\frac{\rho_0^2 + \rho^2}{4Dt}} I_0\left(\frac{\rho\rho_0}{2Dt}\right) \frac{1}{1 - \rho/\rho_0}, \quad \rho \leq \rho_0 \quad (34)$$

For $\rho = \rho_0/4$, $\chi_0/4 \geq 5$, and we may use the large argument expansion of I_0 (11). We then have, for $0 < \rho \leq \rho_0/4$

$$|\Delta g(\rho, t)| < |\Delta g(\rho_0/4, t)| \approx \frac{1}{3} \frac{e^{-\frac{9\chi_0}{32}}}{\sqrt{\frac{\pi\chi_0}{2}}} \left[1 + \frac{1}{2\chi_0} \dots\right] \sim e^{-7} \quad (35)$$

Hence we observe that $\Delta g(\underline{\rho}, \underline{t})$ is negligible for $\rho \leq \rho_0/4$. Equation (34) is an upper bound for $|\Delta g(\underline{\rho}, \underline{t})|$, since, in it, we have replaced all of the modified Bessel functions by I_0 . For example, Eqn. (34) gives $|\Delta g(0, \underline{t})| \lesssim e^{-10}$ while $\Delta g(0, \underline{t}) \equiv 0$ (for all \underline{t}) from Eqn. (27).

For $\rho_0/4 < \rho \leq \rho_0$, we may use the large argument expansion of the modified Bessel functions in Eqn. (25) throughout the entire range of the integration.

$$\begin{aligned} \Delta g(\chi, t) &= -e^{-\beta\chi_0} \int_{\chi_0/4}^{\chi} e^{-\beta y} e^y \frac{dy}{\sqrt{2\pi y}} \left(1 - \frac{3}{8y} \dots\right) \\ &= - \int_{\chi_0/4}^{\chi} e^{-\beta(\chi_0 - y)} \frac{dy}{\sqrt{2\pi y}} \left(1 - \frac{3}{8y} \dots\right) \end{aligned} \quad (36)$$

Since $\chi_0/4 > 5$, it is straightforward to integrate Eqn. (36). Hence

$$\Delta g(\rho, t) = \begin{cases} -1/2 \left(1 - \operatorname{erf}\left(\frac{\rho_0 - \rho}{2\sqrt{Dt}}\right)\right) - \frac{1}{2\sqrt{\pi}} \frac{\sqrt{Dt}}{\rho_0} \times \\ \quad e^{-\frac{(\rho_0 - \rho)^2}{4Dt}} + 0 \left(\left(\frac{\sqrt{Dt}}{\rho_0}\right)^3\right) & \frac{\rho_0}{4} < \rho \leq \rho_0 \\ 0 & \rho \leq \frac{\rho_0}{4} \end{cases} \quad (37)$$

Expression (37) may be obtained directly from Eqn. (20) by taking $\rho = \rho_0 - \Delta$ and letting $\Delta \rightarrow 0$ after the integration. If we set $\rho = \rho_0$ in Eqn. (20), the integrand is indeterminate at $q = 0$; when the integration is now performed, only the second term of Eqn. (37), evaluated at $\rho = \rho_0$, is obtained.

Since the derivative of $g(\underline{\rho}, \underline{t})$ is continuous for $\underline{t} > 0$, we may use an expression similar to Eqn. (25) to evaluate $g(\underline{\rho}, \underline{t})$ for $\rho > \rho_0$

$$\begin{aligned} \Delta g(\rho, t) &= 1 + \Delta g(\rho_0, t) - \frac{\rho_0}{2Dt} \int_{\rho_0}^{\rho} I_1\left(\frac{\rho' \rho_0}{2Dt}\right) \times \\ &\quad e^{-\frac{(\rho') + \rho_0^2}{4Dt}} d\rho' \quad , \quad \rho > \rho_0 \end{aligned}$$

$$= \frac{1}{2} \left(1 - \operatorname{erf} \left(\frac{\rho - \rho_0}{2\sqrt{Dt}} \right) \right) - \frac{1}{2\sqrt{\pi}} \frac{\sqrt{Dt}}{\rho_0} \times e^{-\frac{(\rho - \rho_0)^2}{4Dt}} + o \left(\left(\frac{\sqrt{Dt}}{\rho_0} \right)^3 \right) \quad (38)$$

The next term in Eqns. (37) or (38) is negligible for the times of interest. Since $f(0, \underline{t}) = 1$, the deviation of $\underline{C}^I(\rho, 0, \underline{t})$ from \underline{C}^0 for $\rho \leq \rho_0$ is \underline{C}^0 times Expression (37).

D. Sources for and Calculation of $\underline{C}^{II}(\rho, z, \underline{t})$. $g(\rho, \underline{t})$ is plotted as a function of ρ for various values of \underline{t} in Fig. 2. It is evident that, for $\underline{t} \lesssim 25$ sec, deviations from the step-function initial condition are important only within 0.03 to 0.04 cm of the edge of the electrode. Therefore, we need a current source of radius of about 0.01 cm at the perimeter of the electrode, placed so that the outer edge of the source is at $\rho = \rho_0$ if the boundary condition [Eqn. (7)] is to be satisfied for all times. Such a time-dependent source, which arises from the decomposition of the concentration in Eqn. (6), defines the diffusion problem for $\underline{C}^{II}(\rho, z, \underline{t})$.

As a first approximation, we consider a time-independent source at $\rho = \rho_0$. This should be a good approximation for short times since, for short times, Eqn. (37) shows that the source is essentially at the edge and, as is evident from the large argument expansion of the modified Bessel functions, Eqn. (33) shows that $\underline{\Delta i} / \pi \rho_0^2$ is essentially time independent.

$$\frac{\underline{\Delta i}}{A} = \frac{n\mathcal{F}D^2C^0}{\pi\rho_0^2} \left\{ 1 + o \left(\frac{Dt}{\rho_0^2} \right) \right\} \quad (39)$$

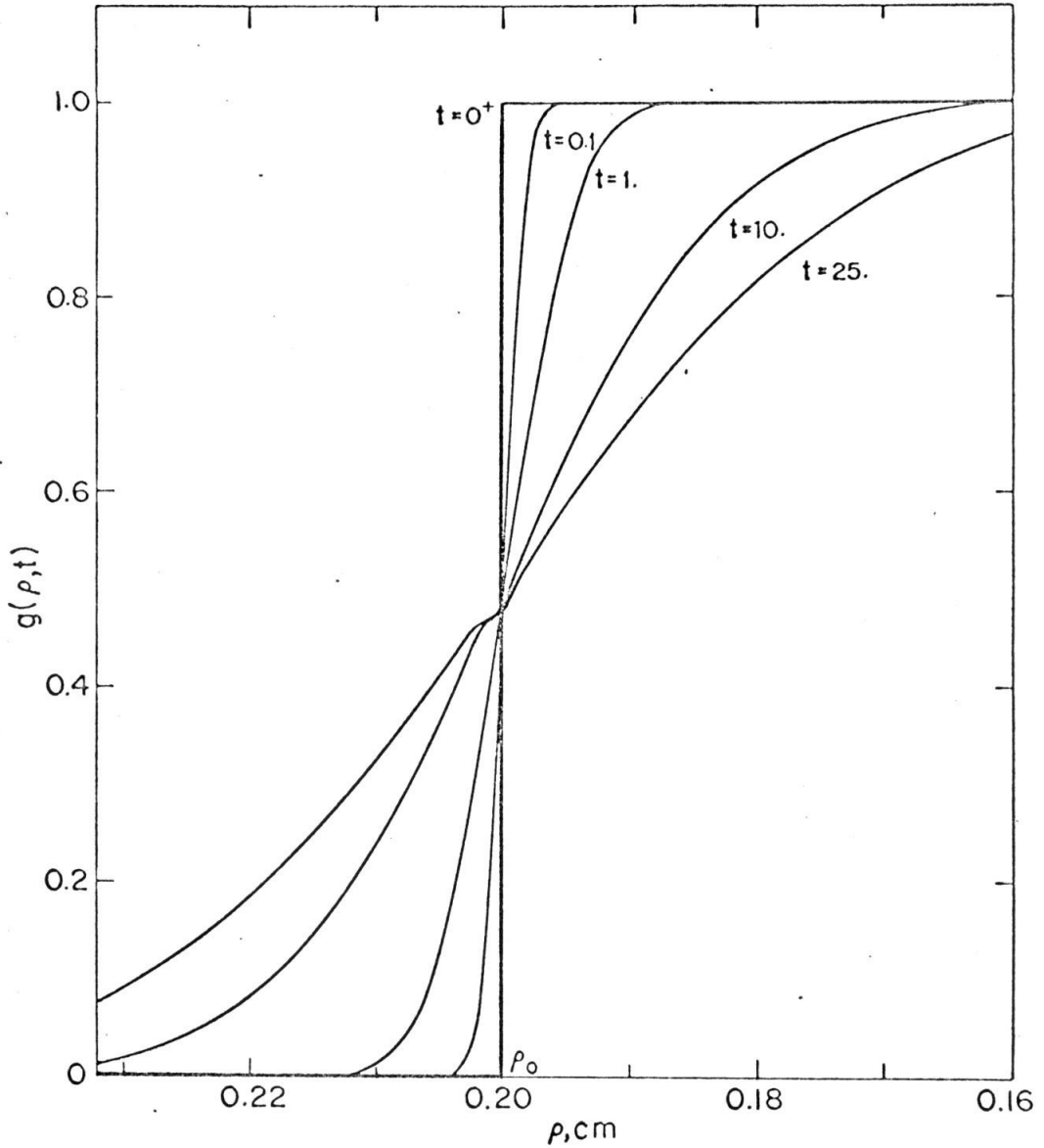


Figure 2. Plot of $g(\rho, t)$ as a function of ρ illustrating the redistribution of the sources of $C^I(\rho, z, t)$.

$\rho_0 = 0.2 \text{ cm}$, $\underline{D} = 1 \times 10^{-5} \text{ cm}^2/\text{sec}$.

In the same spirit, we may, for short times, approximate the source by an infinitely long, straight wire and express the concentration at a distance \underline{r} from the wire as

$$C^{II}(r,t) = \frac{C^0\alpha}{2\pi} \int_{r/2\sqrt{Dt}}^{\infty} \frac{dx}{x} e^{-x^2} = -\frac{C^0\alpha}{4\pi} Ei\left(-\frac{r^2}{4Dt}\right) \quad (40)$$

where $Ei(x)$ is the exponential integral. α is the strength of the source and will be evaluated below. This solution is borrowed from the analogous heat conduction problem (12).

It is not convenient to satisfy the boundary condition [Eqn. (4)] by requiring that the sum of $C^I(\rho, z, t)$ and $C^{II}(\rho, z, t)$ be uniform and time independent at the face of the electrode, since, by lumping the corrections into a line source, we have introduced a singularity. We may, however, as an alternative condition, match fluxes. Since the exact sources of $C^{II}(\rho, z, t)$ have "radii" of about 0.01 cm for $t \lesssim 25$ sec, the approximation of a line source should be excellent for $\underline{r} \gtrsim 0.01$ cm (cf. Fig. 2). Once outside the source distribution, its detailed composition becomes unimportant; as in a multipole expansion, the major effect is found by putting a point source at the center of the distribution. We will approximate even further and place the source at the edge of the electrode instead of near the edge.

(12) L. R. Ingersol, O. J. Zobel, and A. C. Ingersol, "Heat Conduction," McGraw-Hill Book Co., New York, N.Y., 1948, p. 146.

The current flowing from a straight wire is radial by symmetry. At a line source of strength α , the current per unit length is

$$i_s = n\bar{v}D2\pi r \frac{\partial}{\partial r} C^{\text{II}}(r,t)|_{r=0} = -n\bar{v}DC^0\alpha \quad (41)$$

It is evident from Fig. 1 that the symmetry in the $\underline{z} = 0$ plane requires that the flux flowing into the region where $\underline{z} > 0$ be just half the total flux from a source whose intensity is twice the intensity of the actual source. Thus Eqn. (41) will be correct if α is taken to be the actual intensity per unit length of the line source. Furthermore, at least for short times, the flux into the region $\rho < \rho_0$ is the same, by symmetry, as the flux into the region $\rho > \rho_0$. The total flux from a line source of length $2\pi\rho_0$ is

$$\frac{i_s}{\pi\rho_0^2} = -\frac{2}{\rho_0} n\bar{v}DC^0\alpha \quad (42)$$

Half of this current will flow into the region $\underline{z} > 0$, $\rho < \rho_0$. Hence

$$1/2i_s = -\Delta i \quad (43)$$

where Δi is given by Eqn. (33). These two currents have opposite signs since the source for $C^{\text{II}}(\rho, z, t)$ is to correct for the effects of radial diffusion. Thus we obtain

$$\alpha = \frac{2}{\pi} \quad (44)$$

The correction current density is therefore

$$\frac{i_s}{\pi\rho_0^2} = -\frac{n\bar{v}DC^0}{\sqrt{\pi Dt}} \frac{4}{\sqrt{\pi}} \frac{\sqrt{Dt}}{\rho_0} \quad (45)$$

E. Total Current Density and Concentration Profiles. The total current density is the sum of the current sources for $C^I(\rho, z, t)$ and Eqn. (45). The total current density due to the sources of $C^I(\rho, z, t)$ is [cf. Eqn. (12)]

$$\begin{aligned} \frac{i_1}{\pi \rho_0^2} &= -n\mathfrak{F}C^0 \sqrt{\frac{D}{\pi t}} \int_0^\infty g(\rho, t) \rho d\rho \\ &= -n\mathfrak{F}C^0 \sqrt{\frac{D}{\pi t}} \left\{ 1 + o\left(\frac{Dt}{\rho_0^2}\right) \right\} \end{aligned} \quad (46)$$

Therefore, the total current is

$$\frac{i}{\pi \rho_0^2} = -\frac{n\mathfrak{F}DC^0}{\sqrt{\pi Dt}} \left\{ 1 + \frac{4}{\sqrt{\pi}} \frac{\sqrt{Dt}}{\rho_0} + o\left(\frac{Dt}{\rho_0^2}\right) \right\} \quad (47)$$

Although the boundary condition [Eqn. (4)] is not satisfied in detail on the electrode, it is evident that, if the line charge is redistributed near the edge, the concentration could be calculated even at the face of the electrode. The current correction would, however, be very nearly the same since the flux from a source distribution may be found by calculating the flux from the equivalent point source.

We have overestimated the correction in Eqn. (43) since the center of the correction source is actually at $\rho < \rho_0$, rather than at $\rho = \rho_0$. Thus slightly more than half of the flux goes into the region $\rho < \rho_0$. This effect is only of the order of a few per cent for $t \lesssim 25$ sec. At longer times, when this effect becomes larger, the assumption that the added current is a line source approximated by a straight wire also becomes untenable.

$C^I(\rho, z, t)$ and $C^{II}(\rho, z, t)$ are given by Eqns. (7), (9), (37), (38),

and (40). As discussed above, $\underline{C}^{\text{II}}(\rho, z, t)$ is a poor approximation for distances smaller than the dimensions of the sources of $\underline{C}^{\text{II}}(\rho, z, t)$. The dimensions of the sources of $\underline{C}^{\text{II}}(\rho, z, t)$ may be estimated from Fig. 2 which shows the region for $\rho < \rho_0$ where $\Delta g(\rho, t)$ is appreciably different from zero. For $\underline{t} \lesssim 25$ sec, a distance of about 0.01 cm from the edge of the electrode is sufficient to ensure being outside the source. We therefore have, for $\underline{t} \lesssim 25$ sec and $\underline{r} \gtrsim 0.01$ cm.

$$C(\rho, z, t) = C^{\text{I}}(\rho, z, t) + C^{\text{II}}(\rho, z, t)$$

$$C^{\text{I}}(\rho, z, t) = C^0 \begin{cases} 1 - \operatorname{erf}\left(\frac{z}{2\sqrt{Dt}}\right) & 0 \leq \rho < \frac{\rho_0}{4} \\ \left[\frac{1}{2} \left(1 + \operatorname{erf}\left(\frac{\rho_0 - \rho}{2\sqrt{Dt}}\right) \right) - \frac{1}{2\sqrt{\pi}} \frac{\sqrt{Dt}}{\rho_0} e^{-\left(\frac{\rho_0 - \rho}{4Dt}\right)^2} \right] \left(1 - \operatorname{erf}\left(\frac{z}{2\sqrt{Dt}}\right) \right) & \frac{\rho_0}{4} \leq \rho \leq \rho_0 \\ \left[\frac{1}{2} \left(1 - \operatorname{erf}\left(\frac{\rho - \rho_0}{2\sqrt{Dt}}\right) \right) - \frac{1}{2\sqrt{\pi}} \frac{\sqrt{Dt}}{\rho_0} e^{-\left(\frac{\rho - \rho_0}{4Dt}\right)^2} \right] \left(1 - \operatorname{erf}\left(\frac{z}{2\sqrt{Dt}}\right) \right) & \rho_0 < \rho \leq \infty \end{cases} \quad (48)$$

$$C^{\text{II}}(\rho, z, t) = C^0 \begin{cases} -\frac{1}{2\pi^2} \operatorname{Ei}\left(-\frac{r^2}{4Dt}\right) & 0 < r < \frac{\rho_0}{2} \\ 0 & \frac{\rho_0}{2} \leq r < \infty \end{cases} \quad (49)$$

where $\underline{r} = [\underline{z}^2 + (\rho - \rho_0)^2]^{\frac{1}{2}}$.

Near the electrode, the concentration may be found more accurately by replacing our line source by a series of line sources and then replacing each line source by a finite source. The strength of such sources is still determined by $\Delta g(\rho, t)$. As is evident, such a procedure approximates the exact solution more and more accurately. However, in order to obtain the exact solution, both the location and the strength of the sources for $\underline{C}^{\text{II}}(\rho, z, t)$ must be time-dependent. Thus, the mathe-

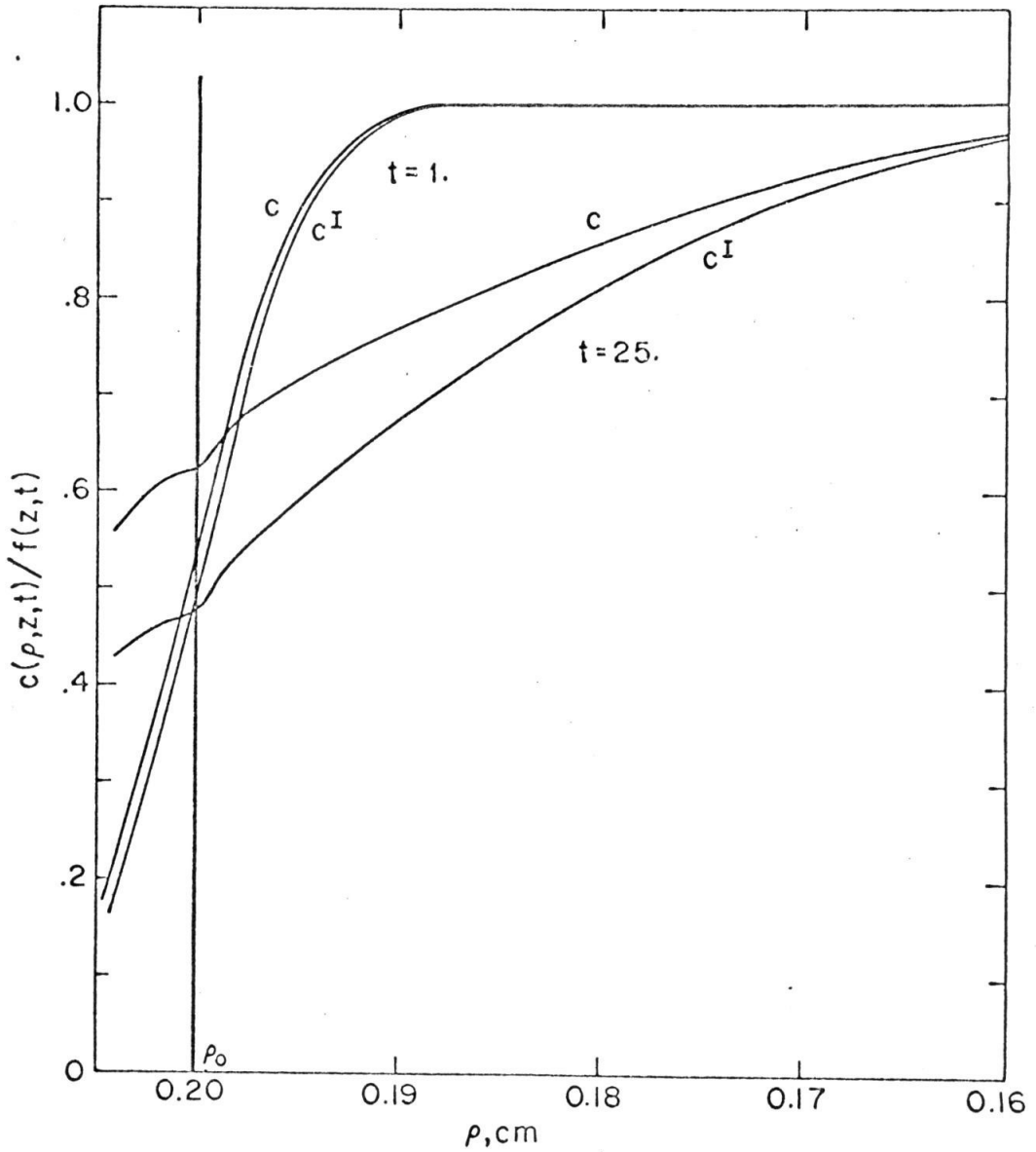


Figure 3. Typical concentration profiles for $C(\rho, z, t)$ and $C^I(\rho, z, t)$: $z = 0.01$ cm.,
 $\rho_0 = 0.2$ cm, $D = 1 \times 10^{-5}$ cm²/sec.

matics becomes considerably less tractable. The simple model discussed in this dissertation is useful because it predicts an accurate value of the total current density and, except very near the electrode, accurate concentration profiles.

Discussion

A. Generalization. Our solution can be readily converted into the more usual situation where the solution originally contains the electroactive species at concentration C^0 and the product is insoluble. This is done by the simple transformation

$$C'(\rho, z, t) = C^0 - C(\rho, z, t) \quad (50)$$

where $C'(\rho, z, t)$ is the transformed concentration and $C(\rho, z, t)$ is given by Eqn. (6). Under these conditions, Eqn. (47) will be valid at all points on the i-E curve if C^0 is replaced by $C^0 - C(\rho, 0, t, E)$.

This treatment could be extended to include the more general system where both the oxidized and reduced species are soluble and the solution is initially free of the reduced species. We would decompose the concentration of both the oxidized and reduced species into the two components $C_i^I(\rho, z, t)$ and $C_i^{II}(\rho, z, t)$. We would require the additional boundary conditions that the ratio of the concentrations of the two components at the outer Helmholtz plane is fixed by the Nernst equation and that the sum of their fluxes is zero at the electrode (7). For the purposes of the next chapter, however, it is sufficient to note that the current on the diffusion plateau is independent of the reduced species.

and is given by Eqn. (47).

B. Comparison with Experiment. The theoretical value of the chronoamperometric constant is obtained by rearranging Eqn. (47).

$$\frac{i^{1/2}}{AC^0} = n\bar{F} \sqrt{\frac{D}{\pi}} \left\{ 1 + \frac{4}{\sqrt{\pi}} \frac{\sqrt{Dt}}{\rho_0} + O\left(\frac{Dt}{\rho_0^2}\right) \right\} \quad (51)$$

The coefficient of the first term is evaluated experimentally for $\rho_0 = 0.258$ cm and $0.01 < \sqrt{Dt}/\rho_0 < 0.08$ for a variety of systems in the next portion of this thesis. The experimental value of this coefficient is 2.12 ± 0.11 (95% confidence level) and is in agreement with the theoretical value of 2.26; the agreement is especially good since the latter is a slight overestimate.

CHAPTER 2.

Evaluation of the Experimental Chronopotentiometric
and Chronoamperometric Constants*

Introduction

In the preceding chapter, we demonstrated that the chronoamperometric constant obtained with unshielded, circular, planar electrodes is expected to differ from the Cottrell equation by a multiplicative power series in the square root of the time.

$$\frac{\underline{i}t^{\frac{1}{2}}}{\underline{AC}} = \frac{nFD^{\frac{1}{2}}}{\pi^{\frac{1}{2}}} \left(1 + R \left(\frac{Dt}{\rho_0^2} \right)^{\frac{1}{2}} + \dots \right) \quad (1)$$

\underline{D} is the diffusion coefficient, \underline{t} is the time, $\underline{i}/\underline{A}$ is the current density, and ρ_0 is the radius of the electrode. The purpose of this chapter is to verify this expression experimentally. In addition, we have shown that the chronopotentiometric constant for unshielded, circular, planar electrodes can be expressed as the product of the Sand equation and a power series in the square root of the transition time.

$$\frac{\underline{i}\underline{\tau}^{\frac{1}{2}}}{\underline{AC}} = \frac{nF\pi^{\frac{1}{2}}\underline{D}^{\frac{1}{2}}}{2} \left(1 + S \left(\frac{D\underline{\tau}}{\rho_0^2} \right)^{\frac{1}{2}} + \dots \right) \quad (2)$$

The dependencies of these expressions on the diffusion coefficient and on the time were determined explicitly and the dependence on the

* A summary of this work appeared in Anal. Chem., 36, 1723 (1964).

electrode radius was assumed on the basis of the preceding theoretical work. It is shown that only the zeroth-order and square root terms contribute to the measured values of the constants under the usual experimental conditions.

Results

The experimental values of the chronopotentiometric constant are plotted in Fig. 4 as a function of $(D\tau/\rho_0^2)^{\frac{1}{2}}$; representative values of the chronoamperometric constant are plotted in Fig. 5 as a function of $(Dt/\rho_0^2)^{\frac{1}{2}}$. These plots were constructed by plotting the experimental values vs. $\tau^{\frac{1}{2}}$ or $t^{\frac{1}{2}}$ and calculating D from the intercept value. The experimental values were then replotted vs. $(D\tau/\rho_0^2)^{\frac{1}{2}}$ or $(Dt/\rho_0^2)^{\frac{1}{2}}$.

It is evident in Fig. 5 that the experimental values deviate from the simple $(Dt/\rho_0^2)^{\frac{1}{2}}$ straight line at sufficiently long times, $t > t_{\text{max}}$. It is thought that this indicates the onset of convective stirring. The deviations have been suppressed by excluding all data pairs--i. e., all i, t pairs, for $t > t_{\text{max}}$. The values listed in Table I under the column heading "t_{max}" correspond to the largest value of the time used in calculating the slope and the intercept. In many of the entries, this value is considerably before the onset of the deviation from the straight line and where this is true it is indicated by the symbol ">".

The confidence intervals corresponding to the deviations of $i\tau^{\frac{1}{2}}/\underline{AC}$ or $it^{\frac{1}{2}}/\underline{AC}$ from the least-squares line are generally less than $\pm 1\%$. Therefore, these deviations are due principally to the experimental

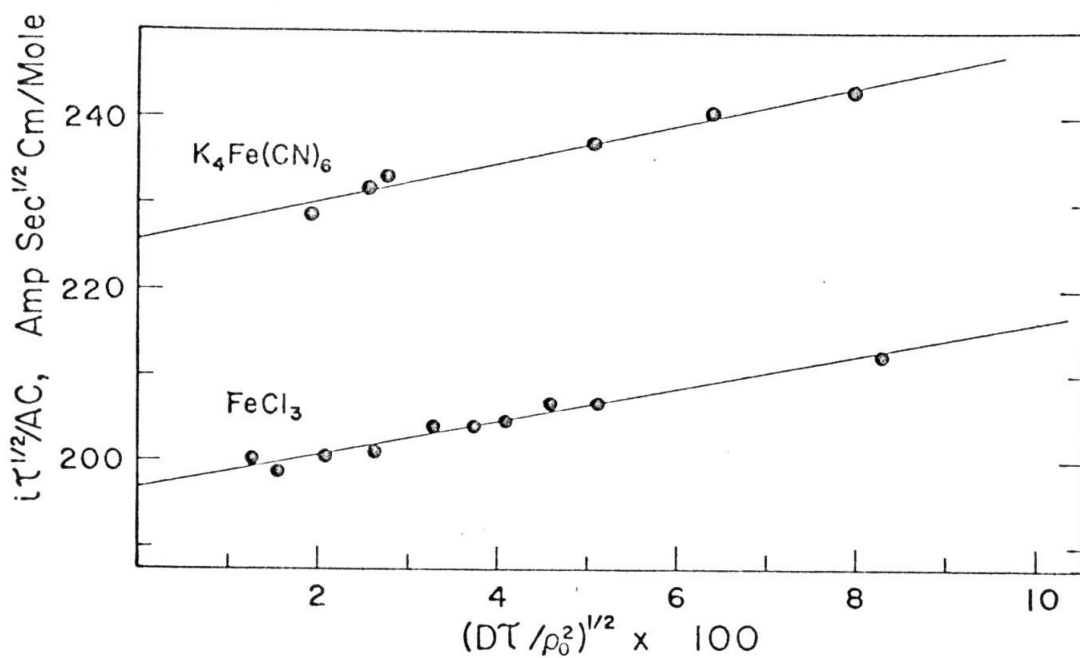


Figure 4. $i\tau^{1/2}/AC$ is plotted vs. $(D\tau/\rho_0^2)^{1/2}$ for the reduction of 10.49 mF ferric chloride in 1.00 F hydrochloric acid and for the oxidation of 9.99 mF potassium ferrocyanide in 0.100 F potassium chloride. Each point represents the average of at least three determinations.

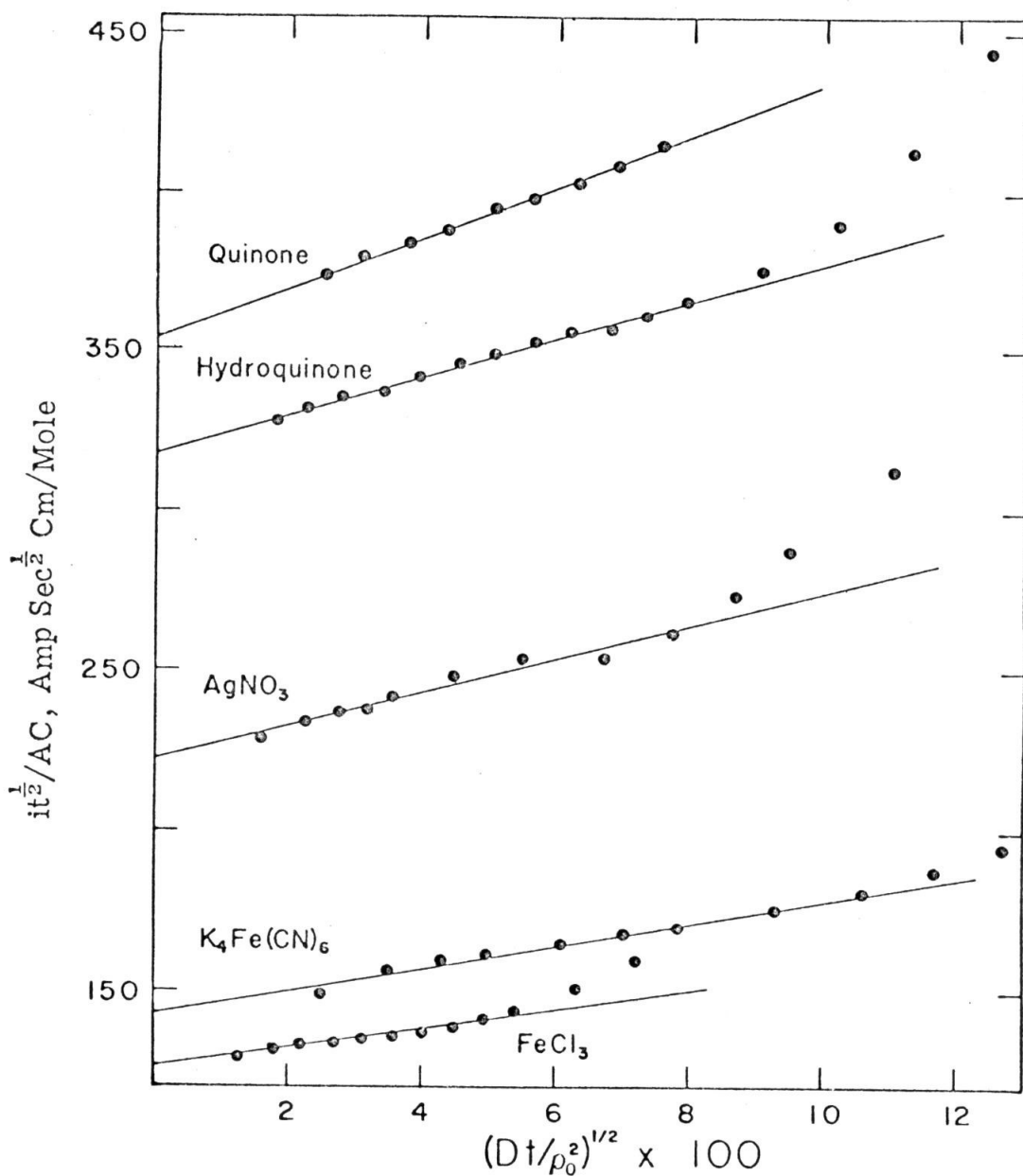


Figure 5. i_t^2/AC is plotted vs. $(Dt/\rho_0^2)^{1/2}$ for the oxidation of 4.72 mF potassium ferrocyanide in 0.100 F potassium chloride, for the reduction of 4.83 mF silver nitrate in 0.1 F nitric acid, for the reduction of 4.63 mF ferric chloride in 1.00 F hydrochloric acid, for the reduction of 10.53 mF quinone and for the oxidation of 5.20 mF hydroquinone, both in 1.03 F perchloric acid. The platinum electrode was potentiostated at +0.40, 0.00, and +0.15 v. vs. S.C.E. and at 0.00 and +0.75 v. vs. NaCl-S.C.E., respectively. Each point represents the average of at least three determinations.

TABLE I

The Chronoamperometric Data Were Fitted to the Straight Line

$$\frac{it^{\frac{1}{2}}}{AC} = \frac{nFD^{\frac{1}{2}}}{\pi^{\frac{1}{2}}} \left[1 + R \left(\frac{Dt}{\rho_0^2} \right)^{\frac{1}{2}} \right]$$

Stated Confidence Intervals Correspond to 95% Confidence Level. Platinum Electrode, $\rho_0 = 0.2578$ cm

System	Conc., mF	t_{\max} , sec	Intercept, amp. $\text{sec}^{\frac{1}{2}}$ cm/mole	R	$D \times 10^6$ cm^2/sec
AgNO ₃ 0.1 F HNO ₃ 0.00 v.	4.83	18	222.4 ± 5.1	2.36 ± 0.56	16.7
Quinone 1.03 F HClO ₄ 0.00 v.	10.20 10.53 ^a	> 36 > 36	354.0 ± 2.9 354.2 ± 2.1	2.36 ± 0.16 2.25 ± 0.12	10.6 10.6
Hydroquinone 1.03 F HClO ₄ 0.75 v.	10.58 _b 10.58 ^b 5.20	> 36 > 36 49	326.2 ± 1.7 327.3 ± 2.0 318.2 ± 1.8	1.96 ± 0.11 1.97 ± 0.13 1.87 ± 0.11	8.97 9.03 8.54
K ₄ Fe(CN) ₆ 0.100 F KCl 0.40 v.	10.08 10.08 ^c 4.72 1.008 0.504	> 36 > 36 84 > 36 > 36	140.5 ± 0.78 142.0 ± 0.97 142.8 ± 3.6 139.6 ± 1.8 142.8 ± 1.4	2.16 ± 0.14 2.00 ± 0.17 2.51 ± 0.41 2.02 ± 0.32 1.49 ± 0.24	6.66 6.80 6.88 6.58 6.88
FeCl ₃ 1.00 F HCl 0.10 v.	9.25 ^d 9.25 ^d 4.63 ^d	42 42 25	124.0 ± 1.2 124.4 ± 0.44 126.8 ± 0.81	2.42 ± 0.26 2.38 ± 0.092 2.04 ± 0.20	5.19 5.22 5.42
FeCl ₂ 1.00 F HCl 0.70 v.	9.25 9.25 ^e	49 42	140.8 ± 1.1 142.2 ± 0.91	2.00 ± 0.16 1.76 ± 0.15	6.69 6.82

^a0.05 v., ^b1.20, ^c0.35, ^d0.15, ^e0.65.

TABLE II

The Chronopotentiometric Data Were Fitted to the Straight Line

$$\frac{i\tau^{\frac{1}{2}}}{AC} = \frac{nF\pi^{\frac{1}{2}}D^{\frac{1}{2}}}{2} \left[1 + S \left(\frac{D\tau}{\rho_0^2} \right)^{\frac{1}{2}} \right]$$

Stated Confidence Intervals Correspond to 95% Confidence Level. Platinum Electrode, $\rho_0 = 0.2578$ cm

<u>System</u>	<u>Conc., mF</u>	<u>t_{max}, sec</u>	<u>intercept, amp. sec^{1/2} cm/mole</u>	<u>S</u>	<u>D × 10⁶ sq cm/sec</u>
K ₄ Fe(CN) ₆ 0.100 <u>F</u> KCl	9.99	> 62	225.7 ± 2.3	0.99 ± 0.21	6.97
FeCl ₃ 1.00 <u>F</u> HCl	10.49	> 74	196.9 ± 1.2	0.98 ± 0.15	5.30

uncertainty associated with the individual data pairs.

The diffusion coefficients calculated from the intercept values of the chronopotentiometric and chronoamperometric constants agree well with those determined independently (Table III). This indicates that the slope is not kinetically controlled and suggests, as we would expect, that the intercepts correspond to the simple Cottrell or Sand equations, Eqn. (1) or Eqn. (2).

The apparent diffusion coefficient of quinone decreased from 10.6×10^{-6} cm²/sec 30 minutes after the solution has been prepared to 9.6×10^{-6} cm²/sec 150 minutes after the solution had been prepared. This suggests that quinone is undergoing an acid-catalyzed decomposition at a rate of about 2% per hour (13). Therefore, the true diffusion coefficient of quinone in 1 F perchloric acid is 10.8×10^{-6} cm²/sec.

The 16 chronopotentiometric data pairs were normalized to a single line by plotting

$$\frac{i\tau^{\frac{1}{2}}}{AC} / \frac{i\tau^{\frac{1}{2}}}{AC} \Big|_{\text{int.}} \quad \text{vs.} \quad \left(\frac{D\tau}{\rho_0^2} \right)^{\frac{1}{2}}$$

In a similar fashion, the 199 chronoamperometric data pairs were normalized to a single line by plotting

$$\frac{it^{\frac{1}{2}}}{AC} / \frac{it^{\frac{1}{2}}}{AC} \Big|_{\text{int.}} \quad \text{vs.} \quad \left(\frac{Dt}{\rho_0^2} \right)^{\frac{1}{2}}$$

(13) L. F. Fieser and M. Fieser, "Advanced Organic Chemistry," Reinhold, New York, N.Y., 1961, p. 846.

TABLE III

Comparison of Diffusion Coefficients Calculated from Intercept Value of Chronopotentiometric and Chronoamperometric Constants with Selected Literature Values

(In units of 10^{-6} cm²/sec)

Technique	K ₄ Fe(CN) ₆ 0.100F KCl	FeCl ₃ 1.00F HCl	FeCl ₂ 1.00F HCl	AgNO ₃ 0.1F NH ₄ O ₃	Quinone 1.03F HClO ₄	Hydro- quinone 1.03F HClO ₄
Unshielded Electrodes						
Chronopotentiometric	6.97					
Chronoamperometric ^a	6.70 ± 0.18	5.29 ± 0.15	6.75 ± 0.07	16.7 ^b	10.8 ^c	8.89 ± 0.26
Shielded Electrodes						
Chronopotentiometric (14)						
Chronoamperometric (2)	7.18					
(3)	6.87 ± 0.08			13.8 ^d		
(15)	6.50			15.5 ^d		
(1)				17.4 ^d		
Polarographic: (16)						
(15)				15.4 ^d		
					10.2 ^{d,e}	8.7 ^{d,e}
					9.5 ^f	

^aValues and confidence intervals are based on a single extrapolation of all data pairs for each system and are not simple averages of the data in Table I.

^bThree data pairs, $t > 36$ sec, were neglected in computing this value.

^cSee text.

(Cont.)

TABLE III (continued)

^d0.1M KNO₃.

^eRecalculated on the basis of the experimentally modified Ilkovic equation.

^f1.0M KNO₃.

(14) J. J. Lingane, J. Electroanal. Chem., 2, 46 (1961).

(15) M. von Stackelberg, M. Pilgram, and V. Toome, Z. Electrochem., 57, 342 (1953).

(16) I. M. Kolthoff and E. F. Orlemann, J. Am. Chem. Soc., 63, 664 (1941).

The experimental intercepts were determined to be 1.000 and 0.998, respectively; the slopes were determined to be

$$S = 0.98 \pm 0.10$$

$$R = 2.12 \pm 0.11$$

This experimental value for R is in excellent agreement with the value of 2.26 derived in the preceding chapter.

Discussion

Since the Sand equation and the Cottrell equation are strictly applicable only under condition of one-dimensional linear diffusion, shielded planar electrodes have been employed in accurate chronopotentiometric (17) and chronoamperometric (1,2,3) experiments. A great deal of enthusiasm has been generated for the use of cylindrical wire electrodes because they are far easier to work with than shielded electrodes and yet are of a sufficiently simple geometry that solutions have been obtained for the chronopotentiometric (18) and chronoamperometric (19) constants.

The work reported here illustrates that both of these alternatives are generally unnecessary and that excellent results are obtained with

(17) A. J. Bard, Anal. Chem., 33, 11 (1961).

(18) D. G. Peters and J. J. Lingane, J. Electroanal. Chem., 2, 1 (1961).

(19) Paul Delahay, "New Instrumental Methods in Electrochemistry," Interscience, New York, 1954, Chapter 3.

the more convenient unshielded planar electrodes. For $(Dt/\rho_0^2)^{\frac{1}{2}} < 0.02$, the deviation of the measured chronoamperometric constant from the Cottrell value will be less than 5 per cent; the limits are even more generous for the chronopotentiometric constant. These criteria are readily satisfied in investigations of preceding chemical reactions or of adsorption where high current densities are employed. These criteria may not be met in certain analytical applications but in those cases Eqns. (1) or (2) can be applied directly. Alternatively, replicate determinations can be made at different current densities and the data extrapolated to the $\underline{t}^{\frac{1}{2}} = 0$ or the $\underline{\tau}^{\frac{1}{2}} = 0$ intercept.

Experimental

The chronopotentiometric setup was usual. The constant current was obtained by putting large dropping resistors in series with a 270-volt battery bank. A Clare mercury-wetted, make-before-break, d. c. relay was used for switching. A Philbrick P2 differential amplifier was used as a follower. The constant currents were determined during the experiment since currents measured prior to the experiment (when a dummy resistor is substituted for the cell) were about 0.3% greater than those observed during the experiment. The E - \underline{t} curve was displayed on a Sargent-SR recorder; the chart was driven at a rate of 12 inches/min by a synchronous motor. The transition times were measured directly from the chart paper by the method of Kuwana (20).

(20) C. D. Russell and J. M. Peterson, J. Electroanal. Chem., 5, 467 (1963).

The chronoamperometric experiments employed a Wenking TR potentiostat (Brinkmann Instruments, Inc., Cantague Road, Westbury, N. Y.), and the current was determined by measuring the iR drop developed across a precision resistor. The Sargent recorder, equipped with a 5-mv range plug, was used to monitor this current continuously.

A jacketed, single-compartment cell of about 125-ml capacity was employed. The Teflon cap was fitted with openings for the various nitrogen inlets, for the salt bridge, for the reference electrode, and for the working and auxiliary electrodes. The salt bridge was of the cracked glass type. The auxiliary electrode was not placed in a separate compartment because it was desired to keep the rest potentials of the auxiliary and working electrodes identical; the make-before-break relay, used in the chronopotentiometric circuit to minimize current transients, momentarily shorts these two electrodes together and hence undesired electrochemistry takes place if these two potentials are not identical (21). The cell was stirred with a magnetic stirrer and de-aerated with "prepurified" nitrogen. No attempt was made to shock-mount the cell. The cell was thermostated at $25.0 \pm 0.1^\circ\text{C}$.

The electrode employed in this study was a Beckman No. 39273 platinum button electrode. The projected area was determined to be 0.2088 ± 0.0004 sq cm by measuring mutually perpendicular diameters with an optical comparator. As received, the electrode surface was dull in color and deeply scratched; therefore, it was polished with 4/0

(21) F. C. Anson, Anal. Chem., 36, 520 (1964).

emery paper and cleaned with aqua regia prior to its initial use. The electrode was mounted horizontally in the center of the cell and oriented so that the diffusion was upwards. The auxiliary electrode was positioned parallel to and about 1 cm from the working electrode.

All potentials are with respect to the saturated calomel electrode (S.C.E.) with the exception of the experiments involving perchloric acid where a NaCl-S.C.E. was employed. The potential of this electrode was measured to be -14 mv vs. S.C.E. in 1 F sulfuric acid supporting electrolyte.

The potassium ferrocyanide was Baker and Adamson $K_4Fe(CN)_6 \cdot 3H_2O$ and was used directly without assay. The silver solution was prepared by weight and the ferric chloride solution was standardized vs. potassium dichromate. The quinone was twice sublimed prior to use and solutions were discarded within 30 minutes of their preparation (see text). The hydroquinone and ferrous chloride solutions were prepared by potentiostatic reduction of quinone or ferric chloride in situ at a large platinum gauze electrode. All solutions were prepared with triply distilled water of specific conductivity less than 1.3×10^{-6} mho/cm.

Background currents were measured at potentiostated electrodes in perchloric and hydrochloric acids and were negligible at the concentration levels studied.

In all cases, except for the reduction of silver ion, the electrode was also potentiostated 50 mv less anodic or cathodic in at least one experiment to demonstrate that the electrode was being potentiostated

on the plateau of the current-potential curve.

The slopes, intercepts, and confidence intervals were determined by a least-squares analysis. All the data pairs were weighted equally. The stated confidence intervals correspond to the 95% confidence level and were calculated from the usual equations (22).

Acknowledgment

It is a pleasure to thank Martin S. Itzkowitz for assistance in the least-squares programming.

(22) H. A. Laitinen, "Chemical Analysis," McGraw-Hill, New York, 1960, Chapter 26.

II. APPLICATIONS OF POTENTIAL STEP CHRONOCOULOMETRY

In applying the potential step technique to the study of electrochemical problems, the potential of the indicator electrode is initially adjusted to a value such that no faradaic current passes through the electrode. For example, if the solution were free of the reduced species, the initial potential would be chosen to lie in the potential region anodic to the foot of the polarographic wave, cf. Fig. 6. If the solution were to contain appreciable amounts of both oxidation states of the redox couple, the initial potential would be the equilibrium potential (23). The potential step experiment is initiated by abruptly shifting the potential of the indicator electrode to a value such that faradaic current flows; the value of this new potential, relative to the polarographic wave, governs the type of information which can be obtained about the system. Cf. Fig. 6.

If the new potential lies in the potential region of the polarographic diffusion plateau, the current will be limited by the rate of transport of material to the electrode. If the new potential is in the vicinity of the half-wave potential, the current will be limited, for sufficiently short times, by the rate of the electron-transfer step. Therefore, the potential region corresponding to the polarographic diffusion plateau is utilized for the measurement of the rates of solution

(23) H. Gerischer, Z. Elektrochem., 64, 29 (1960).

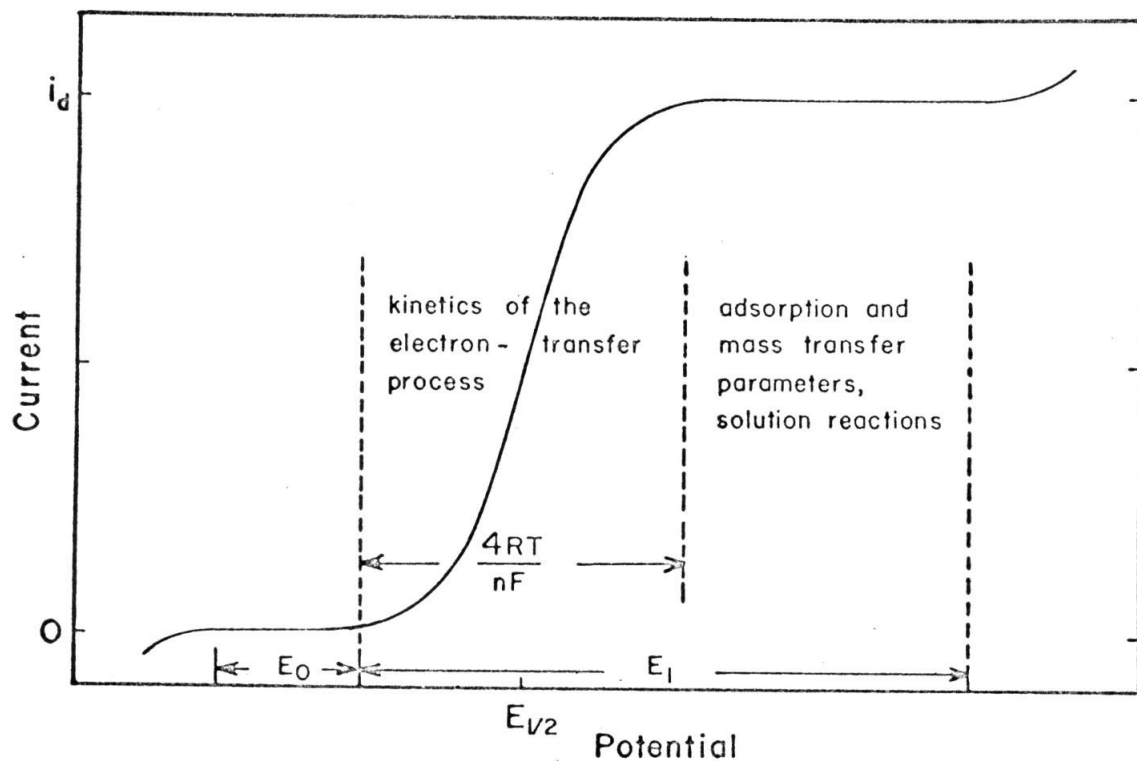


Figure 6. The characteristic potential regions for the applications of potential step chronocoulometry superimposed on an idealized polarographic current-potential curve.

reactions, for the determination of the quantity of electroactively adsorbed species, and for the determination of diffusion coefficients; the potential region in the vicinity of the half-wave potential is utilized for the determination of the kinetics of the electrode-transfer process.

The unique contribution of Anson, Christie, Lauer, and Osteryoung to the development of potential step techniques is their decision to observe the integral of the current, rather than the current itself, as the experimental quantity. An immediate advantage is that the integrator averages out the noise superimposed on the output of the high-gain current-measuring amplifier and thus the current integral can generally be determined more precisely than the current itself.

A more important advantage of an integral technique concerns its "memory capacity." For example, the current could be enhanced for a brief period following the application of the potential step by the electrolysis of a substance adsorbed on the surface of the electrode. One can determine the extent of this adsorption by making charge measurements on a time scale which is long compared to the half time for the electrolysis of the adsorbed species. Furthermore, the quantity of electroactive adsorption is obtained directly and thus the adsorption isotherms are independent of any mechanistic assumptions about the rate and order of the electrolysis process.

A third advantage of an integral technique lies in the simplicity with which a correction for double-layer charging may be effected. By operating on a time scale long compared to the time constant for

the charging of the electrode/solution interface, one can correct the measured values of the charge for the effects of double-layer charging by simply shifting the zero-charge axis by an amount equal to the change in electronic charge on the electrode.

The original application of the potential step chronocoulometric technique and the one which has absorbed the continuing interest of these investigators is the measurement of the extent of electroactive adsorption on the surface of electrodes (24-28). Subsequent chapters discuss specific applications of the potential step chronocoulometric technique to the determination of the kinetics of solution reactions and of electron-transfer processes at electrodes.

(24) F. C. Anson, Anal. Chem., 36, 932 (1964).

(25) J. H. Christie, G. Lauer, and R. A. Osteryoung, J. Electroanal. Chem., 7, 60 (1964).

(26) R. A. Osteryoung and F. C. Anson, Anal. Chem., 36, 975 (1964).

(27) F. C. Anson, J. H. Christie, and R. A. Osteryoung, J. Electroanal. Chem., in press, 1966.

(28) J. H. Christie, R. A. Osteryoung, and F. C. Anson, J. Electroanal. Chem., in press, 1966.

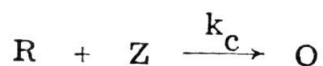
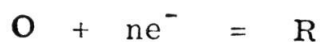
CHAPTER 3.

The Evaluation of Working Curves for the
Study of the Rates of Solution Reactions

The purpose of this chapter is to discuss the calculation of the working curves and working tables to be used in conjunction with double potential step chronocoulometry for the determination of the first order rate constants of those catalytic or following reactions which occur after electrode processes.

The Catalytic Reaction

The model for the catalytic regeneration of the electroactive species is



where k_c is the first order or pseudo first order rate constant for the catalytic reaction. Christie (29) has solved this problem and has obtained the following solutions for the faradaic charge as a function of time.

(29) J. H. Christie, J. Electroanal. Chem., in press, 1966.

$$\begin{aligned}
 Q(t \leq \tau) &= \frac{nFAD^{\frac{1}{2}}C_0}{\beta} \left[(\beta^2 t + \frac{1}{2}) \operatorname{erf} \sqrt{\beta^2 t} + \beta \sqrt{\frac{t}{\pi}} e^{-\beta^2 t} \right] \\
 Q(t > \tau) &= \frac{nFAD^{\frac{1}{2}}C_0}{\beta} \left[(\beta^2 t + \frac{1}{2}) \operatorname{erf} \sqrt{\beta^2 t} + \beta \sqrt{\frac{t}{\pi}} e^{-\beta^2 t} \right. \\
 &\quad \left. - [\beta^2(t - \tau)] \operatorname{erf} \sqrt{\beta^2(t - \tau)} - \beta \sqrt{\frac{t - \tau}{\pi}} e^{-\beta^2(t - \tau)} \right]
 \end{aligned} \tag{1}$$

The reverse potential step is initiated at $t = \tau^+$, $\beta^2 = k_c(Z)$, and $D_0 = D_r \equiv D$. The quantity used for the determination of β^2 is the ratio

$$\left| \frac{Q_b}{Q_f} \right| = 2 - \frac{(2\beta^2\tau + \frac{1}{2}) \operatorname{erf} \sqrt{2\beta^2\tau} + \sqrt{\frac{2\beta^2\tau}{\pi}} e^{-2\beta^2\tau}}{(\beta^2\tau + \frac{1}{2}) \operatorname{erf} \sqrt{\beta^2\tau} + \sqrt{\frac{\beta^2\tau}{\pi}} e^{-\beta^2\tau}} \tag{2}$$

because this ratio is independent of the numerical value of D , of the electrode area, and of the bulk concentration C_0 .

Values of $|Q_b/Q_f|$ were calculated directly from Eqn. (2) for $0.01 \leq \beta\tau^{\frac{1}{2}} \leq 2.00$ in increments of $\beta\tau^{\frac{1}{2}} = 0.01$. The results of these calculations are presented in Appendix A and Fig. 7.

Values of $\beta\tau^{\frac{1}{2}}$ were obtained as a function of equally spaced values of $|Q_b/Q_f|$ by inverse interpolation from Appendix A. A quadratic interpolation formula was employed. The results of this interpolation are presented in Appendix B. The calibration table, $\beta^2\tau$ as

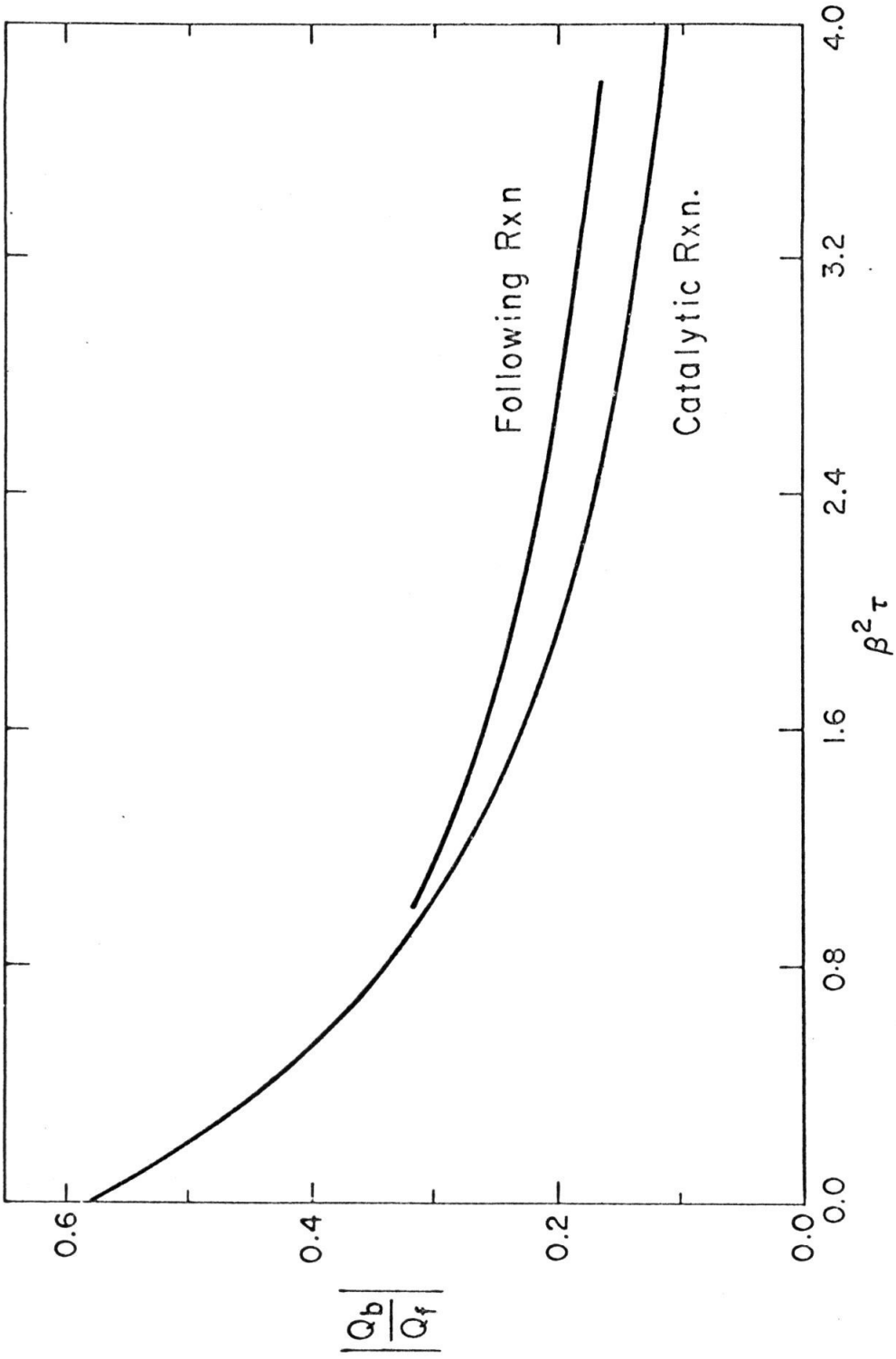
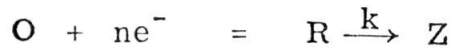


Figure 7. Theoretical plot of $\left| \frac{Q_b}{Q_f} \right|$ as a function of $\beta^2 \tau$ for the first-order catalytic and following reactions.

a function of $|Q_p/Q_f|$, is presented in Appendix C.

The Following Reaction

The model for the chemical reaction of the product of the electrode process to yield an electro-inactive species is



where k is the first order rate constant for the following reaction.

Christie (29) has obtained the following solutions for the faradaic charge as a function of time when the reverse step is initiated at $t = \tau^+$.

$$\begin{aligned} Q(t \leq \tau) &= 2nFAD_0^{\frac{1}{2}} C_0 \sqrt{\frac{t}{\pi}} \\ Q(t > \tau) &= \frac{2nFAD_0^{\frac{1}{2}} C_0}{\sqrt{\pi}} \left[\sqrt{t} - \sqrt{t-\tau} \psi \right] \end{aligned} \quad (3)$$

where

$$\begin{aligned} \psi &= -e^{-kt} \left\{ \sum_{n=1}^{\infty} \frac{{}_1F_1\left(n+\frac{1}{2}, n+1, k\tau\right)}{n!} \left[\frac{k(t-\tau)^{n-1}}{2} \right. \right. \\ &+ \left. \left. \sum_{i=1}^{n-1} \frac{[k(t-\tau)]^{n-i-1}}{2^{i+1}} \frac{(2n-1)!!}{(2n-2i-1)!!} \right] \right\} \\ &+ \frac{\sqrt{\pi}}{2} \frac{\text{erf}[k(t-\tau)]^{\frac{1}{2}}}{[k(t-\tau)]^{\frac{1}{2}}} e^{-k\tau} \left[{}_1F_1\left(\frac{1}{2}, 1, k\tau\right) + \right. \end{aligned}$$

$$\sum_{n=1}^{\infty} \frac{{}_1F_1\left(n+\frac{1}{2}, n+1, k\tau\right)}{2^n(n!)} (2n-1)!! \quad (4)$$

where $(2n-1)!! = 1 \cdot 3 \cdot 5 \cdots (2n-1)$.

We attempted the computation of ψ directly from Eqn. (4). The values of the necessary confluent hypergeometric functions were calculated directly from their definition (30).

$${}_1F_1(a, b, z) = 1 + \frac{az}{b} + \frac{(a+1)z^2}{(b+1)} + \dots \quad (5)$$

The series was terminated when the last term was less than 0.0001% of the sum. Unfortunately, Eqn. (4) converges very slowly, if at all.

We rearranged Eqn. (4) by using the identity (30)

$$\operatorname{erf}(x) = \frac{2x}{\sqrt{\pi}} {}_1F_1\left(\frac{1}{2}, \frac{3}{2}, -x^2\right) = \frac{2x}{\sqrt{\pi}} e^{-x^2} {}_1F_1\left(1, \frac{3}{2}, x^2\right) \quad (6)$$

to obtain at $t = (1+R)\tau$,

$$\psi = e^{-(1+R)k\tau} \left\{ \sum_n \frac{{}_1F_1\left(n+\frac{1}{2}, n+1, k\tau\right)}{n!} \left[\frac{(2n-1)!!}{2^n} {}_1F_1\left(1, \frac{3}{2}, Rk\tau\right) \right. \right. \\ \left. \left. - \frac{(Rk\tau)^{n-1}}{2^n} - \frac{(2n-1)!!}{2^n} \sum_i \frac{(Rk\tau)^{n-i-1} 2^i}{(2n-2i-1)!!} \right] \right. \\ \left. + {}_1F_1\left(1, \frac{3}{2}, Rk\tau\right) {}_1F_1\left(\frac{1}{2}, 1, k\tau\right) \right\} \quad (7)$$

(30) L. J. Slater, Confluent Hypergeometric Functions, Cambridge University Press, 1960.

This series converges satisfactorily. ψ was taken to be equal to the sum of the first 15 terms. The last term was less than 0.0001% of ψ in all cases for $t = 2\tau$ ($R = 1$) and $0 < k\tau \leq 4.0$. Values of ψ calculated from Eqn. (7) are tabulated in Appendix D as a function of $k\tau$ for $t = 2\tau$.

It is again convenient to form the ratio

$$\left| \frac{Q_b}{Q_f} \right| = \left| \frac{Q[(1+R)\tau] - Q(\tau)}{Q(\tau)} \right| = (\psi\sqrt{R} - \sqrt{1+R} + 1) \quad (8)$$

Values of this ratio for $t = 2\tau$ are presented graphically in Fig. 7, and in tabular form in Appendix E, as a function of $k\tau = \beta^2\tau$. Values of $k\tau$ as a function of equally spaced values of $|Q_b/Q_f|$ were obtained by inverse interpolation from Appendix E. A quadratic interpolation formula was again used. The resulting working table is presented in Appendix F.

APPENDIX B

 βT^2 as a Function of $\frac{Q_b}{Q_r}$; Interpolated from Appendix A

$\frac{Q_b}{Q_r}$	0.000	0.001	0.002	0.003	0.004	0.005	0.006	0.007	0.008	0.009
0.15	1.6766	1.6699	1.6632	1.6565	1.6500	1.6434	1.6370	1.6305	1.6242	1.6179
0.16	1.6116	1.6054	1.5992	1.5931	1.5870	1.5810	1.5750	1.5691	1.5632	1.5574
0.17	1.5516	1.5458	1.5401	1.5345	1.5288	1.5232	1.5177	1.5122	1.5067	1.5013
0.18	1.4959	1.4905	1.4852	1.4799	1.4746	1.4694	1.4642	1.4591	1.4540	1.4489
0.19	1.4438	1.4388	1.4338	1.4289	1.4239	1.4190	1.4142	1.4093	1.4045	1.3997
0.20	1.3950	1.3903	1.3856	1.3809	1.3762	1.3716	1.3670	1.3625	1.3579	1.3534
0.21	1.3489	1.3444	1.3400	1.3356	1.3312	1.3268	1.3224	1.3181	1.3138	1.3095
0.22	1.3053	1.3010	1.2968	1.2926	1.2884	1.2842	1.2801	1.2760	1.2719	1.2678
0.23	1.2637	1.2597	1.2557	1.2517	1.2477	1.2437	1.2398	1.2358	1.2319	1.2280
0.24	1.2241	1.2203	1.2164	1.2126	1.2088	1.2050	1.2012	1.1974	1.1937	1.1899
0.25	1.1862	1.1825	1.1788	1.1751	1.1714	1.1678	1.1642	1.1605	1.1569	1.1533
0.26	1.1497	1.1462	1.1426	1.1391	1.1356	1.1320	1.1285	1.1250	1.1216	1.1181
0.27	1.1146	1.1112	1.1078	1.1043	1.1009	1.0975	1.0941	1.0908	1.0874	1.0841
0.28	1.0807	1.0774	1.0741	1.0707	1.0674	1.0642	1.0609	1.0576	1.0543	1.0511
0.29	1.0478	1.0446	1.0414	1.0382	1.0350	1.0318	1.0286	1.0254	1.0222	1.0191
0.30	1.0159	1.0128	1.0096	1.0065	1.0034	1.0003	0.9972	0.9941	0.9910	0.9879
0.31	0.9849	0.9818	0.9787	0.9757	0.9726	0.9696	0.9666	0.9636	0.9605	0.9575
0.32	0.9545	0.9515	0.9486	0.9456	0.9426	0.9396	0.9367	0.9337	0.9308	0.9278
0.33	0.9249	0.9220	0.9190	0.9161	0.9132	0.9103	0.9074	0.9045	0.9016	0.8987
0.34	0.8958	0.8929	0.8901	0.8872	0.8843	0.8815	0.8786	0.8758	0.8729	0.8701
0.35	0.8673	0.8644	0.8616	0.8588	0.8560	0.8532	0.8504	0.8476	0.8448	0.8420
0.36	0.8392	0.8364	0.8336	0.8308	0.8280	0.8253	0.8225	0.8197	0.8170	0.8142
0.37	0.8114	0.8087	0.8059	0.8032	0.8005	0.7977	0.7950	0.7922	0.7895	0.7868
0.38	0.7840	0.7813	0.7786	0.7759	0.7731	0.7704	0.7677	0.7650	0.7623	0.7596
0.39	0.7569	0.7542	0.7515	0.7488	0.7461	0.7434	0.7407	0.7380	0.7353	0.7326
0.40	0.7299	0.7272	0.7245	0.7218	0.7192	0.7165	0.7138	0.7111	0.7084	0.7057
0.41	0.7031	0.7004	0.6977	0.6950	0.6923	0.6897	0.6870	0.6843	0.6816	0.6789
0.42	0.6763	0.6736	0.6709	0.6682	0.6656	0.6629	0.6602	0.6575	0.6548	0.6522
0.43	0.6495	0.6468	0.6441	0.6414	0.6387	0.6360	0.6334	0.6307	0.6280	0.6253
0.44	0.6226	0.6199	0.6172	0.6145	0.6118	0.6091	0.6064	0.6037	0.6010	0.5982
0.45	0.5955	0.5928	0.5901	0.5874	0.5846	0.5819	0.5792	0.5764	0.5737	0.5710
0.46	0.5682	0.5655	0.5627	0.5600	0.5572	0.5544	0.5517	0.5489	0.5461	0.5433
0.47	0.5405	0.5378	0.5350	0.5322	0.5294	0.5265	0.5237	0.5209	0.5181	0.5152
0.48	0.5124	0.5096	0.5067	0.5038	0.5010	0.4981	0.4952	0.4923	0.4894	0.4865
0.49	0.4836	0.4807	0.4778	0.4748	0.4719	0.4690	0.4660	0.4630	0.4600	0.4570
0.50	0.4540	0.4510	0.4480	0.4450	0.4419	0.4389	0.4358	0.4328	0.4297	0.4266
0.51	0.4234	0.4203	0.4172	0.4140	0.4109	0.4077	0.4045	0.4013	0.3980	0.3948
0.52	0.3915	0.3882	0.3849	0.3816	0.3783	0.3749	0.3715	0.3681	0.3647	0.3613
0.53	0.3578	0.3543	0.3508	0.3473	0.3437	0.3402	0.3365	0.3329	0.3292	0.3255
0.54	0.3218	0.3180	0.3142	0.3104	0.3065	0.3026	0.2987	0.2947	0.2906	0.2866

APPENDIX C

 B^2r as a Function of $\frac{c_b}{c_r}$; Interpolated from Appendix A

$\frac{c_b}{c_r}$	0.000	0.001	0.002	0.003	0.004	0.005	0.006	0.007	0.008	0.009
0.15	2.8111	2.7885	2.7662	2.7441	2.7224	2.7009	2.6796	2.6587	2.6380	2.6175
0.16	2.5973	2.5773	2.5575	2.5380	2.5187	2.4996	2.4808	2.4621	2.4437	2.4255
0.17	2.4075	2.3896	2.3720	2.3546	2.3373	2.3203	2.3034	2.2867	2.2702	2.2538
0.18	2.2376	2.2216	2.2058	2.1901	2.1746	2.1592	2.1440	2.1290	2.1140	2.0993
0.19	2.0847	2.0702	2.0559	2.0417	2.0276	2.0137	1.9999	1.9862	1.9727	1.9593
0.20	1.9460	1.9328	1.9198	1.9068	1.8940	1.8813	1.8688	1.8563	1.8439	1.8317
0.21	1.8195	1.8075	1.7956	1.7837	1.7720	1.7604	1.7488	1.7374	1.7261	1.7148
0.22	1.7037	1.6926	1.6817	1.6708	1.6600	1.6493	1.6387	1.6281	1.6177	1.6073
0.23	1.5971	1.5869	1.5767	1.5667	1.5567	1.5468	1.5370	1.5273	1.5176	1.5080
0.24	1.4985	1.4890	1.4797	1.4704	1.4611	1.4519	1.4428	1.4338	1.4248	1.4159
0.25	1.4071	1.3983	1.3895	1.3809	1.3723	1.3637	1.3553	1.3468	1.3385	1.3302
0.26	1.3219	1.3137	1.3056	1.2975	1.2895	1.2815	1.2736	1.2657	1.2579	1.2501
0.27	1.2424	1.2347	1.2271	1.2196	1.2120	1.2046	1.1972	1.1898	1.1824	1.1752
0.28	1.1679	1.1607	1.1536	1.1465	1.1394	1.1324	1.1254	1.1185	1.1116	1.1048
0.29	1.0980	1.0912	1.0845	1.0778	1.0712	1.0646	1.0580	1.0515	1.0450	1.0385
0.30	1.0321	1.0257	1.0194	1.0131	1.0068	1.0006	0.9944	0.9882	0.9821	0.9760
0.31	0.9699	0.9639	0.9579	0.9520	0.9460	0.9401	0.9343	0.9284	0.9226	0.9169
0.32	0.9111	0.9054	0.8998	0.8941	0.8885	0.8829	0.8774	0.8718	0.8663	0.8609
0.33	0.8554	0.8500	0.8446	0.8393	0.8339	0.8286	0.8233	0.8181	0.8129	0.8077
0.34	0.8025	0.7974	0.7922	0.7871	0.7821	0.7770	0.7720	0.7670	0.7620	0.7571
0.35	0.7522	0.7473	0.7424	0.7375	0.7327	0.7279	0.7231	0.7184	0.7136	0.7089
0.36	0.7042	0.6995	0.6949	0.6903	0.6857	0.6811	0.6765	0.6720	0.6674	0.6629
0.37	0.6585	0.6540	0.6495	0.6451	0.6407	0.6363	0.6320	0.6276	0.6233	0.6190
0.38	0.6147	0.6105	0.6062	0.6020	0.5978	0.5936	0.5894	0.5852	0.5811	0.5770
0.39	0.5729	0.5688	0.5647	0.5607	0.5566	0.5526	0.5486	0.5446	0.5407	0.5367
0.40	0.5328	0.5288	0.5249	0.5211	0.5172	0.5133	0.5095	0.5057	0.5019	0.4981
0.41	0.4943	0.4905	0.4868	0.4831	0.4793	0.4756	0.4719	0.4683	0.4646	0.4610
0.42	0.4573	0.4537	0.4501	0.4465	0.4430	0.4394	0.4359	0.4323	0.4288	0.4253
0.43	0.4218	0.4183	0.4149	0.4114	0.4080	0.4045	0.4011	0.3977	0.3943	0.3910
0.44	0.3876	0.3843	0.3809	0.3776	0.3743	0.3710	0.3677	0.3644	0.3611	0.3579
0.45	0.3547	0.3514	0.3482	0.3450	0.3418	0.3386	0.3354	0.3323	0.3291	0.3260
0.46	0.3229	0.3198	0.3166	0.3136	0.3105	0.3074	0.3043	0.3013	0.2982	0.2952
0.47	0.2922	0.2892	0.2862	0.2832	0.2802	0.2772	0.2743	0.2713	0.2684	0.2655
0.48	0.2626	0.2596	0.2567	0.2539	0.2510	0.2481	0.2452	0.2424	0.2395	0.2367
0.49	0.2339	0.2311	0.2283	0.2255	0.2227	0.2199	0.2171	0.2144	0.2116	0.2089
0.50	0.2062	0.2034	0.2007	0.1980	0.1953	0.1926	0.1899	0.1873	0.1846	0.1820
0.51	0.1793	0.1767	0.1740	0.1714	0.1688	0.1662	0.1636	0.1610	0.1584	0.1558
0.52	0.1533	0.1507	0.1482	0.1456	0.1431	0.1406	0.1380	0.1355	0.1330	0.1305
0.53	0.1280	0.1256	0.1231	0.1206	0.1182	0.1157	0.1133	0.1108	0.1084	0.1060
0.54	0.1036	0.1011	0.0987	0.0963	0.0940	0.0916	0.0892	0.0868	0.0845	0.0821

Appendix D
 DPSCC: First Order Following Reaction
 ψ as a Function of kr ; Calculated from Equation 7

ψ	0.00	0.02	0.04	0.06	0.08	0.10	0.12	0.14	0.16	0.18
0.	1.0000	0.9901	0.9806	0.9713	0.9623	0.9535	0.9450	0.9368	0.9287	0.9209
0.2	0.9134	0.9060	0.8989	0.8919	0.8852	0.8786	0.8722	0.8660	0.8600	0.8541
0.4	0.8484	0.8429	0.8375	0.8322	0.8271	0.8222	0.8173	0.8126	0.8080	0.8036
0.6	0.7992	0.7950	0.7909	0.7869	0.7830	0.7791	0.7754	0.7718	0.7683	0.7648
0.8	0.7615	0.7582	0.7550	0.7519	0.7488	0.7458	0.7429	0.7401	0.7373	0.7346
1.0	0.7320	0.7294	0.7269	0.7244	0.7220	0.7196	0.7173	0.7150	0.7128	0.7106
1.2	0.7085	0.7064	0.7044	0.7024	0.7004	0.6985	0.6966	0.6948	0.6930	0.6912
1.4	0.6894	0.6877	0.6860	0.6844	0.6828	0.6812	0.6796	0.6781	0.6765	0.6751
1.6	0.6736	0.6721	0.6707	0.6693	0.6680	0.6666	0.6653	0.6639	0.6626	0.6614
1.8	0.6601	0.6589	0.6576	0.6564	0.6552	0.6541	0.6529	0.6518	0.6506	0.6495
2.0	0.6484	0.6473	0.6462	0.6452	0.6441	0.6431	0.6420	0.6410	0.6400	0.6390
2.2	0.6380	0.6370	0.6361	0.6351	0.6342	0.6332	0.6323	0.6314	0.6305	0.6296
2.4	0.6287	0.6278	0.6269	0.6260	0.6252	0.6243	0.6234	0.6226	0.6218	0.6209
2.6	0.6201	0.6193	0.6185	0.6177	0.6169	0.6161	0.6153	0.6145	0.6137	0.6130
2.8	0.6122	0.6114	0.6107	0.6099	0.6092	0.6084	0.6077	0.6070	0.6062	0.6055
3.0	0.6048	0.6041	0.6034	0.6027	0.6020	0.6013	0.6006	0.5999	0.5992	0.5985
3.2	0.5979	0.5972	0.5965	0.5959	0.5952	0.5945	0.5939	0.5932	0.5926	0.5920
3.4	0.5913	0.5907	0.5900	0.5894	0.5888	0.5882	0.5876	0.5869	0.5863	0.5857
3.6	0.5851	0.5845	0.5839	0.5833	0.5827	0.5821	0.5815	0.5810	0.5804	0.5798
3.8	0.5792	0.5787	0.5781	0.5775	0.5770	0.5764	0.5758	0.5753	0.5747	0.5742

Appendix E

DPSCC: First Order Following Reaction

 $|Q_b/Q_f|$ as a Function of kr ; Calculated from Equation 8.

$ Q_b/Q_f $	0.00	0.02	0.04	0.06	0.08	0.10	0.12	0.14	0.16	0.18
0.	0.5858	0.5759	0.5664	0.5571	0.5481	0.5393	0.5308	0.5225	0.5145	0.5067
0.2	0.4992	0.4916	0.4846	0.4777	0.4710	0.4644	0.4580	0.4518	0.4458	0.4399
0.4	0.4342	0.4287	0.4233	0.4180	0.4129	0.4080	0.4031	0.3984	0.3938	0.3894
0.6	0.3850	0.3808	0.3767	0.3727	0.3687	0.3649	0.3612	0.3576	0.3540	0.3506
0.8	0.3472	0.3440	0.3408	0.3376	0.3346	0.3316	0.3287	0.3259	0.3231	0.3204
1.0	0.3178	0.3152	0.3126	0.3102	0.3077	0.3054	0.3031	0.3008	0.2986	0.2964
1.2	0.2943	0.2922	0.2902	0.2882	0.2862	0.2843	0.2824	0.2806	0.2787	0.2770
1.4	0.2752	0.2735	0.2718	0.2702	0.2686	0.2670	0.2654	0.2638	0.2623	0.2608
1.6	0.2594	0.2579	0.2565	0.2551	0.2537	0.2524	0.2510	0.2497	0.2484	0.2472
1.8	0.2459	0.2447	0.2434	0.2422	0.2410	0.2399	0.2387	0.2375	0.2364	0.2353
2.0	0.2342	0.2331	0.2320	0.2309	0.2299	0.2289	0.2278	0.2268	0.2258	0.2248
2.2	0.2238	0.2228	0.2219	0.2209	0.2200	0.2190	0.2181	0.2172	0.2163	0.2153
2.4	0.2144	0.2136	0.2127	0.2118	0.2109	0.2101	0.2092	0.2084	0.2075	0.2067
2.6	0.2059	0.2051	0.2043	0.2035	0.2027	0.2019	0.2011	0.2003	0.1995	0.1987
2.8	0.1980	0.1972	0.1965	0.1957	0.1950	0.1942	0.1935	0.1928	0.1920	0.1913
3.0	0.1906	0.1899	0.1892	0.1885	0.1878	0.1871	0.1864	0.1857	0.1850	0.1843
3.2	0.1836	0.1830	0.1823	0.1816	0.1810	0.1803	0.1797	0.1790	0.1784	0.1777
3.4	0.1771	0.1765	0.1758	0.1752	0.1746	0.1740	0.1733	0.1727	0.1721	0.1715
3.6	0.1709	0.1703	0.1697	0.1691	0.1685	0.1679	0.1673	0.1667	0.1662	0.1656
3.8	0.1650	0.1644	0.1639	0.1633	0.1627	0.1622	0.1616	0.1611	0.1605	0.1600

Appendix F

DPSCC: First Order Following Reaction

 $k\tau$ as a Function of $|Q_b/Q_f|$: Interpolated from Appendix E

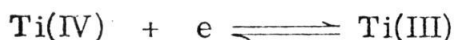
$ Q_b/Q_f $	0.000	0.001	0.002	0.003	0.004	0.005	0.006	0.007	0.008	0.009
0.16	3.9789	3.9426	3.9066	3.8709	3.8356	3.8005	3.7658	3.7314	3.6973	3.6635
0.17	3.6299	3.5967	3.5638	3.5311	3.4987	3.4666	3.4347	3.4032	3.3719	3.3408
0.18	3.3101	3.2796	3.2493	3.2193	3.1896	3.1601	3.1309	3.1019	3.0732	3.0447
0.19	3.0165	2.9887	2.9608	2.9332	2.9060	2.8790	2.8522	2.8256	2.7993	2.7733
0.20	2.7474	2.7218	2.6965	2.6713	2.6464	2.6218	2.5973	2.5731	2.5492	2.5254
0.21	2.5019	2.4786	2.4555	2.4327	2.4101	2.3877	2.3655	2.3436	2.3218	2.3003
0.22	2.2790	2.2580	2.2371	2.2165	2.1961	2.1759	2.1559	2.1361	2.1165	2.0971
0.23	2.0780	2.0590	2.0403	2.0217	2.0034	1.9852	1.9673	1.9496	1.9320	1.9146
0.24	1.8975	1.8805	1.8637	1.8471	1.8307	1.8144	1.7984	1.7825	1.7668	1.7512
0.25	1.7359	1.7207	1.7057	1.6908	1.6762	1.6616	1.6473	1.6331	1.6190	1.6052
0.26	1.5914	1.5778	1.5644	1.5511	1.5380	1.5250	1.5122	1.4994	1.4869	1.4744
0.27	1.4621	1.4500	1.4379	1.4260	1.4142	1.4026	1.3911	1.3796	1.3684	1.3572
0.28	1.3461	1.3352	1.3244	1.3137	1.3031	1.2926	1.2822	1.2719	1.2617	1.2517
0.29	1.2417	1.2318	1.2220	1.2124	1.2028	1.1933	1.1839	1.1746	1.1654	1.1562
0.30	1.1472	1.1383	1.1294	1.1206	1.1119	1.1033	1.0947	1.0863	1.0779	1.0696
0.31	1.0614	1.0532	1.0451	1.0371	1.0292	1.0213	1.0135	1.0058	0.9981	0.9905
0.32	0.9830	0.9755	0.9681	0.9608	0.9535	0.9463	0.9391	0.9320	0.9250	0.9180
0.33	0.9111	0.9042	0.8974	0.8907	0.8840	0.8773	0.8707	0.8642	0.8577	0.8512
0.34	0.8449	0.8385	0.8322	0.8260	0.8198	0.8136	0.8075	0.8015	0.7955	0.7895
0.35	0.7836	0.7777	0.7718	0.7660	0.7603	0.7546	0.7489	0.7433	0.7377	0.7321
0.36	0.7266	0.7211	0.7157	0.7103	0.7049	0.6996	0.6943	0.6890	0.6838	0.6786
0.37	0.6735	0.6684	0.6633	0.6582	0.6532	0.6482	0.6433	0.6384	0.6335	0.6286
0.38	0.6238	0.6190	0.6142	0.6095	0.6048	0.6001	0.5954	0.5908	0.5862	0.5817
0.39	0.5771	0.5726	0.5681	0.5637	0.5592	0.5548	0.5505	0.5461	0.5418	0.5375
0.40	0.5332	0.5289	0.5247	0.5205	0.5163	0.5122	0.5080	0.5039	0.4998	0.4957
0.41	0.4917	0.4877	0.4837	0.4797	0.4757	0.4718	0.4679	0.4640	0.4601	0.4563
0.42	0.4524	0.4486	0.4448	0.4410	0.4373	0.4336	0.4298	0.4261	0.4225	0.4188
0.43	0.4152	0.4115	0.4079	0.4043	0.4008	0.3972	0.3937	0.3902	0.3867	0.3832
0.44	0.3797	0.3763	0.3728	0.3694	0.3660	0.3626	0.3593	0.3559	0.3526	0.3492
0.45	0.3459	0.3427	0.3394	0.3361	0.3329	0.3296	0.3264	0.3232	0.3200	0.3169
0.46	0.3137	0.3106	0.3074	0.3043	0.3012	0.2981	0.2950	0.2920	0.2889	0.2859
0.47	0.2829	0.2799	0.2769	0.2739	0.2709	0.2679	0.2650	0.2620	0.2591	0.2562
0.48	0.2533	0.2504	0.2476	0.2447	0.2418	0.2390	0.2362	0.2334	0.2305	0.2277
0.49	0.2250	0.2222	0.2194	0.2167	0.2139	0.2112	0.2085	0.2058	0.2031	0.2004
0.50	0.1977	0.1951	0.1924	0.1898	0.1871	0.1845	0.1819	0.1793	0.1767	0.1741
0.51	0.1715	0.1689	0.1664	0.1638	0.1613	0.1588	0.1563	0.1537	0.1512	0.1487
0.52	0.1463	0.1438	0.1413	0.1389	0.1364	0.1340	0.1315	0.1291	0.1267	0.1243
0.53	0.1219	0.1195	0.1171	0.1148	0.1124	0.1100	0.1077	0.1054	0.1030	0.1007
0.54	0.0984	0.0961	0.0938	0.0915	0.0892	0.0869	0.0847	0.0824	0.0801	0.0779
0.55	0.0756	0.0734	0.0712	0.0690	0.0668	0.0646	0.0624	0.0602	0.0580	0.0558

CHAPTER 4.

Catalytic Reactions: The Ti(III)-Hydroxylamine Reaction*Introduction

The oxidation of Ti(III) by hydroxylamine in the presence of oxalic acid was originally and most thoroughly studied by Blažek and Koryta polarographically (31). These authors obtained a rate constant at 25°C of 42.1 ± 1.5 liters/mole-second and an activation energy of 7.9 kcal/mole. This value of the rate constant was subsequently confirmed polarographically by Delahay, Mattax, and Berzins (32).

Blažek and Koryta (31) also determined the rate constant by mixing hydroxylamine and Ti(III) solutions and following the rate of disappearance of Ti(III) polarographically. The rate constant obtained under these conditions was 42.0 ± 0.2 liters/mole-second. Blažek and Koryta concluded that their results were consistent with the previously proposed mechanism of Davis, Evans, and Higginson (33):

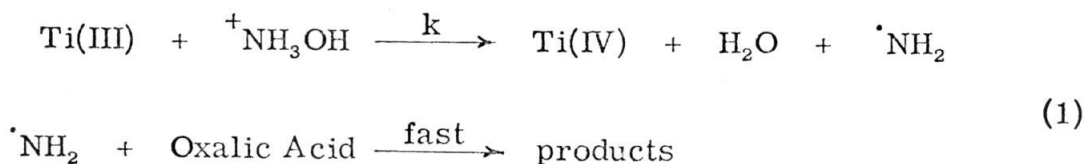


* This work was performed in collaboration with Joseph H. Christie. A summary will appear in J. Electroanal. Chem., 1966.

(31) A. Blažek and J. Koryta, Collection Czech. Chem. Commun., 18, 326 (1953).

(32) P. Delahay, C. C. Mattax, and T. Berzins, J. Am. Chem. Soc., 76 5319 (1954).

(33) P. Davis, M. G. Evans, and G.C.E. Higginson, J. Chem. Soc., 2563 (1951).



The oxalic acid serves as a radical scavenger (33).

Fischer, Dracka, and Fischerova (34) have studied this system by chronopotentiometry at low concentrations of hydroxylamine (5-10 mF) under conditions where the catalytic reaction is relatively slow and of second order. Under these conditions they obtain a rate constant of 45.9 ± 0.4 liters/mole-second.

Saveant and Vianello (35) have employed linear sweep chronoamperometry for the study of this reaction. They obtained a rate constant of $42. \pm 1.7$ liters/mole-second.

In the case of a controlled potential experiment such as polarography, the presence of a catalytic reaction simply means that a larger current is flowing at any given time and the precision with which this larger current can be measured is not affected. But in the case of a controlled current experiment such as chronopotentiometry, the presence of a catalytic reaction greatly decreases the rate of potential change of the indicator electrode, especially in the vicinity of the transition time, and thus renders the determination of the transition time substantially more difficult. For this reason we expect chrono-

(34) O. Fischer, O. Dracka, and E. Fischerova, Collections Czech. Chem. Commun., 26, 1505 (1961).

(35) J. M. Saveant and E. Vianello, Electrochim. Acta, 10, 905 (1965).

potentiometry to be a substantially poorer tool than a controlled potential technique for the study of fast catalytic reactions.

This is borne out by the investigation of Delahay, Mattax, and Berzins (32). These authors found a quite low value of 24 liters/mole-second for the rate constant (recalculated from their value at 30°C using an activation energy of 7.9 kcal/mole) in a chronopotentiometric study of the Ti(III)-hydroxylamine reaction. They concluded that they had obtained an incorrect value of the rate constant because of the poor definition of the chronopotentiometric transition times.

Christie and Lauer (36) were able to circumvent some difficulties by the use of reverse current chronopotentiometry. Under these conditions, the forward time is a quite well defined quantity. Since the shape of the Ti(III) oxidation wave is essentially unaffected by the catalytic reaction, a normal potential inflection is obtained at the transition time for the reverse wave. Christie and Lauer obtained a value of $32. \pm 2$. liters/mole-second for the rate constant (recalculated from their value at 27°C (37) using an activation energy of 7.9 kcal/mole).

Herman and Bard (38) considered the application of cyclic chronopotentiometry to the study of Ti(III)-hydroxylamine reaction. Their experimental results were inconsistent with a single rate con-

(36) J. H. Christie and G. Lauer, Anal. Chem., 36, 2037 (1964).

(37) G. Lauer, private communication.

(38) H. B. Herman and A. J. Bard, Anal. Chem., 36, 510 (1964).

stant and they suggested that the system is more complicated than previously assumed. This conclusion may not be completely justified (36).

Christie (29) has recently investigated the application of double potential step chronocoulometry to the study of electrode reactions. In this chapter we undertake the application of the double step chronocoulometric technique to the study of the Ti(III)-hydroxylamine reaction.

Results and Discussion

Our solutions are initially free of Ti(III) and the concentration of hydroxylamine is sufficiently large (100-200 mF) that the rate of reaction is well described by a pseudo first-order rate constant, $k(^+\text{NH}_3\text{OH})$. E_0 , the initial potential of the indicator electrode, is such that no current flows through the cell. The potential is stepped to E_1 which is sufficiently cathodic that the reduction of Ti(IV) is diffusion limited. After a time τ , the potential of the electrode is stepped to E_2 which is sufficiently anodic that the oxidation of Ti(III) is diffusion limited.

Ignoring the effects of double layer charging, the faradaic currents and the total faradaic charge are (29)

$$I(t \leq \tau) = nFA\sqrt{D} * C_0\beta \left[\text{erf} \sqrt{\beta^2 t} + \frac{1}{\beta\sqrt{\pi t}} e^{-\beta^2 t} \right]$$

$$I(t > \tau) = nFA\sqrt{D} * C_0\beta \left[\text{erf} \sqrt{\beta^2 t} + \frac{1}{\beta\sqrt{\pi t}} e^{-\beta^2 t} - \text{erf} \sqrt{\beta^2 (t-\tau)} - \frac{1}{\beta\sqrt{\pi(t-\tau)}} e^{-\beta^2 (t-\tau)} \right].$$

$$Q(t \leq \tau) = \frac{nFA\sqrt{D}^* C_0}{\beta} \left[(\beta^2 t + \frac{1}{2}) \operatorname{erf} \sqrt{\beta^2 t} + \beta \sqrt{\frac{t}{\pi}} e^{-\beta^2 t} \right]$$

$$Q(t > \tau) = \frac{nFA\sqrt{D}^* C_0}{\beta} \left[(\beta^2 t + \frac{1}{2}) \operatorname{erf} \sqrt{\beta^2 t} + \beta \sqrt{\frac{t}{\pi}} e^{-\beta^2 t} \right. \\ \left. - \{ \beta^2 (t-\tau) + \frac{1}{2} \} \operatorname{erf} \sqrt{\beta^2 (t-\tau)} - \beta \sqrt{\frac{t-\tau}{\pi}} e^{-\beta^2 (t-\tau)} \right]$$

where $\beta^2 = k(^+ \text{NH}_3\text{OH})$, $D_{\text{Ti(IV)}}$ is assumed equal to $D_{\text{Ti(III)}} \equiv D$, and $^* C_0$ is the bulk concentration of Ti(IV). Figure 8 reproduces experimental I-t and Q-t traces for extreme values of $\beta\tau^{\frac{1}{2}}$.

Forming the ratio of the charge due to the oxidation of Ti(III) to the charge due to the reduction of Ti(IV), we obtain

$$\left| \frac{Q_b}{Q_f} \right| = \left| \frac{Q(2\tau) - Q(\tau)}{Q(\tau)} \right| = 2 - \frac{(2\beta^2\tau + \frac{1}{2}) \operatorname{erf} \sqrt{2\beta^2\tau} + \sqrt{\frac{2\beta^2\tau}{\pi}} e^{-2\beta^2\tau}}{(\beta^2\tau + \frac{1}{2}) \operatorname{erf} \sqrt{\beta^2\tau} + \sqrt{\frac{\beta^2\tau}{\pi}} e^{-\beta^2\tau}} \quad (2)$$

Note that this ratio is independent of the numerical value of D, of the electrode area, and of the bulk concentration of Ti(IV).

The curve illustrated in Fig. 7 is a plot of $|Q_b/Q_f|$, calculated from Eqn. (2), versus $\beta^2\tau$. In the limiting case of no catalytic reaction ($k \rightarrow 0$), the simple diffusion limited value of 0.586 is obtained (29). As the catalytic reaction becomes very fast ($k \rightarrow \infty$), no charge is recovered on the reverse step and the ratio goes to zero. A table of $\beta^2\tau$ as a function of $|Q_b/Q_f|$, Chapter 3, Appendix C, was used for the

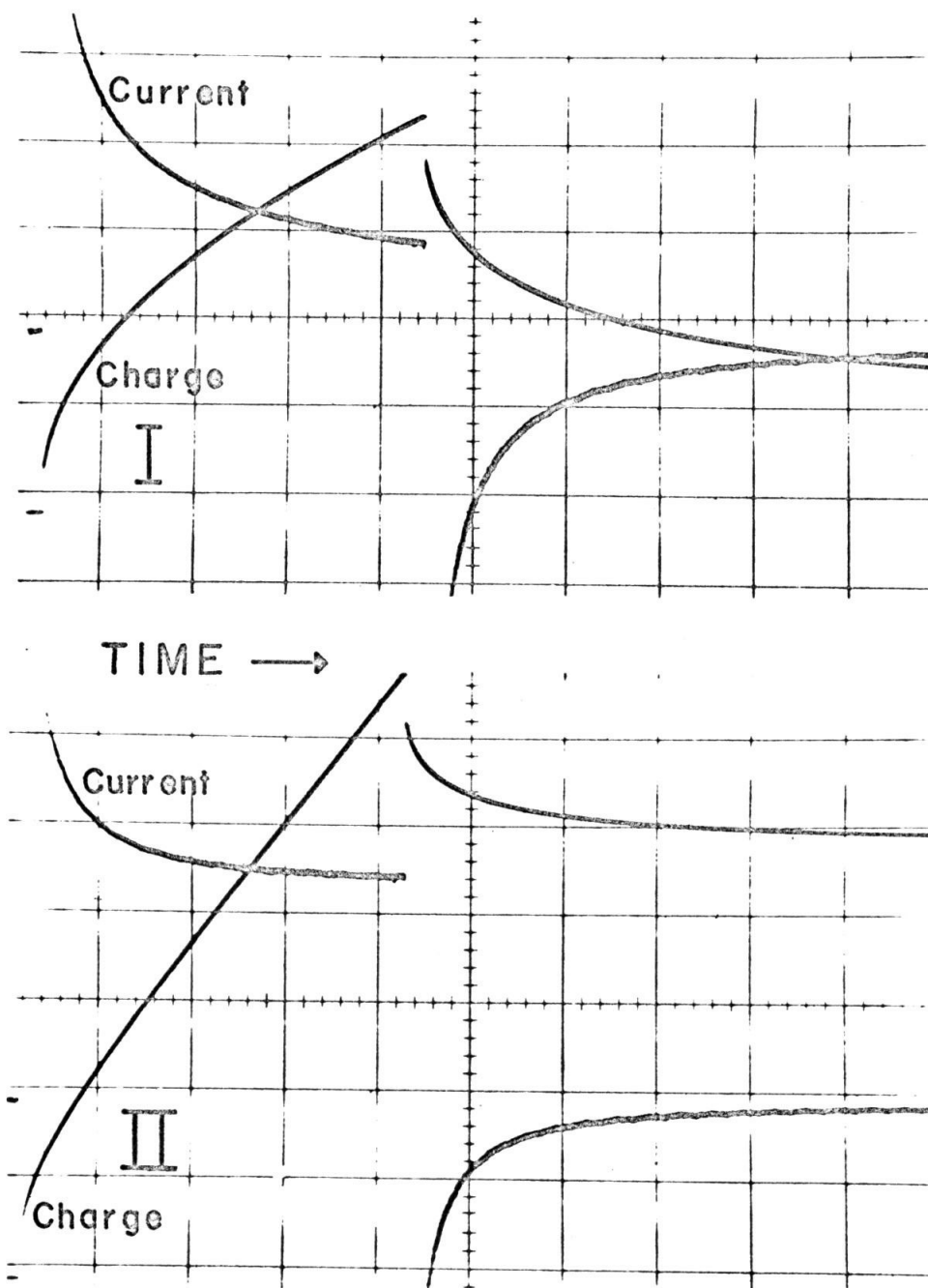


Figure 8. Experimental I-t and Q-t traces for extreme values of $\beta\tau^2$. I. $\beta\tau^2 = 0$ (no hydroxylamine); II. $\beta\tau^2 \sim 1.3$. The current, charge, and time scales are identical in I. and II.

evaluation of β^2 from the experimental data.

A striking advantage of any integral technique lies in the simplicity with which a correction for double layer charging can be effected. In the present case we write

$$\left| \frac{^*Q_b}{^*Q_f} \right| = \frac{|Q_\tau - Q_{2\tau}| - |q_b|}{|Q_\tau| - |q_f|} \quad (3)$$

where Q_τ and $Q_{2\tau}$ are the experimentally observed values of Q at $t = \tau$ and 2τ respectively and q_f and q_b represent the charge required to charge the double layer for the forward (cathodic) and backward (anodic) steps respectively. The asterisks signify that the measured quantities have been corrected for double layer charging. In the present investigation, q_f and q_b were determined by repeating the experiment in solutions identical to the ones being investigated but which contained no titanium.

The results of double potential step chronocoulometric experiments in the absence of hydroxylamine are given in Table I; each entry is the average of four determinations. The values of q_f and q_b , determined for the same step intervals, are 0.50 and 0.60 μ coulombs respectively. The average value of $|^*Q_b/^*Q_f|$ is 0.576 and is some 1.7 per cent smaller than the theoretical value of 0.586. The reason for this small discrepancy is unknown. This discrepancy is not due to a significant error in the correction for double layer charging since an error in q_b or q_f would introduce a trend with τ .

TABLE I

2.0mF Ti(IV), 0.20 F Oxalic Acid, pH = 1.1

$E_0 = -100$ mv, $E_1 = -600$ mv, $E_2 = 000$ mv

25.0°C

τ , ms	$*Q_T$, μ coulombs	$*Q_b/*Q_f$
440.	16.8	0.57
215.	11.7	.58
90.	7.81	.57
42.	5.56	.58
21.	4.03	.58
		<hr/> 0.576 \pm 0.002

Similar experiments in which E_1 was varied from -600 to -800 mv and E_2 was varied from -100 to +200 mv were performed and results similar to those of Table I were obtained. We conclude that the reduction of Ti(IV) and the oxidation of Ti(III) are diffusion limited at -600 and 000 mv vs. S.C.E. respectively; all subsequent experiments employed these step potentials.

The data obtained in the presence of 0.1 and 0.2 \underline{F} hydroxylamine are presented in Tables II and III. Each entry is the average of at least four experiments. The confidence intervals listed correspond to the standard deviation of the mean. Values of q_f and q_b were determined for the same step interval for the various solutions and only small variations were observed among them. Therefore, q_f and q_b were taken to be 0.50 and 0.60 μ coulombs in all solutions. Variation of q_f and q_b with temperature was not investigated.

For any given temperature and hydroxylamine concentration, β^2 should be independent of τ . In certain experiments performed with unrecrystallized oxalic acid (which appeared to contain a trace of reducible impurity), β^2 was observed to increase dramatically with decreasing values of τ at any given temperature and concentration of hydroxylamine. The constancy of β^2 over a wide range of values of τ appears to be a sensitive and useful diagnostic test for impurities and other irregularities in the system and for the correctness of q_b and q_f .

In performing the experiments, it was necessary to decide over what range to vary $\beta^2\tau$. We have rejected all values of β^2 corresponding

TABLE II

2.0 mF Ti(IV), 0.20 F Oxalic Acid, pH = 1.0

0.204 F Hydroxylamine

 $E_0 = -100$ mv, $E_1 = -600$ mv, $E_2 = 000$ mv

τ , ms	Q_T , μ coulombs	$^*Q_b/^*Q_f$	$\beta^2\tau$	β^2 , sec $^{-1}$
15.0°				
412.	16.5	0.262	1.30	3.17 \pm 0.021
210.	10.4	.362	0.69	3.3 \pm 0.19
93.	6.4	.461	.32	3.44 \pm 0.071
			AVERAGE	3.32 \pm 0.033
25.0°				
402.†	25.8	0.134	3.17	7.90 \pm 0.15
207.	15.1	.213	1.78	8.6 \pm 0.14
79.	7.6	.371	0.65	8.24 \pm 0.065
41.†	5.2	.457	.33	8.1 \pm 0.12
20.†	3.6	.516	.17	8.4 \pm 0.13
			AVERAGE	8.35 \pm 0.092
210.	16.7	0.220	1.70	8.14 \pm 0.081
84.	8.9	.357	0.72	8.6 \pm 0.19
44.	5.9	.447	.36	8.4 \pm 0.11
			AVERAGE	8.37 \pm 0.086
35.0°				
92.	11.8	0.195	2.01	22.0 \pm 0.32
43.	6.8	.313	0.95	22.4 \pm 0.31
20.	4.0	.429	.42	21.8 \pm 0.71
			AVERAGE	22.0 \pm 0.26

† Neglected in the average. See text.

TABLE III

2.0 mF Ti(IV), 0.20 F Oxalic Acid, pH = 1.1

0.102 F Hydroxylamine				
E ₀ = -100 mv, E ₁ = -600 mv, E ₂ = 000 mv				
τ , ms	Q_T , $\mu\text{coulombs}$	$^*Q_D/^*Q_f$	$\beta^2\tau$	β^2 , sec^{-1}
25.0°				
414.	22.4	0.203	1.90	4.60 ± 0.019
220.	13.6	.300	1.03	4.71 ± 0.079
90.	7.8	.430	0.42	4.67 ± 0.049
43.†	5.1	.500	.21	4.8 ± 0.13
22.†	3.7	.547	.088	4.2 ± 0.35
			AVERAGE	4.70 ± 0.040
35.0°				
86.	10.1	0.293	1.08	12.5 ± 0.28
42.	6.3	.404	.52	12.2 ± 0.28
21.	4.4	.489	.24	11.2 ± 0.24
			AVERAGE	12.0 ± 0.23
45.0°				
37.	7.6	0.30	1.04	28. ± 1.6
19.	4.7	.41	.50	27. ± 2.0
8.6	3.2	.49	.25	29. ± 1.1
			AVERAGE	27.9 ± 0.92

† Neglected in the average. See text.

to values of the ratio $|\frac{*Q_b}{*Q_f}|$ less than 0.2 or greater than 0.5. Where available, such values have been included in Tables II and III and it is evident that including them in the averages would not have altered the rate constant substantially.

The slope of the working curve (Fig. 7) has a value of about 6 in the vicinity of $\beta^2 \tau = 1$. Therefore, an error of about 1 per cent in the ratio of $|\frac{*Q_b}{*Q_f}|$ in this region results in an error of about 6 per cent in the rate constant. The precision for the determination of Q_T and Q_{2T} is not better than 1 per cent and so we are somewhat surprised, and gratified, by the low standard deviations associated with the experimental determination of β^2 .

The activation energy was determined from the plot in Fig. 9. Since the standard deviations associated with the various values of the rate constant vary by only a factor of three, all of the data pairs were weighted equally in the calculation of the least squares slope and intercept. The results are

$$\begin{aligned} k_{298} &= 43.4 \pm 1.1 \text{ liters/mole-second} \\ E_a &= 17.2 \pm 1.1 \text{ kcal/mole} \end{aligned}$$

where the confidence intervals now correspond to the 95 per cent confidence level. This value of k_{298} confirms the polarographic value of Blažek and Koryta (31) and the chronopotentiometric value of Fischer, et al. (34).

The activation energy determined in this study is larger by a factor of two than the value of 7.9 kcal/mole found by Blažek and

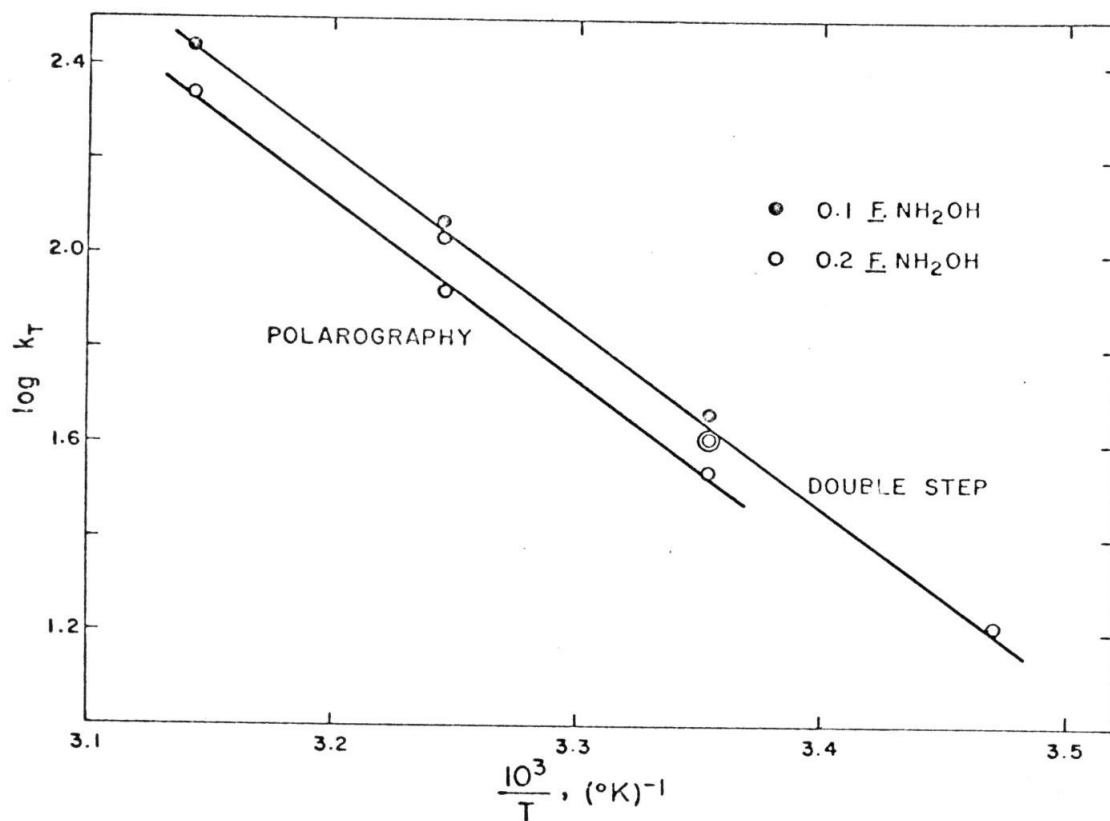


Figure 9. Plot of $\log k_T$ versus T^{-1} for the evaluation of k_{298} and of the Arrhenius activation energy.

Koryta (31). We were unable to resolve this large disagreement by repeating their calculations and therefore we have redetermined the activation energy polarographically. The polarographically and double potential step chronocoulometrically determined rate constants are plotted in Fig. 9. The slope of the polarographic line corresponds to an activation energy of 17.3 kcal/mole and is in excellent agreement with the value determined by the double potential step technique.

Conclusion

Double potential step chronocoulometry compares very favorably with polarography for determining the kinetic parameters of catalytic reactions. This technique can probably be used to measure values of β^2 of at least 100-200 seconds⁻¹, well into the polarographic range. $\beta^2\tau$ can be varied over a far wider range than is possible with polarography and this flexibility makes possible the useful diagnostic test for systematic irregularities described above. Although the experiments were easily performed, obtaining the data from Polaroid prints is somewhat tedious. But it is evident that the experiments could be modified in any of a variety of ways so as to obtain Q_T and Q_{2T} directly in digital form and thereby increase the ease and simplicity of the experiment (39).

(39) G. Lauer and R. A. Osteryoung, Anal. Chem., in press, 1966.

Experimental

Potassium Oxo(bisoxalato)titanate(IV). -- Fisher technical grade $K_2TiO(C_2O_4)_2 \cdot 2H_2O$ was twice recrystallized from water and then dried to constant weight at 60 per cent relative humidity. Solutions were prepared by weight and were allowed to equilibrate 24 hours before use. Solutions investigated prior to such equilibration appeared to contain two reducible species.

Oxalic Acid. -- Mallinckrodt "AR" $H_2C_2O_4 \cdot 2H_2O$ contained small amounts of some oxidizing impurity which was removed by a single recrystallization. The salt was dried for 2 hours at $80^\circ C$ and weighed as the dihydrate.

Hydroxylamine. -- Matheson, Coleman, and Bell $(NH_2OH) \cdot H_2SO_4$, > 99% purity, was recrystallized from an 80% ethanol-water solution and dried 1 hour at $105^\circ C$. Stock solutions were standardized by titration with permanganate according to the method of Bray, et al. (40) and the titer of these solutions changed less than 0.1% during the course of these experiments.

Mercury. -- Mallinckrodt "AR" mercury was employed in the experiments with the hanging mercury drop. The DME experiments employed triply distilled mercury from Bethlehem Apparatus Co., Hellertown, Pa.; total nonvolatile impurities were reported to

(40) W. C. Bray, M. E. Simpson, and A. A. Mackenzie, J. Am. Chem. Soc., 41, 1363 (1919).

be less than 0.25 ppm.

All solutions were prepared from triply distilled water and deaerated with Matheson "prepurified" nitrogen (< 8 ppm oxygen) which was further deoxygenated by passage through a vanadous washing tower prior to entry into the cell.

The electronic circuitry is shown schematically in Fig. 10 and is analagous to that of Christie, Lauer, and Osteryoung (41). Relay 2 controls the reverse step and is fired by a variable delay timing circuit (42). The measured rise time of the potentiostat is less than 20 μ sec. The Q-t and I-t curves were displayed simultaneously on the screen of a Tektronix Type 564 "storage" oscilloscope equipped with Type 3A72 and 3B3 plug-in units. Satisfactory displays were recorded on Polaroid film. The area of the Kemula-type hanging mercury drop was 0.0407 cm^2 at 25°C .

The polarographic setup employed the equipment shown in Fig. 4 and a three electrode cell; the output of the current measuring amplifier was fed to a Sargent SR recorder and the maximum polarographic currents were recorded at -500 , -600 , and $-700 \text{ mv vs. S.C.E.}$ Under our conditions, the catalytic I-t curve was observed to be a $2/3$ order parabola and the catalytic current was observed to be independent of the mercury head. The rate constant was calculated

(41) J. H. Christie, G. Lauer, and R. A. Osteryoung, J. Electroanal. Chem., 7, 60 (1964).

(42) G. Lauer, H. Schlein, and R. A. Osteryoung, Anal. Chem., 35, 1789 (1963).

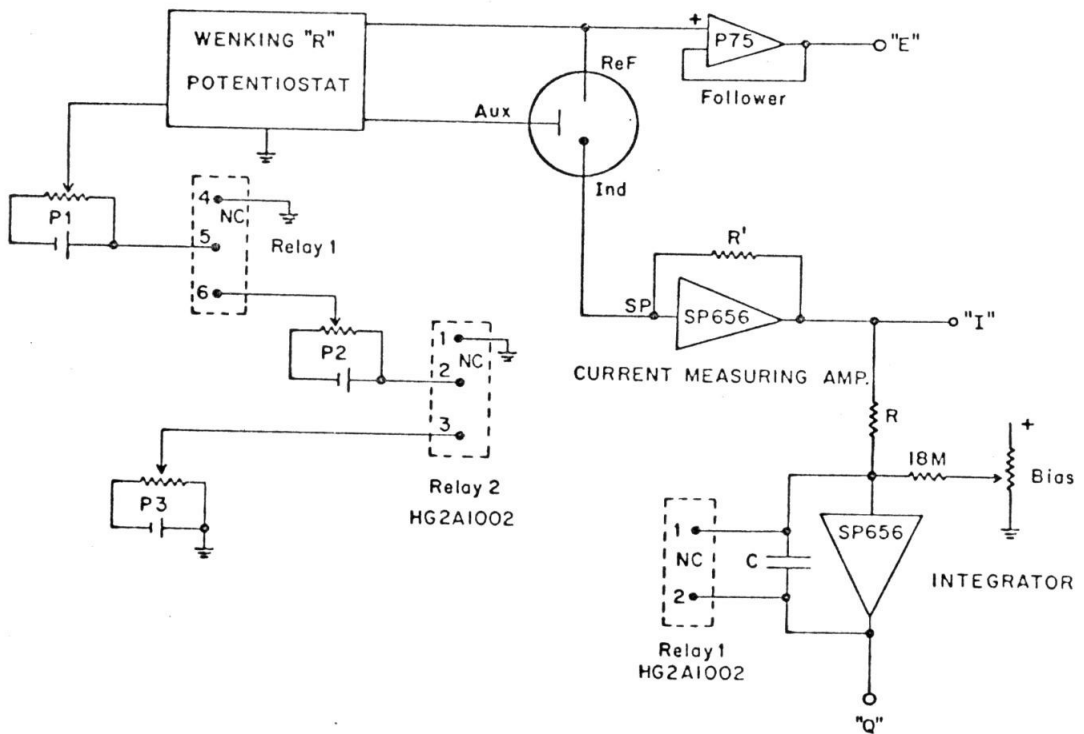


Figure 10. Block diagram of the electronic apparatus employing G. A. Philbrick Researches, Inc. solid state operational amplifiers and C. P. Clare and Co. mercury-wetted relays.

according to Koutecky (43).

$$\frac{i_{\text{cat}}}{i_{\text{d}}} = \sqrt{\frac{3}{7}} \pi \beta \tau^{\frac{1}{2}} \quad (4)$$

The cell was thermostated at the stated temperatures with a precision of about $\pm 0.2^{\circ}\text{C}$.

Acknowledgment

It is a pleasure to thank George Lauer for his collaboration on certain preliminary experiments.

(43) J. Koutecky, Collection Czech. Chem. Commun., 18, 311 (1953).

CHAPTER 5.

Improved Method for the Determination of the
Kinetic Parameters of Electrode Reactions*Introduction

The study of electrode kinetics by the potential-step method of Gerischer and Vielstich involves the measurement of the current as a function of time following the application of a potential step. For sufficiently short times, the kinetic parameters may be determined from the slope and the intercept of a linear $I - t^{\frac{1}{2}}$ plot (44,45). A recent paper describes the study of electrode kinetics by the measurement of the total charge passed following application of a potential step. For sufficiently long times, the kinetic parameters may be determined from the slope and the intercept of a linear $Q - t^{\frac{1}{2}}$ plot (46). It is obvious that the long or the short time criteria place severe restrictions on the magnitudes of the rate constants which may be studied. The present work reports a method which allows the determination of the kinetic

* The work of this and the following chapter was performed in collaboration with Joseph H. Christie. A summary has appeared in J. Electroanal. Chem., 10, 284 (1965).

(44) H. Gerischer and W. Vielstich, Z. physik. Chem. (Frankfurt), 3, 16 (1955); W. Vielstich and H. Gerischer, Z. physik. Chem., 4, 10 (1955).

(45) Y. Okinaka, S. Toshima, and H. Okiniwa, Talanta, 11, 203 (1964).

(46) J. H. Christie, G. Lauer, and R. A. Osteryoung, J. Electroanal. Chem., 7, 60 (1964).

parameters of the system by simultaneous measurement of both I and Q and which is valid for all values of the rate constant.

Theoretical

The equations for the current-time behavior of an electrochemical system following the application of a potential step are (44)

$$I = K \exp(y^2) \operatorname{erfc}(y) \quad (1)$$

$$y = \lambda t^{\frac{1}{2}} \quad (2)$$

$$K = nFAk_a^0 C_o \exp \left[- \frac{\alpha nF}{RT} (E - E^0) \right] \quad (3)$$

$$\lambda = k_a^0 \left\{ \frac{\exp \left[- \frac{\alpha nF}{RT} (E - E^0) \right]}{D_o^{\frac{1}{2}}} + \frac{\exp \left[\frac{(1 - \alpha)nF}{RT} (E - E^0) \right]}{D_R^{\frac{1}{2}}} \right\} \quad (4)$$

It is assumed that only the oxidized form of the electroactive species is initially present in the solution. k_a^0 is the apparent standard heterogeneous rate constant; the other symbols have their usual significance.

For small values of y ($y \lesssim 0.1$), $\exp(y^2) \operatorname{erfc}(y)$ may be replaced by $(1 - \frac{2}{\sqrt{\pi}} y)$ and Eqn. (1) becomes

$$I = K - \frac{2}{\sqrt{\pi}} K \lambda t^{\frac{1}{2}}; \quad \lambda t^{\frac{1}{2}} < 0.1 \quad (5)$$

Extrapolation of the $I - t^{\frac{1}{2}}$ plot to $t = 0$ gives K as the intercept (44, 45).

λ can be determined from the ratio of the slope to the intercept.

The charge-time behavior is obtained by integrating Eqn. (1)

$$Q = \int_0^t I dt = \frac{K}{\lambda^2} \left[\exp(y^2) \operatorname{erfc}(y) + \frac{2}{\sqrt{\pi}} y - 1 \right] \quad (6)$$

Since $\operatorname{erfc}(y)$ approaches $\exp(-y^2)/y\sqrt{\pi}$ for large values of y ($y \geq 5$), the first term in Eqn. (6) becomes negligible with respect to the others and Q approaches the asymptote

$$Q|_{\text{asym}} = \frac{2K}{\lambda\sqrt{\pi}} t^{\frac{1}{2}} - \frac{K}{\lambda^2}; \quad \lambda t^{\frac{1}{2}} > 5 \quad (7)$$

If the potential is sufficiently cathodic that the second term in Eqn. (4) becomes negligible

$$\frac{K}{\lambda} = nFAD_0^{\frac{1}{2}}C_0 \quad (\text{independent of } E) \quad (8)$$

The $Q - t^{\frac{1}{2}}$ plot therefore attains the same limiting slope as that predicted by the integral of the Cottrell equation for a planar electrode, viz.,

$$Q = \int_0^t \frac{nFAD_0^{\frac{1}{2}}C_0}{\sqrt{\pi t}} dt = \frac{2}{\sqrt{\pi}} nFAD_0^{\frac{1}{2}}C_0 t^{\frac{1}{2}} \quad (9)$$

It should be noted that even though the Cottrell slope is attained for sufficiently long times, i.e., all electrochemical systems approach diffusion control for $\lambda t^{\frac{1}{2}} > 5$, the intercept on the Q axis is not zero and is given by

$$a = - \frac{nFAD_0C_0}{k_a^0} \exp \left[\frac{\alpha nF}{RT} (E - E^0) \right] \quad (10)$$

In the method previously reported (46), the parameters K and λ were obtained from the slope and the intercept of the linear portion of the $Q - t^{\frac{1}{2}}$ plot. No criterion, other than apparent linearity, was used to determine if the asymptotic region had been attained. It may be seen from Fig. 11 that apparent linearity is observed even for $\lambda t^{\frac{1}{2}} \sim 2$. It is therefore obvious that serious errors can be made if apparent linearity and $\lambda t^{\frac{1}{2}} > 5$ are assumed to coincide. An analogous criticism can be made of the Gerischer-Vielstich method.

It is preferable to determine the kinetic parameters from a function which is linear in $\lambda t^{\frac{1}{2}}$ for all values of $\lambda t^{\frac{1}{2}}$. Since

$$\frac{4}{\pi} (\tau^{\frac{1}{2}})^2 = \frac{1}{\lambda^2} \quad (11)$$

where $\tau^{\frac{1}{2}}$ is the intercept of the Q asymptote on the $t^{\frac{1}{2}}$ axis

$$\frac{4}{\pi} (\tau^{\frac{1}{2}})^2 I = \frac{K}{\lambda^2} \exp(y^2) \operatorname{erfc}(y) \quad (12)$$

Hence, the function

$$A^* = Q - \frac{4}{\pi} (\tau^{\frac{1}{2}})^2 I = \frac{K}{\lambda^2} \left[\frac{2}{\sqrt{\pi}} \lambda t^{\frac{1}{2}} - 1 \right] = b t^{\frac{1}{2}} + a \quad (13)$$

has the desired property. Since A^* is identical with the Q asymptote, K and λ may be determined from the slope and the intercept of the $A^* - t^{\frac{1}{2}}$ plot in a manner identical to that previously described. The method for the estimation of a and b is discussed below.

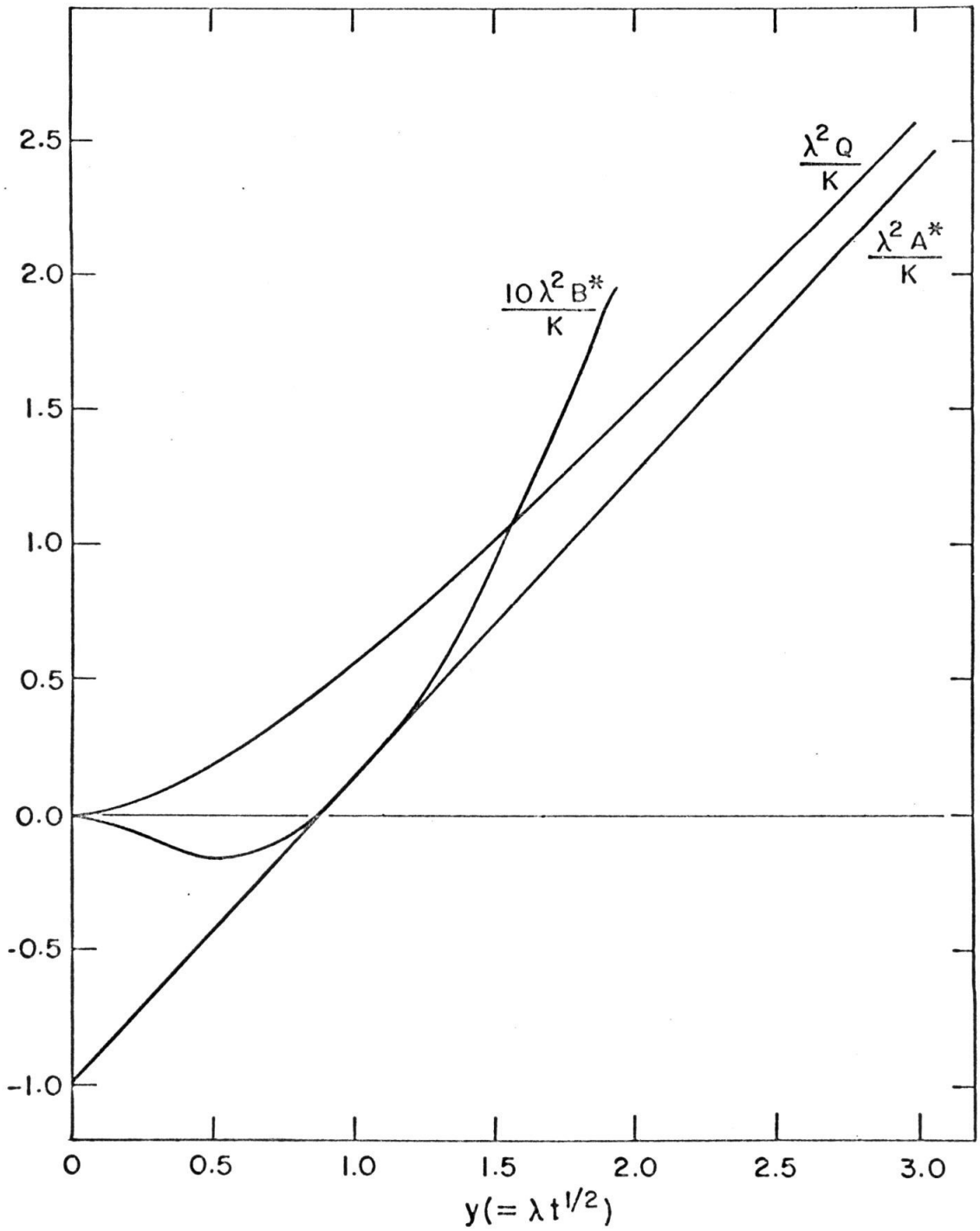


Figure 11. Q , A^* , and B^* , calculated from Eqns. (6), (13), and (23) plotted vs. $\lambda t^{1/2}$.

The potential dependence of K and λ has been discussed previously (46). The kinetic parameters α and k_a^0 may be determined from the plot of $\log K$ vs. E : α from the slope and k_a^0 from the value of K at $E = E^0$.

The Least Squares Estimation of a and b

We observe that our data are subject to N equations of condition (47, 48, 49)

$$F(\bar{Q}_j, \bar{I}_j, t_j, \bar{a}, \bar{b}) = \bar{Q}_j - \frac{4}{\pi} \frac{\bar{a}}{\bar{b}^2} \bar{I}_j - \bar{a} - \bar{b}t_j^{\frac{1}{2}} = 0 \quad (14)$$

where \bar{a} and \bar{b} are the intercept and the slope of the $A^* - t^{\frac{1}{2}}$ curve and obey the geometrical relationship

$$\tau^{\frac{1}{2}} = -a/b \quad (15)$$

The index j is taken over the $N(Q_j, I_j, t_j)$ data points. $(\bar{Q}_j, \bar{I}_j, t_j)$, \bar{a} , \bar{b} are the least squares adjusted values of these quantities as opposed to the experimental values (Q_j, I_j, t_j) and the preliminary values a_0 and b_0 .

If the equations of condition are evaluated at the experimental data points with preliminary values of the slope and the intercept, they

(47) W. E. Deming, Statistical Adjustment of Data, John Wiley & Sons, New York, 1943, Chap. 8.

(48) E. T. Whittaker and G. Robinson, The Calculus of Observations, Blackie and Son, London, 1937, Chap. 9.

(49) W. P. Schaefer, Inorg. Chem., 4, 642 (1965).

will not be satisfied exactly, in general, but will equal some small quantity f^j .

$$F(Q_j, I_j, t_j, a_0, b_0) = f^j \neq 0 \quad (16)$$

f^j may be linearized by expanding it in a Taylor's series about $F(\bar{Q}_j, \bar{I}_j, t_j, \bar{a}, \bar{b})$ and then neglecting the higher order terms.

$$f^j = F_a^j \Delta a + F_b^j \Delta b + F_Q^j \Delta Q_j + F_I^j \Delta I_j + \dots \quad (17)$$

where F_a^j denotes the derivative $(\partial F / \partial a)_{Q_j, I_j, t_j, a_0, b_0}$ and $\Delta Q_j, \Delta I_j, \dots$ are called residuals and are defined by

$$\begin{aligned} \Delta Q_j &= V_{Q_j} = Q_j - \bar{Q}_j \\ \Delta I_j &= V_{I_j} = I_j - \bar{I}_j \\ \Delta t_j &= 0 \\ \Delta a &= a_0 - \bar{a} \\ \Delta b &= b_0 - \bar{b} \end{aligned} \quad (18)$$

The method of least squares consists in determining those values of \bar{a} and \bar{b} which minimize the sum, \underline{S} , of the squares of the weighted residuals of the experimental points.

$$S = \sum_{j=1}^N (W_{Q_j} V_{Q_j}^2 + W_{I_j} V_{I_j}^2) \quad (19)$$

W_{Q_j} and W_{I_j} are the weights associated with the individual experimental values Q_j and I_j . The minimizing is done by obtaining the total differential of S and equating this to zero. The constraints imposed on the sum, S , by the N equations of condition are introduced by the method of Lagrange multipliers. The deduced values of these multipliers are (47)

$$l_j = \frac{1}{L_j} (f^j - F_a^j \Delta a - F_b^j \Delta b) \quad (20)$$

where

$$L_j = \frac{F_Q^j F_Q^j}{W_{Q_j}} + \frac{F_I^j F_I^j}{W_{I_j}} \quad (21)$$

The residuals Δa and Δb are then determined from the matrix equation

$$\begin{bmatrix} \sum \frac{F_a^j F_a^j}{L_j} & \sum \frac{F_b^j F_a^j}{L_j} \\ \sum \frac{F_a^j F_b^j}{L_j} & \sum \frac{F_b^j F_b^j}{L_j} \end{bmatrix} \begin{bmatrix} \Delta a \\ \Delta b \end{bmatrix} = \begin{bmatrix} \sum \frac{F_a^j f^j}{L_j} \\ \sum \frac{F_b^j f^j}{L_j} \end{bmatrix} \quad (22)$$

and \bar{a} and \bar{b} are determined finally from Eqn. (18). These values are improved by iterating. The preliminary values a_0 and b_0 were obtained by observing that the function

$$B^*(t) = Q - \frac{4}{\pi} It = \frac{4}{\pi} K \left[(\tau - t) \exp(\lambda^2 t) \operatorname{erfc}(\lambda t^{\frac{1}{2}}) + \tau^{\frac{1}{2}}(t^{\frac{1}{2}} - \tau^{\frac{1}{2}}) \right] \quad (23)$$

passes through zero at $t^{\frac{1}{2}} = \tau^{\frac{1}{2}}$. Cf. Fig. 11.

The Q and I residuals are given by the equations

$$V_{Q_j} = \frac{1}{W_{Q_j}} \ell_j F_{Q_j}^j \quad (24)$$

$$V_{I_j} = \frac{1}{W_{I_j}} \ell_j F_{I_j}^j$$

The weights W_{Q_j} and W_{I_j} are defined as the reciprocal of the square of the standard deviation for the measurement of the individual Q_j or I_j data points. Since $\sigma_{Q_j}^2$ and $\sigma_{I_j}^2$ are not known, we approximate them by the square of the estimated reading error for the individual Q_j or I_j data points. The standard deviations associated with the calculated values of \bar{a} and \bar{b} can be estimated from the diagonal elements of the inverse of the coefficient matrix of Eqn. (22), viz.

$$s_a^2 = \sum \frac{F_b^j F_b^j}{L_j} \Big/ |\text{DET}|$$

$$s_b^2 = \sum \frac{F_a^j F_a^j}{L_j} \Big/ |\text{DET}| \quad (25)$$

where $|\text{DET}|$ is the determinant of the coefficient matrix.

We applied the CHI-SQUARE test (49, 50, 51) in order to estimate the confidence level at which our data conforms to Eqns. (1) and (6). The parameter $\chi^2(M)$ can be defined as the minimum value of the weighted sum of the square of the residuals. $M = N - P - 1$ is the number of degrees of freedom, less one, of a system of N independent measurements where P parameters have been estimated from the data. For example, The CHI-SQUARE estimate associated with the A^* technique is

$$\chi^2(N-3) = \sum_{j=1}^N \frac{1}{L_j} f^j f^j - \sum_{j=1}^N \frac{1}{L_j} f^j F_a^j \Delta a - \sum_{j=1}^N \frac{1}{L_j} f^j F_b^j \Delta b \quad (26)$$

as can be shown by substituting Eqns. (20), (21), and (23) into (19).

The distribution function for $\chi^2(M)$ is

$$P(\chi^2(M))d\chi^2 = \frac{1}{2^{M/2} \Gamma(\frac{M}{2})} \chi^2 \left[\frac{M}{2} - 1 \right] \exp(-\frac{1}{2}\chi^2) d\chi^2 \quad (27)$$

and the expectation value of $\chi^2(M)$ is M .

$$\langle \chi^2(M) \rangle = \int_0^\infty \chi^2 P(\chi^2) d\chi^2 = M \quad (28)$$

$P(\chi^2(30))$ is plotted as a function of $\chi^2/30$ in Fig. 12.

(50) K. A. Brownlee, Statistical Methods and Methodology in Science and Engineering, John Wiley & Sons, New York, 1960, Chapters 2 and 5.

(51) W. G. Cochran, Annals of Math. Stat., 23, 315 (1952).

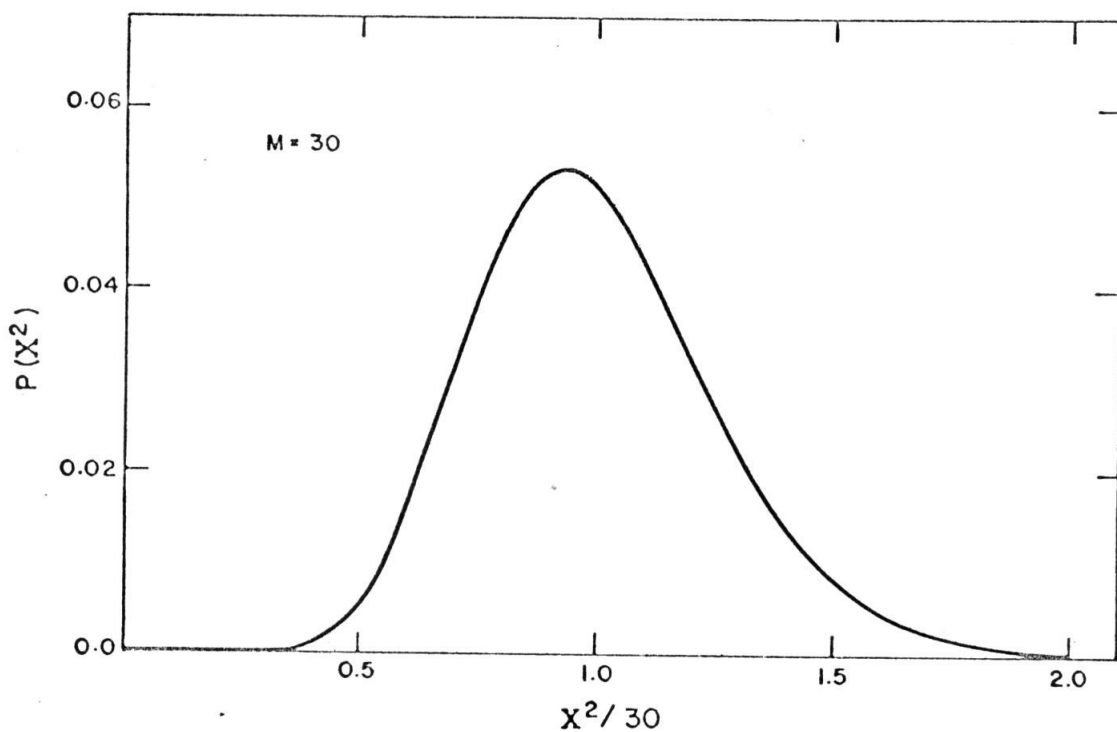


Figure 12. The probability of observing a particular value of CHI-SQUARE calculated from Eqn. (27). $M = 30$.

Hence, if our estimates of the standard deviations associated with the individual data points are correct and if the system is accurately described by Eqns. (1) and (6), then the experimental estimates of the CHI-SQUARE should, on the average, equal the number of degrees of freedom of the system and should be distributed according to Eqn. (27). We can calculate the probability of observing a value of $\chi^2 \geq \chi_1^2$ or of $\chi^2 \leq \chi_2^2$. Cf. Fig. 12.

$$\alpha \equiv \Pr(\chi^2 \geq \chi_1^2) = \int_{\chi_1^2}^{\infty} P(\chi^2) d\chi^2$$

$$\beta \equiv \Pr(\chi^2 \leq \chi_2^2) = \int_0^{\chi_2^2} P(\chi^2) d\chi^2$$
(29)

Selected values of α and β for $M = 30$ are tabulated in Table I.

The following chapter discusses the application of this method to the study of the kinetics of the Zn(II)/Zn(Hg) and Cd(II)/Cd(Hg) couples. The computer program, written in Fortran IV and used in the treatment of this data, is included as an Appendix at the end of this chapter.

TABLE I
Confidence Levels Associated with Selected Values
of χ^2 ($M = 30$)

α, β	30%	20%	10%	5%	1%	0.5%	0.1%
$\chi_1^2 / 30$	1.12	1.21	1.34	1.46	1.70	1.79	1.99
$\chi_2^2 / 30$	0.85	0.78	0.69	0.62	0.50	0.46	


```

$IBFTC ASTAR   DECK       SINGLE POTENTIAL STEP CHRONOCQUOMETRY
C
C   PROGRAMMED BY PETER JAMES LINGANE, JULY 22, 1964
C
C   *****
C
C           TABLE OF DEFINED SYMBOLS
C
C   AI       CURRENT, MICROAMPERES/ELECTRODE AREA
C   Q        CURRENT INTEGRAL, MICROCOULOMBS/ELECTRODE AREA
C   T        TIME, SECONDS
C   TIME     TIME, MILLISECONDS
C   A        ASTAR INTERCEPT
C   AO       APPROXIMATE ASTAR INTERCEPT
C   ALPHA    WEIGHT OF A
C   ALM      LAGRANGE MULTIPLIER
C   AL       LAMBDA, KINETIC PARAMETER
C   B        SLOPE OF ASTAR VS. SQRT(T)
C   BO       APPROXIMATE SLOPE
C   BETA     WEIGHT OF B
C   TI       ROOT TIME INTERCEPT, SQUARED
C   Z        SQRT(T)
C   N        NUMBER OF DATA PAIRS
C   DL       CHANGE IN DOUBLE LAYER CHARGE
C   FO        $Q - (4./PIE)*AI*(AO/BO)**2 - AO - BO*Z$ 
C   FA       DERIVATIVE OF FO, A, CALCULATED AT AO, BO, DATA POINT
C   FB       DERIVATIVE OF FO, B, CALCULATED AT AO, BO, DATA POINT
C   FQ       DERIVATIVE OF FO, Q, CALCULATED AT AO, BO, DATA POINT
C   FI       DERIVATIVE OF FO, I, CALCULATED AT AO, BO, DATA POINT
C   ITER     NUMBER OF ITERATIONS
C   S        MINIMUM SUM OF WEIGHTED SQUARED RESIDUALS
C   SIGMA    VARIANCE OF AN OBSERVATION OF UNIT WEIGHT
C
C   *****
C
C   DATA MUST BE ENTERED IN ASCENDING ORDER OF TIME
C
C   DIMENSION Q(100), AI(100), TIME(100), T(100), TI(100), ASTAR(100),
*   BSTAR(100), COMMT(12), Z(100), AQ(100), W(100), ERRORQ(100),
*   ERRORI(100), RESA(100), RESQ(100), RESI(100), FO(100), FA(100),
*   FB(100), ALM(100)
C   PIE = 3.1416
C   RTPIE = 1.7725
10 WRITE(6,1)
C   1 FORMAT(1H1)
C   DO 3 I=1,2
C   READ(5,2) COMMT
C   2 FORMAT(12A6)
C   3 WRITE(6,6) COMMT
C   6 FORMAT(1X, 12A6)
C   READ(5,5) N, DL ,E
C   5 FORMAT(15,2E15.8)
C   READ(5,32) ITER
C   32 FORMAT(15)
C   WRITE(6,11) N, DL,ITER
11 FORMAT (///, 23H NUMBER OF DATA PAIRS = , I3, // 24H DOUBLE LAYER
*   COULOMBS =, E15.8, 16H MICROCOULOMBS, // 13H ITERATIONS = , I3)
C   READ(5,4) (TIME(I), AI(I),AQ(I), ERRORI(I), ERRORQ(I), I=1,N)
C   4 FORMAT(5E10.8)
C   DO 21 I=1,N
C   Q(I) = AQ(I) - DL
C   T(I) = 0.001*TIME(I)
C   BSTAR(I) = Q(I) - (4./PIE)*AI(I)*T(I)
C   21 Z(I) = SQRT(T(I))

```

C THIS SECTION CHOOSES VALUES FOR AO AND BO BY OBSERVING WHERE
 C BSTAR = 0.
 C

```

I = 1
18 IF (BSTAR(I).LT.0.) GO TO 8
I = I + 1
GO TO 18
8 WRITE(6,19) I
19 FORMAT(/, 29H FIRST BSTAR .LT. 0. = BSTAR(, I2, 1H))
12 I = I + 1
IF (BSTAR(I)) 12,13,14
13 TI(1) = T(I)
GO TO 9
14 L = I - 1
TI(1) = -(BSTAR(L)*T(I)-BSTAR(I)*T(L))/(BSTAR(I)-BSTAR(L))
9 DO 23 I=1,N
23 ASTAR(I) = Q(I) - (4./PIE)*TI(1)*AI(I)
CALL FIT1(N, Z, ASTAR, A, B)

```

C
 C
 C

LEAST SQUARES ADJUSTMENT OF AO AND BO

```

DO 27 J=1,ITER
AO = A
BO = B
K=J+1
TI(K) = (AO/BO)**2
WRITE(6,29) AO,BO, TI(K)
29 FORMAT (/, 4H AO=, E15.8, 16H MICROCOULOMBS,10X,4H BO=, E15.8,
* 29H MICROCOULOMBS SECONDS*-1/2 ,10X, 4H TI=, E15.8, 8H SECONDS)
DO 25 I=1,N
FO(I) = Q(I) - (4./PIE)*AI(I)*(AO/BO)**2 -AO - BO*Z(I)
FA(I) = -8.*AO*AI(I)/(PIE*BO**2) -1.
FB(I) = 8.*AO**2*AI(I)/(PIE*BO**3) - Z(I)
25 W(I) = ERRORQ(I)**2 + (16./PIE**2) *ERRORI(I)**2*(AO/BO)**4
C11 = 0.
C12 = 0.
C22 = 0.
PHI1 = 0.
PHI2 = 0.
PHI3 = 0.
DO 26 I=1,N
C11 = C11 + FA(I)*FA(I)/W(I)
C12 = C12 + FA(I)*FB(I)/W(I)
C22=C22 + FB(I)*FB(I)/W(I)
PHI1 = PHI1 + FA(I)*FO(I)/W(I)
PHI3 = PHI3 + FO(I)*FO(I)/W(I)
26 PHI2 = PHI2 + FB(I)*FO(I)/W(I)
DET = C22*C11 -C12**2
DELTA A = (C22*PHI1 - C12*PHI2)/DET
DELTA B = (-C12*PHI1 + C11*PHI2)/DET
A = AO - DELTA A
27 B = BO - DELTA B
30 DO 28 I=1,N
ALM(I)= (FO(I) - FA(I)*DELTA A- FB(I)*DELTA B)/W(I)
RESQ(I) =ALM(I)*(ERRORQ(I)**2)
RESI(I) =ALM(I)*(-4./PIE)*(A*ERRORI(I)/B)**2
RESA(I) = RESQ(I) - (4./PIE)*RESI(I)*(A/B)**2
28 ASTAR(I)= Q(I) -(4./PIE)*AI(I)*(A/B)**2
S = PHI3 - PHI1*DELTA A - PHI2*DELTA B
SIGMA = S/(FLOAT(N) - 3.)
AL = -RTPIE*B/(2.*A)

```

```

C   95 PERCENT CONFIDENCE INTERVALS, ASSUMES N IS INFINITE
    SIGMAA= 1.96*SQRT(C22/DET)
    SIGMAB=1.96*SQRT(C11/DET)
    AK = - 0.001*PIE*B**2/(4.*A)
C   KAPPA HAS UNITS OF MILLIAMPERES/ELECTRODE AREA
    ALOGK  = ALOG10(AK)
    SIGMAK=SQRT((PIE*B/(2.*A))**2*(SIGMAB**2+(B/(2.*A))**2*SIGMAA**2))
    SIGMAK = 0.001* SIGMAK
C   THIS CONVERTS SIGMAK TO MILLIAMPERES
    SIGNAL  = SQRT((RTPIE/(2.*A))**2*(SIGMAB**2 + (B/A)**2*SIGMAA**2))
    SALOGK = SIGMAK/AK
C   CONFIDENCE INTERVALS, PERCENT
    SIGAP  = 100.*(SIGMAA/A)
    SIGBP  =(SIGMAB/B)*100.
    SIGKP  =(SIGMAK/AK)*100.
    SIGLP  =(SIGNAL/AL)*100.
    SLGKP  =(SALOGK/ALOGK)*100.

C
C   OUTPUT OF DATA
C
    WRITE(6,15) A, SIGMAA, SIGAP
15  FORMAT(//, 8H A      =, E15.8, 27H MICROCOULOMBS      ,5X,
*11H C.I.(95) =, E16.8, 2H =, E16.8, 8H PERCENT)
    WRITE(6,41)
41  FORMAT(//, 50(2H *))
    WRITE(6,51) B, SIGMAB, SIGBP
51  FORMAT(//, 8H B      =, E15.8, 27H MICROCOULOMBS SECONDS-1/2 ,5X,
*11H C.I.(95) =, E16.8, 2H =, E16.8, 8H PERCENT)
    WRITE(6,52) AK, SIGMAK, SIGKP
52  FORMAT(//, 8H KAPPA =, E15.8, 27H MILLIAMPERES      ,5X,
*11H C.I.(95) =, E16.8, 2H =, E16.8, 8H PERCENT)
    WRITE(6,53) AL, SIGNAL, SIGLP
53  FORMAT(//, 8H LAMBDA=, E15.8, 27H SECONDS*-1/2      ,5X,
*11H C.I.(95) =, E16.8, 2H =, E16.8, 8H PERCENT)
    WRITE(6,41)
    WRITE(6,54) ALOGK, SALOGK, SLGKP
54  FORMAT(//, 8H ALOGK =, E15.8, 27H                      ,5X,
*11H C.I.(95) =, E16.8, 2H =, E16.8, 8H PERCENT)
    WRITE(6,40) DET, S, SIGMA
40  FORMAT(//, 6H DET =, E15.8, // 36H MINIMUM WEIGHTED SUM OF RESIDUAL
*S =, E15.8, // 20H VARIANCE WEIGHT=1 =, E15.8,9X)
    WRITE(6,33)
33  FORMAT(1H1, // 1X, 19H QCOR,MICROCOULOMBS, 5X, 11H Q RESIDUAL,9X,
* 16H AI,MICROAMPERES, 9X, 12H AI RESIDUAL, 10X, 14H TIME,MILLISEC
* , 4X, 20H BSTAR,MICROCOULOMBS,///)
    WRITE(6,31) (Q(I),RESQ(I),AI(I),RESI(I),TIME(I),BSTAR(I), I=1,N)
31  FORMAT (E15.8, 5E23.8)
    WRITE(6,34)
34  FORMAT(1H1, // 6X, 2H Z, 18X, 6H ASTAR, 14X, 15H ASTAR RESIDUAL,
* 11X, 7H ERRORQ, 17X, 7H ERRORI, 18X, 2H W,/)
    WRITE(6,31)(Z(I),ASTAR(I), RESA(I),ERRORQ(I),ERRORI(I),W(I),I=1,N)
C   PUNCHED OUTPUT FOR USE IN LEAST SQUARES LOGK VS E PLOTS
    PUNCH 42,E, ALOGK, SALOGK
42  FORMAT( F10.0,2E15.8)
    GO TO 10
    STOP
    END

```

```

SUBROUTINE FIT1(N,X,Y,A,B)
C
C   2 PARAMETER LINEAR LEAST SQUARES ANALYSIS
C   X COORDINATE FREE OF ERROR, Y COORDINATE
C   ASSOCIATED WITH CONSTANT ABSOLUTE PRECISION.
C   PROGRAMMED FOR P.J.LINGANE BY M.S.ITZKOWITZ 10/18/63
C
C   A           INTERCEPT ON Y AXIS
C   B           DY/DX
C
DIMENSION X(100),Y(100)
SUMY=0
  SUMX=0
SUMXY=0
SUMX2=0
DO3I=1,N
SUMY=SUMY+Y(I)
SUMX=SUMX+X(I)
SUMXY=SUMXY+X(I)*Y(I)
SUMX2=SUMX2+X(I)*X(I)
3 CONTINUE
  DET=FLOAT(N)*SUMX2-SUMX*SUMX
  A=(SUMY*SUMX2-SUMX*SUMXY)/DET
  B=(FLOAT(N)*SUMXY-SUMX*SUMY)/DET
RETURN
END

```

CHAPTER 6.

Investigation of the Kinetic Parameters of the
Zn(II)/Zn(Hg) and Cd(II)/Cd(Hg) Couples

The purpose of the work described in this chapter is to verify the validity and the usefulness of the A^* approach to the determination of the kinetic parameters of electrode reactions. The second purpose of this study is to investigate the apparent concentration dependence of the rate constant for the reduction of cadmium from sulfate solutions. This effect appears to be characteristic of fast reactions and is independent of the method of data treatment.

Results and Discussion

The iterative least squares computer program described in Chapter 5 appeared to work very well; the \bar{a} and \bar{b} values became very constant after 3-4 iterations. The χ^2 values, cf. Eqn. (26), Chapter 5, are listed in the tables and indicate that the weighting scheme is essentially correct. The experimental weights vary over a range of about 100:1 with the short time points being weighted most heavily.

The experimental values of Q were corrected for "double-layer charging" by measuring Q in the absence of the electroactive species for each step potential; this correction had little effect on the results.

The results for the reduction of Zn(II) in 1 \underline{F} NaClO₄ are summarized in Table I. The values of K determined from A* - t^{1/2} plots for t ≥ 2.0 msec and from I - t^{1/2} plots for t ≤ 1.8 msec are in good agreement. The rate constant, calculated from the value of K at (E - E⁰) = 0, is 3.04 × 10⁻³ cm/sec and α, calculated from the slope, is 0.19, in agreement with the values k_a⁰ = 3.26 ± 0.12 × 10⁻³ cm/sec and α = 0.30 determined by faradaic impedance (52).

The limiting slope of the A* - t^{1/2} plots does not appear especially constant, but it should be realized that the confidence intervals corresponding to this slope are in the 5-10% range. If we assume that the limiting slope has the value 350 μcoulombs/sec^{1/2}, we calculate a diffusion coefficient from Eqn. (9), p.75, for Zn(II) of 1.3 ± 0.3 × 10⁻⁵ cm²/sec. This seems to be high.

Experimental values for Q and A* are plotted vs. t^{1/2} in Fig. 13. This figure shows clearly that it would be impossible to apply the Q - t^{1/2} procedure to a couple as slow as Zn(II)/Zn(Hg) since t ≥ 6 sec for λt^{1/2} > 5 and at times this long the sphericity of the hanging drop will be very important. The point at which the I - t^{1/2} plot becomes valid (λt^{1/2} ≤ 0.1) is also indicated.

Thus we have demonstrated that this least squares method of data treatment is capable of choosing a and b so as to achieve a linear A* - t^{1/2} plot over the entire range of λt^{1/2}. The kinetic parameters

(52) J. H. Sluyters and J.J.C. Oomen, Rec. trav. chim., 79, 101 (1960).

TABLE I

11.1 mF Zn(II) in 1.0 F NaClO₄, pH 3.4 $E_{\text{initial}} = -0.850$ v. $E_{\frac{1}{2}} = -1.002$ v. vs. S.C.E. $k_a^0 = 3.04 \times 10^{-3}$ cm/sec, $\alpha = 0.19$

$-E$ mv. vs. S.C.E.	χ^2	b $\mu\text{coulombs}$ $\text{sec}^{-\frac{1}{2}}$	λ $\text{sec}^{-\frac{1}{2}}$	K^b m amp	K^c m amp
984	1.48	93. \pm 2.4 ^a	2.1 \pm 0.13 ^a	0.171 \pm 0.013 ^a	0.194
994	2.28	143. \pm 4.	1.7 \pm 0.12	0.215 \pm 0.019	0.222
1004	1.20	199. \pm 7.	1.6 \pm 0.14	0.286 \pm 0.030	0.273
1014	0.77	226. \pm 10.	1.6 \pm 0.17	0.317 \pm 0.040	0.328
1024	0.44	275. \pm 14.	1.7 \pm 0.20	0.405 \pm 0.059	0.407
1034	1.28	344. \pm 15.	1.4 \pm 0.14	0.441 \pm 0.054	0.475
1044 ^d	2.88	159. \pm 1.2	9.5 \pm 0.17	1.34 \pm 0.030	0.522
1064	1.11	378. \pm 17.	2.0 \pm 0.23	0.67 \pm 0.092	0.720
1084	0.45	359. \pm 8.	2.8 \pm 0.17	0.89 \pm 0.062	0.897
1124	1.67	308. \pm 4.	7.4 \pm 0.50	2.03 \pm 0.14	1.400

^a95% confidence intervals^bfrom $A^* - t^{\frac{1}{2}}$ plots^cfrom $I - t^{\frac{1}{2}}$ plots^dneglected

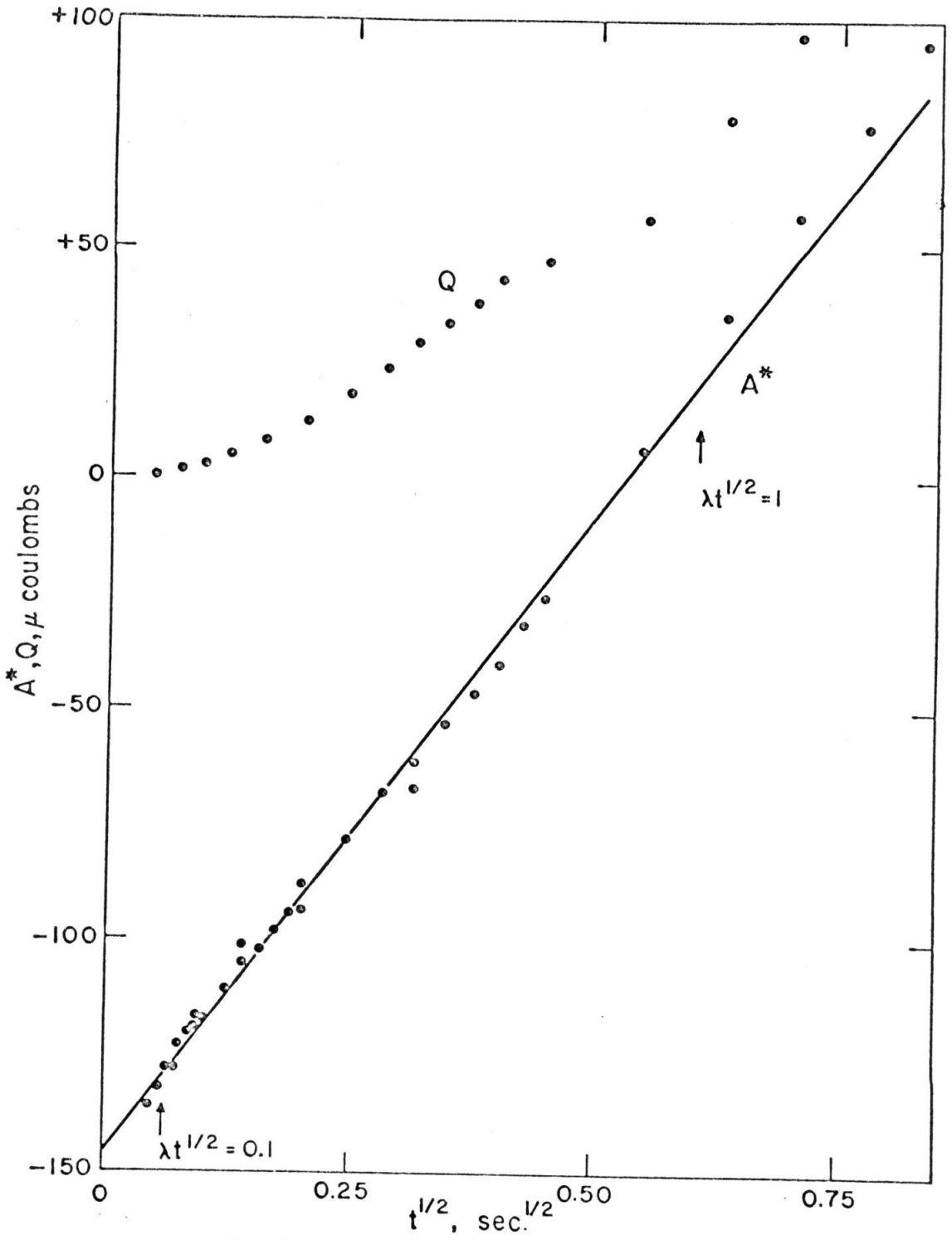


Figure 13. A^* and Q vs. $t^{1/2}$ for the reduction of 11.1 mF Zn(II) in 1.0 F NaClO₄, pH = 3.4, 24.8 ± 0.2°C. $E - E_{1/2} = -22$ mv.

calculated from a and b are in agreement with those determined by other techniques. The $A^* - t^{\frac{1}{2}}$ approach to the determination of kinetic parameters has been experimentally verified.

Data for the reduction of Cd(II) in sulfate and perchlorate media are presented in Tables II, III, and IV. The limiting values of b yield values of the diffusion coefficients of 0.60 and 0.74×10^{-5} cm²/sec for the 9.25 and 18.5 mF cadmium sulfate solutions respectively, in agreement with the value in nitrate media (53).

The rate constants determined for these solutions are substantially in error. The value of k_a^0 obtained from the cadmium sulfate data are in agreement only with the values obtained by the $Q - t^{\frac{1}{2}}$ method (46). Plots of $\log K$ vs. E are shown in Fig. 14; this figure shows clearly the anomalous fact that K is essentially independent of the concentration of cadmium. The rate constant determined for the reduction of Cd(II) in perchlorate media is more than an order of magnitude smaller than that obtained by faradaic impedance (54).

The $A^* - t^{\frac{1}{2}}$ plots for all the cadmium solutions exhibit excellent linearity; it should be emphasized that the same values of the slope and the intercept would be obtained from the $Q - t^{\frac{1}{2}}$ plots since $\lambda t^{\frac{1}{2}} > 5$ for most of the data points. Therefore, the seemingly anomalous rate

(53) D. J. Macero and C. L. Rulfs, J. Am. Chem. Soc., 81, 2942 (1959).

(54) J.E.B. Randles, in Transactions of the Symposium on Electrode Processes, Philadelphia, May, 1959, edited by E. Yeager, John Wiley & Sons, New York, 1961, p. 209.

TABLE II

9.25 mF Cd(II) in 0.5 F Na₂SO₄, pH = 5.9

$E_{\text{initial}} = -0.470$ v. $E_{\frac{1}{2}} = -0.601$ v. vs. S.C.E.

$k_a^0 = 1.38 \times 10^{-2}$ cm/sec, $\alpha = 0.28$

<u>-E</u> <u>mv. vs.</u> <u>S.C.E.</u>	<u>χ^2</u>	<u>b</u> <u>$\mu\text{coulombs}$</u> <u>$\text{sec}^{-\frac{1}{2}}$</u>	<u>λ</u> <u>$\text{sec}^{-\frac{1}{2}}$</u>	<u>K</u> <u>mA</u>
570	0.53	16.4 \pm 0.3 ^a	34.7 \pm 4.0 ^a	0.505 \pm 0.060 ^a
580	1.14	31.1 \pm 0.5	20.5 \pm 1.8	0.564 \pm 0.052
590	1.23	54.8 \pm 1.0	15.3 \pm 1.2	0.741 \pm 0.064
600	1.04	89.7 \pm 1.9	10.8 \pm 1.0	0.860 \pm 0.086
610	0.83	135. \pm 2.7	8.4 \pm 0.7	1.01 \pm 0.094
620	2.56	152. \pm 2.2	11.9 \pm 0.9	1.61 \pm 0.13
630	0.32	184. \pm 4.4	10.6 \pm 1.1	1.72 \pm 0.19
640	0.62	192. \pm 3.7	13.7 \pm 1.3	2.33 \pm 0.24
650	0.69	202. \pm 4.6	15.5 \pm 1.6	2.76 \pm 0.31
660	0.83	207. \pm 4.1	18.4 \pm 1.7	3.37 \pm 0.34
680	1.02	207. \pm 3.7	26.4 \pm 2.5	4.83 \pm 0.48
700	0.58	198. \pm 3.7	44.8 \pm 7.3	7.89 \pm 1.30

^a95% confidence interval

TABLE III

18.5 mF Cd(II) in 0.5 F Na₂SO₄, pH = 5.9 $E_{\text{initial}} = -0.470$ v. $E_{\frac{1}{2}} = -0.601$ v. vs. S.C.E. $k_a^0 = 0.75 \times 10^{-2}$ cm/sec, $\alpha = 0.22$

<u>-E</u> <u>mv. vs.</u> <u>S.C.E.</u>	<u>χ^2</u>	<u>b</u> <u>$\mu\text{coulombs}$</u> <u>$\text{sec}^{-\frac{1}{2}}$</u>	<u>λ</u> <u>$\text{sec}^{-\frac{1}{2}}$</u>	<u>K</u> <u>m amp</u>
570	0.26	34.9 \pm 0.5 ^a	20.3 \pm 2.2 ^a	0.626 \pm 0.071 ^a
580	0.74	65.2 \pm 1.1	11.9 \pm 1.0	0.690 \pm 0.064
590	0.84	120. \pm 2.5	7.7 \pm 0.6	0.824 \pm 0.069
600	0.69	191. \pm 5.8	5.7 \pm 0.5	0.961 \pm 0.10
610	0.72	265. \pm 7.4	5.1 \pm 0.4	1.20 \pm 0.11
630	0.52	406. \pm 10.	4.7 \pm 0.4	1.69 \pm 0.16
640	0.81	435. \pm 14.	5.6 \pm 0.6	2.17 \pm 0.27
650	2.39	456. \pm 16.	5.8 \pm 0.6	2.34 \pm 0.29
660	1.36	456. \pm 15.	6.9 \pm 0.8	2.78 \pm 0.34
680	3.27	442. \pm 14.	10.6 \pm 1.6	4.17 \pm 0.67
700	1.59	443. \pm 12.	12.7 \pm 1.8	5.00 \pm 0.74

^a95% confidence interval

TABLE IV

9.25 mF Cd(II) in 1.0 F NaClO₄, pH = 1.4 (nitric acid)

$$E_{\text{initial}} = -0.470 \text{ v. } E_{\frac{1}{2}} = -0.564 \text{ vs. S.C.E.}$$

$$k_a^0 = 1.41 \times 10^{-2}, \alpha = 0.26$$

<u>-E</u> mv. vs. S.C.E.	<u>χ^2</u>	<u>b</u> $\mu\text{coulombs}$ $\text{sec}^{-\frac{1}{2}}$	<u>λ</u> $\text{sec}^{-\frac{1}{2}}$	<u>K</u> m amp
570	0.38	89. ± 4.	14. ± 3. ^a	1.13 ± 0.30 ^a
580	0.90	135. ± 5.	11. ± 2.	1.33 ± 0.28
590	0.24	170. ± 9.	11. ± 3.	1.70 ± 0.44
600	0.48	195. ± 9.	13. ± 3.	2.20 ± 0.54
610	1.16	216. ± 11.	14. ± 3.	2.67 ± 0.66
620	1.92	218. ± 10.	18. ± 4.	3.38 ± 0.90
630	2.00	225. ± 9.	20. ± 4.	4.05 ± 0.82
640	0.98	226. ± 9.	26. ± 5.	5.1 ± 1.5
650	1.50	217. ± 8.	45. ± 16.	8.6 ± 3.2
660	1.10	223. ± 9.	37. ± 12.	7.4 ± 2.4
680	0.60	221. ± 8.	56. ± 22.	10.9 ± 4.4
700	1.44	221. ± 7.	69. ± 26.	13.5 ± 5.2

^a95% confidence interval

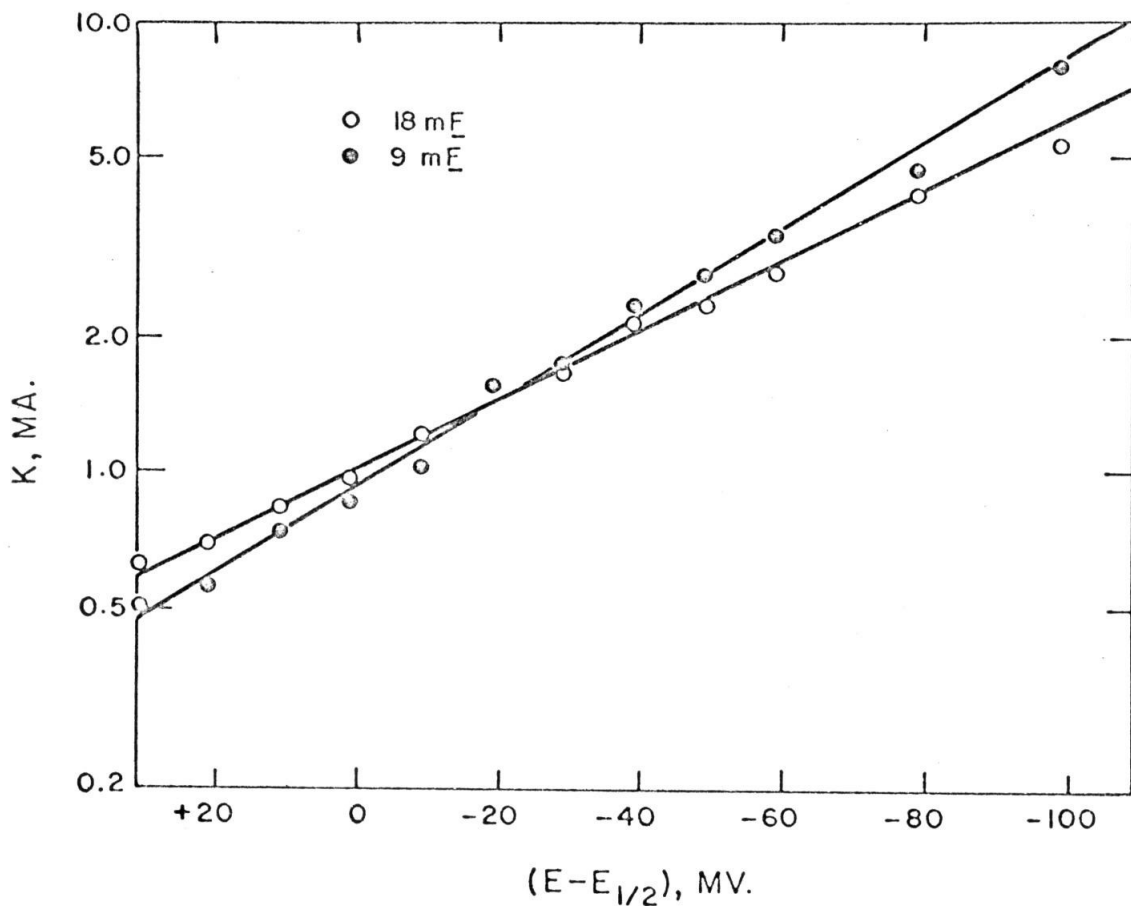


Figure 14. Plot of $\log K$ vs. $(E - E_{1/2})$ for the reduction of Cd(II) in 0.50 \underline{F} Na_2SO_4 , pH = 5.9, 26°C. $E_{1/2} = -0.601$ v. vs. S.C.E. Uncompensated.

constants determined for the cadmium solutions are not due to the particular method of data calculation.

Since the conclusion of this work, Oldham (55) has suggested that the explanation for these effects lies in the consideration of the influence of uncompensated resistance on the performance of an electronic potentiostat. Figure 15 illustrates both the schematic representation of the potentiostated indicator electrode and its equivalent circuit. Within the current and voltage limitations of the potentiostat, the ability of this circuit to maintain the reference electrode E volts above ground potential is independent of the magnitude of R_3 . An ideal potentiostat is powerless however to maintain the potential drop across the faradaic resistance R_f at E volts. The potential drop across the faradaic resistance will be $E - i(R_1 + R_2)$ where R_1 and R_2 are respectively the resistance in the capillary or in the leads to the summing point of the current measuring amplifier and the resistance corresponding to the ohmic drop in the solution between the tip of the reference electrode and the surface of the indicator electrode. The sum of R_1 and R_2 is the uncompensated resistance in the circuit.

Lauer and Osteryoung (56) have ungrounded the positive input of the potentiostat and have fed a voltage back to this point which is proportional to the current passing through the cell. In this way they have minimized the effects of uncompensated resistance and have

(55) K. B. Oldham, J. Electroanal. Chem., 11, 171 (1966).

(56) G. Lauer and R. A. Osteryoung, Anal. Chem., in press, 1966.

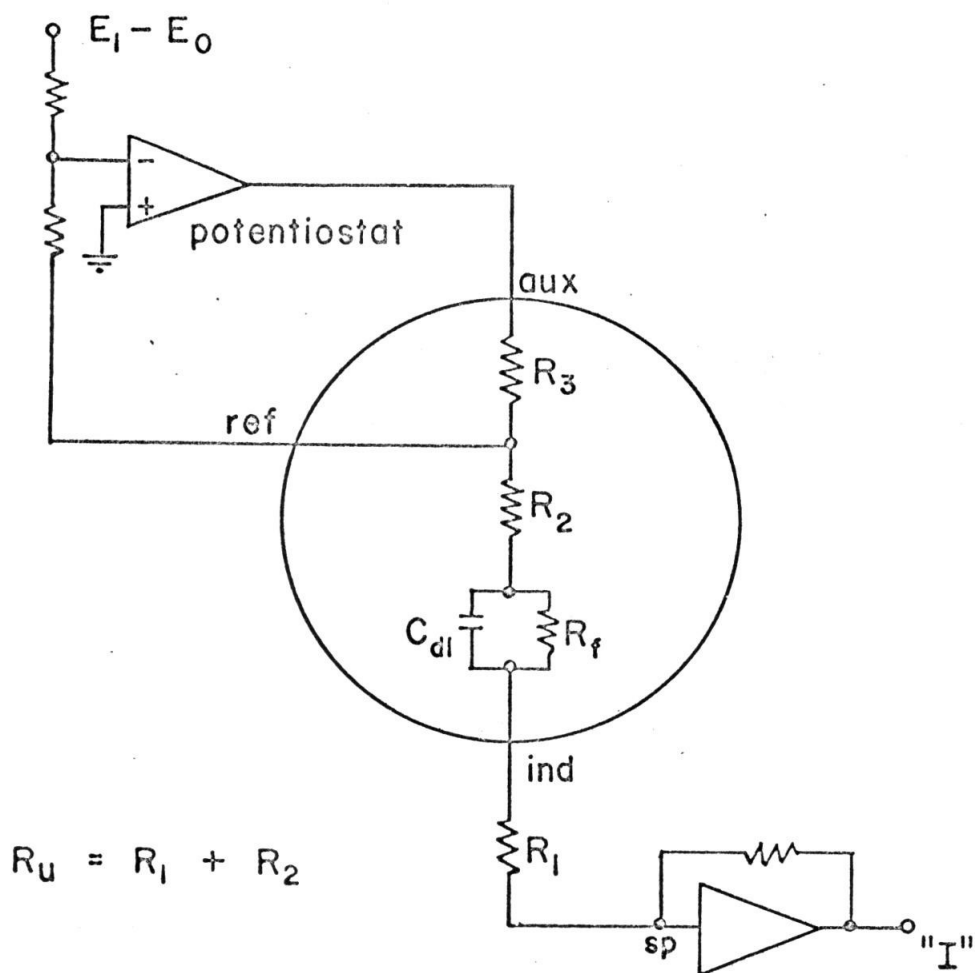


Figure 15. Schematic representation of an electrochemical cell in the presence of uncompensated resistance.

demonstrated that under these conditions the potential step technique yields values for the rate constant which are indeed independent of the concentration of the electroactive species.

Conclusions

This work has shown the necessity for a modified experimental setup such as that developed by Lauer and Osteryoung (56) in order that the influence of uncompensated resistance may be minimized. In addition, the A^* approach to the determination of kinetic parameters from potential step measurements has been shown to be superior to either the $I - t^{\frac{1}{2}}$ or the $Q - t^{\frac{1}{2}}$ methods because it eliminates the need for long or short time criteria and thus the possibility of operator bias in the fitting of the data and because of the capability for the evaluation of statistical parameters from the data.

When applied in the semi-manual fashion outlined here, the A^* approach is prohibitively time consuming. Lauer and Osteryoung (39) however have developed a data acquisition system built around a multichannel analyzer. This system is capable of producing precise data in the form, for example, of punched cards directly compatible with the computing facilities. The method of data treatment outlined here, when used in conjunction with this or a similar data acquisition system, is the best available method for the estimation of kinetic parameters from potential step measurements.

Experimental

A stock solution of 8 F NaClO₄ was prepared by neutralizing 60% perchloric acid with solid sodium carbonate. The solution was boiled while still slightly acid to remove most of the dissolved carbon dioxide and the pH was then adjusted to ca. 7 with sodium hydroxide. The standard cadmium nitrate solution was prepared by weight by dissolving Baker and Adamson Cd metal in nitric acid. The standard zinc perchlorate solution was prepared by weight by dissolving B & A zinc shot in an equivalent quantity of perchloric acid plus excess nitric acid. This was evaporated to decomposition of the zinc perchlorate and redissolved in a minimum amount of dilute perchloric acid; the solution therefore contained a small amount of chloride. All test solutions were prepared by dilution with triply distilled water of specific conductivity less than 2×10^{-6} (ohm-cm)⁻¹.

The electronic arrangement is similar to that described in Chapter 4 (cf. Fig. 10) with the exception that relay 2 was removed from the circuit since it is unnecessary. The supporting equipment is also essentially as described in Chapter 4. Four Polaroid pictures were taken at each potential covering time intervals of 10, 50, 200, and 1000 mseconds.

A Kemula-type hanging mercury drop electrode was used (area = 0.041 cm²). The cell was deaerated with prepurified nitrogen (< 8 ppm O₂).

III. FARADAIC INTEGRATION OF THE DIFFUSE DOUBLE LAYER

General Statement of the Problem

Electrochemical phenomena are divisible into "faradaic" and "non-faradaic" processes. Faradaic processes are characterized by the fact that chemical changes accompany the flow of charge across the electrode/electrolyte interface; non-faradaic processes involve the flow of charge onto the surface of the electrode and are unaccompanied by chemical changes. The presently available techniques for the determination of the net charge residing on the surface of an electrode are non-faradaic in nature. These include those techniques based on the determination of the charge that flows upon changes in the area of the electrode (57-59), the integration of double layer capacitance curves (60,61), and the application of the Lippman equation to the differentiation of electrocapillary curves (60, 62, 69).

(57) F. C. Anson, Anal. Chem., 38, 54 (1966).

(58) J. N. Butler and G. L. Meehan, J. Phys. Chem., 68, 5041 (1965).

(59) G. Lauer, unpublished experiments based on a dipping platinum electrode (1964).

(60) R. Parsons, in "Electrochemistry and Electrochemical Engineering," Vol. I, P. Delahay, Ed., Interscience, N.Y., 1961, Chap. 1.

(61) D. C. Grahame, Chem. Rev., 41, 441 (1947).

(62) H. D. Hurwitz, J. Electroanal. Chem., 10, 35, (1965) and references contained therein.

This problem was undertaken with the hope of developing an electrochemical technique whereby the excess charge in the region of the diffuse double layer, and thus the electronic charge on the electrode in the absence of specific adsorption, could be measured by the direct electrolysis of the ions comprising the diffuse layer. This technique involves the faradaic integration of the excess charge in the diffuse layer rather than the determination of the electronic charge in the surface of the electrode.

The essential premise upon which this investigation is based is that "integral" electrochemical techniques, which determine the quantity of "non-diffusing" reactant "adsorbed" on the surface of the electrode, measure not only the reactant which is chemisorbed to the electrode surface but also that reactant which is electrostatically attracted into the diffuse double layer. This latter quantity is usually too small to be measured because the diffuse layer is usually composed almost entirely of non-electroactive ions because of the presence of a large excess of supporting electrolyte. If, however, the concentration of the supporting electrolyte were decreased to a value comparable to the reactant concentration, significant quantities of reactant should be present in the diffuse layer and should be capable of detection and measurement.

Modification of the Mass Transport Phenomena in the Absence of Supporting Electrolyte

The expressions describing the response of an electrochemical

system to the application of a particular electrochemical technique have generally been derived under the assumption that diffusion is the sole method of mass transport. Since this assumption is not valid under our experimental conditions, it is necessary to consider what modifications are needed.

The modifications of the "diffusion equations" needed, in the absence of supporting electrolyte, to account for the transport of ionic species by "migration" have been fully discussed by Kies (63) and by Morris and Lingane (64, 65). Fick's First Law becomes

$$\vec{J} = -\frac{CD}{RT} \nabla \bar{\mu} = -D(\nabla C + \frac{zFC}{RT} \nabla \phi) \quad (1)$$

where \vec{J} and $\bar{\mu}$ are the flux density and the electrochemical potential of a particular ionic species and ϕ is the electrical potential in the solution. Fick's Second Law becomes

$$\frac{\partial C_j}{\partial t} = \nabla \cdot D_j (\nabla C_j + \frac{z_j FC_j}{RT} \nabla \phi); \quad j = 1, 2, \dots, N \quad (2)$$

When an equation of this form is written for the electroactive species ($j = 1$) in the presence of excess supporting electrolyte, the product $z_1 C_1 \nabla \phi$ is negligible and the more familiar form of this law results.

It is usual to assume that the diffusion coefficient is independent

(63) H. L. Kies, J. Electroanal. Chem., 4, 156 (1962).

(64) M. D. Morris and J. J. Lingane, J. Electroanal. Chem., 6, 300 (1963).

(65) M. D. Morris, J. Electroanal. Chem., 8, 1 (1964).

of position in the solution, i.e., $\nabla D_j = 0$. Thus Eqn. (2) becomes

$$\frac{\partial C_j}{\partial t} = D_j \nabla^2 C_j + \frac{z_j F C_j D_j}{RT} \nabla^2 \phi + \frac{z_j F D_j}{RT} \nabla C_j \cdot \nabla \phi; \quad j = 1, 2, \dots, N \quad (3)$$

In general, an equation of this form must be written for each species in the solution and the resulting system of simultaneous differential equations is solved for the various solution concentrations.

Certain simplifications result if the solution contains only two ionic species. Under these conditions, there are only two equations of the form of Eqn. (3) and $n = z_1$.

$$\frac{\partial C_1}{\partial t} = D_1 \nabla^2 C_1 + \frac{z_1 F C_1 D_1}{RT} \nabla^2 \phi + \frac{z_1 F D_1}{RT} \nabla C_1 \cdot \nabla \phi \quad (4)$$

$$\frac{\partial C_3}{\partial t} = D_3 \nabla^2 C_3 + \frac{z_3 F C_3 D_3}{RT} \nabla^2 \phi + \frac{z_3 F D_3}{RT} \nabla C_3 \cdot \nabla \phi \quad (5)$$

where the subscript "1" denotes the electroactive species and the subscript "3" the counter ion. Using the electroneutrality expression $z_1 C_1 + z_3 C_3 = 0$ (66), we combine Eqn. (4) and (5) to obtain

$$\frac{\partial C_1}{\partial t} = D_S \nabla^2 C_1 \quad (6)$$

where

$$D_S = D_1 D_3 (z_1 - z_3) / (z_1 D_1 - z_3 D_3) \quad (7)$$

(66) The validity of this assumption has been discussed by Levich with an approximate diffusion layer treatment. Cf. V. G. Levich, "Physicochemical Hydrodynamics," Prentice-Hall, Inc., Englewood Cliffs, N.J., 1962, p. 248 ff.

Note that the form of Eqn. (6) is identical to the usual formulation of Fick's Second Law with a different numerical value for the proportionality factor. The current passing through the cell is the sum of the charge flux densities of both the anions and the cations.

$$\frac{\vec{I}}{F} = -z_1 D_1 (\nabla C_1 + \frac{z_1 F}{RT} C_1 \nabla \phi) - z_3 D_3 (\nabla C_3 + \frac{z_3 F}{RT} C_3 \nabla \phi) \quad (8)$$

Since the flux of C_3 is zero at the electrode surface,

$$\frac{\vec{I}}{F} \Big|_{x=0} = \frac{i_0}{z_1 F} = D_1 (\nabla C_1 + \frac{z_1 F}{RT} C_1 \nabla \phi) \cdot \hat{x} \Big|_{x=0} \quad (9)$$

and

$$\nabla \phi \cdot \hat{x} \Big|_{x=0} = - \frac{RT}{z_3 F C_3} \nabla C_3 \cdot \hat{x} \Big|_{x=0} \quad (10)$$

Therefore the current density at the electrode surface is given by

$$\frac{i_0}{z_1 F} = D_1 \frac{z_3 - z_1}{z_3} \nabla C_1 \cdot \hat{x} \Big|_{x=0} \quad (11)$$

Thus the form of the expression relating the current density and the concentration gradient of the reactant is unchanged in the absence of supporting electrolyte and a multiplicative factor " $(z_3 - z_1)/z_3$ " is introduced.

The gradient of the electrical potential is composed of an ohmic and a liquid junction term and can be obtained at any point in the solution by substituting the electroneutrality relationship into Eqn. (8)

$$\nabla \phi = \frac{RT}{FC_1(z_1 D_1 - z_3 D_3)} \left\{ \frac{i_0}{z_1 F} - (D_1 - D_3) \nabla C_1 \right\} \quad (12)$$

These basic equations define the mass transport problem in the absence of supporting electrolyte. Because the form of Fick's Second Law and the form of the boundary conditions are unchanged in the absence of supporting electrolyte, the form of the solutions for C_1 and C_3 are unchanged. The parametric dependences of these solutions on time, current density, bulk concentration, etc. are not altered and the numerical constant " $(z_3 - z_1)/z_3$ " appears in all flux expressions. Specific examples of the solutions under chronopotentiometric and potentiostatic boundary conditions are given in Chapters 8 and 9.

Morris and Lingane (64) have demonstrated that the exact solutions in the presence of small amounts of supporting electrolyte are adequately approximated by solutions of the same form as those obtaining in the presence of supporting electrolyte. In treating our own data, we have adopted the approach of Morris and Lingane and have assumed that the parametric dependences are unaffected by the presence or absence of supporting electrolyte.

Characteristics of the Pilot Ion

Before progressing to the discussion of the measurement of the electroactive charge in the diffuse double layer, it is well to consider the magnitudes of the quantities we will be attempting to measure and the characteristics which influence the choice of the pilot system.

A suitable pilot ion must possess a standard potential several hundred millivolts removed from the decomposition potential of the

supporting electrolyte and a large heterogeneous rate constant so that the electrolysis of the pilot ion can support very high current densities, for a few milliseconds, at 100 per cent current efficiency.

Inspection of tabulations (67, 68) of the electronic charge on the surface of mercury electrodes in the absence of specific adsorption indicates that Q_e becomes as positive as perhaps $+20 \mu\text{C}/\text{cm}^2$ at $+0.2 \text{ v. vs. S.C.E.}$ and as negative as perhaps $-25 \mu\text{C}/\text{cm}^2$ at about $1.8 \text{ v. vs. S.C.E.}$ In reality however, the requirement that the potential at which the electrolysis of the pilot ion occurs be removed from the decomposition potential restricts the range of measurable diffuse layer charge to perhaps $\pm 10 \mu\text{C}/\text{cm}^2$.

Certain electrochemical techniques require the presence of appreciable quantities of supporting electrolyte; e.g., the uncompensated resistance becomes unmanageably large in the absence of supporting electrolyte in the potential step chronocoulometric technique. If the supporting electrolyte and the electroactive ions are of the same charge type, both $+1$ or $+2$ cations for example, the charge in the diffuse layer due to the electroactive material is reduced by approximately the ratio of the bulk concentration of the electroactive cation to the sum of the bulk concentrations of all of the cationic species. On the other hand, the electroactive species would be preferentially attracted into the

(67) D. C. Grahame and B. A. Soderberg, J. Chem. Phys., 22, 449 (1954).

(68) H. Wroblowa, Z. Kovac, and J. O'M. Bockris, Trans. Faraday Soc., 61, 1523 (1965).

diffuse layer if it is more highly charged than the cation of the supporting electrolyte (69). This effect is sufficiently large that a +2 cation composes more than 50 per cent of the charge in the diffuse layer even in the presence of a 10-20 fold excess of +1 supporting electrolyte. Thus it is desirable, nay mandatory, to employ a doubly or triply charged pilot ion and a singly charged indifferent electrolyte.

It would be advantageous if the electrolysis of the pilot ion consumed more charge than the ion contributed to the formation of the diffuse layer, i.e., $|n| > |z|$, because this would improve the absolute precision with which the surface excess of the pilot ion in the diffuse layer could be measured.

Non-Equilibrium Changes in the Composition of the Diffuse Layer

As discussed in detail in Chapter 7, the equilibrium distribution of ions in the diffuse layer can be estimated on the basis of Gouy-Chapman theory. In this section a model is developed to describe the transient response of the diffuse double layer to changes in the magnitude of the electronic charge on the surface of the electrode. The essential characteristic of this model is that the relaxation time of the diffuse double layer is much smaller than that of any diffusion controlled process. The purpose of this model is to provide an approximate estimate for the relaxation time of the diffuse layer and to provide a basis for understanding

(69) K. M. Joshi and R. Parsons, Electrochim. Acta, 4, 129 (1961).

the manner in which the charged components in the diffuse layer change during an electrochemical experiment.

The field arising from the incomplete polarization of the diffuse layer at the surface of a planar electrode does not decrease in intensity as the distance from the electrode increases; the forces acting on an ion in the bulk of the solution are similar to the forces acting on an ion in the vicinity of the electrode. Therefore, we expect that the field arising from the incomplete polarization of the diffuse double layer will accelerate all of the ions of one charge towards the electrode and will repel all of the ions of the other charge, independent of their distance from the electrode. In this fashion, the net change in the charge in the diffuse layer is effected without the creation of any concentration gradients in the solution except at the surface of the electrode, i.e., in the region of the diffuse layer itself.

We can approximate the relaxation time of the diffuse layer in the following fashion. Should the magnitude of the electronic charge on the surface of the electrode exceed that in the diffuse double layer by $\sigma \mu\text{C}/\text{cm}^2$, a field of about $144 \sigma \text{ kv}/\text{cm}$ would exist throughout the solution.

$$\nabla\phi = \frac{\sigma}{K\epsilon_0} = \frac{\sigma \times 10^{-6} \text{ C}/\text{cm}^2}{78.5 \times 8.85 \times 10^{-14} \text{ C}/\text{v. cm}} = 144 \sigma \text{ kv}/\text{cm} \quad (13)$$

Since the mobilities of most ions in aqueous solutions are of the order of $6-8 \times 10^{-4} \text{ cm}^2/\text{volt-sec}$, the ionic components of the solution would achieve velocities of the order of $100 \sigma \text{ cm}/\text{sec}$ under the influence of

this field. A uniform translation, at velocities of this magnitude, of the anionic and cationic lattices would require about $1/10C$ to change the diffuse layer charge by $\sigma \mu\text{C}/\text{cm}^2$. This is of the order of 100 nanoseconds for a symmetrical electrolyte of concentration 10^{-6} equivalents/ cm^3 .

Since the relaxation time of the diffuse layer appears to be considerably smaller than that of any diffusion controlled process, an additional consequence of this model is that diffusive forces do not begin to establish the ultimate equilibrium concentration distributions until after the equalization of the charge in the diffuse layer to that on the surface of the electrode. The equalization of the diffuse layer charge to that on the electrode surface is effected essentially instantaneously by the transport of ionic material in and out of the region of the diffuse layer in proportion to their transport numbers in the bulk of the solution.

We can illustrate this last point by considering the following thought experiment. Suppose that a mixture of 0.5 mF zinc perchlorate, 2. mF sodium perchlorate is in equilibrium with a mercury electrode at its point of zero charge. $-4.95 \mu\text{C}/\text{cm}^2$ of surface charge are instantaneously injected onto the electrode surface and the region of the diffuse double layer is allowed to relax and establish an excess surface charge of $+4.95 \mu\text{C}/\text{cm}^2$ in the diffuse layer. The relative transference numbers of the ionic components in this solution may be calculated using the data in Table I. $2\lambda_{\text{Na}^+} : \lambda_{\text{Zn}^{++}} : 3\lambda_{\text{ClO}_4^-} = 0.28:0.15:0.57$. The net change of $+4.95 \mu\text{C}/\text{cm}^2$ in the excess charge in the

Table I

Diffusion Coefficients and Equivalent Conductivities
of Various Ions at Infinite Dilution at 25°C (70,71)

<u>Ion</u>	<u>λ^0, cm²/ohm</u>	<u>$D \times 10^5$, cm²/sec</u>
Ba ⁺⁺	63.6	0.85
Co ⁺⁺	49.	.66
Cu ⁺⁺	54.	.72
H ⁺	350.	9.34
Li ⁺	39.	1.04
Na ⁺	50.5	1.35
Tl ⁺	75.	2.00
Zn ⁺⁺	54.	0.72
Cl ⁻	76.	2.03
ClO ₄ ⁻	67.3	1.80
NO ₃ ⁻	72.	1.92

(70) R. Parsons, "Handbook of Electrochemical Constants," Academic Press, N.Y., 1959, p. 85.

(71) I. M. Kolthoff and J. J. Lingane, "Polarography," Interscience, Inc., N.Y., 2nd Ed., 1952, p. 52.

diffuse layer is considered to be effected, initially, by the attraction of $1.40 \mu\text{C}/\text{cm}^2$ of Na^+ and of $0.75 \mu\text{C}/\text{cm}^2$ of Zn^{++} into the region of the diffuse layer and by the rejection of $2.80 \mu\text{C}/\text{cm}^2$ of ClO_4^- from this region. Once charge equilibrium has been established, the much slower process of diffusion is considered to reject $0.76 \mu\text{C}/\text{cm}^2$ of Na^+ and to accept $3.34 \mu\text{C}/\text{cm}^2$ of Zn^{++} and $2.60 \mu\text{C}/\text{cm}^2$ of ClO_4^- back into the region of the diffuse layer so as to establish the ultimate equilibrium distributions. (Cf. Chapter 7, Table I, p. 123).

This model is especially useful in interpreting the amount of "adsorption" determined by a particular electrochemical technique. For example, in those cases in which the potential of the electrode changes appreciably during the experiment, e.g., in potential step chronocoulometry or in chronopotentiometric experiments in which the indicator electrode is initially biased to a potential far removed from $E_{1/4}$, the measured value of the surface excess of the electroactive species in the diffuse layer should be given by the following expression,

$$\Gamma_1 |_{\text{obs}} = \Gamma_1(E_0) + \frac{Z_1 C_1 \lambda_1^0}{F \sum |Z_j| C_j \lambda_j^0} Q_{\text{dl}}(E_0, E_1) \quad (14)$$

where $Q_{\text{dl}}(E_0, E_1)$ is the net change in the diffuse layer charge between the potential limits E_0 and E_1 and where $Z_1 C_1 \lambda_1^0 / \sum |Z_j| C_j \lambda_j^0$ is the transference number of the electroactive species.

Let us consider the manner in which charge equilibrium is maintained between the diffuse layer and the electrode surface in the total

absence of supporting electrolyte. This is a very interesting situation because the possibility exists for "trapping" electroactive material in the diffuse layer under these conditions. If the potential of the electrode is changed abruptly from E_0 to E_1 , the change in the surface excess of cations in the diffuse layer should be given by Eqn. (15); this change is

$$\Delta\Gamma_+ = \frac{\lambda_+^0}{\lambda_+^0 - \frac{z_-}{z_+} \lambda_-^0} Q_{dl}(E_0, E_1) \quad (15)$$

represented as the upper shaded region of Fig. 16. It is clear that a quantity of cations equal to the total surface charge in the diffuse layer, the entire shaded region of Fig. 16, cannot react at the electrode because, for it to do so, would result in the elimination of the diffuse layer. Therefore the concentration profile of the material which can react at the electrode is actually given by $|z_-/z_+| C_-!$ Since the charge density of the "reactive" material is reduced by an amount $z_- F \Delta\Gamma_-$ in the region of the diffuse layer (the lower shaded region of Fig. 16) upon the change in electrode potential from E_0 to E_1 , it is clear that the observed surface excess of electroactive material will be less than the equilibrium value characteristic of E_0 .

$$\Gamma_+ |_{obs} = \Gamma_+(E_0) - \frac{z_-}{z_+} \Delta\Gamma_- < \Gamma_+(E_0) \quad (16)$$

The chapters in this section will discuss the results of calculations of the surface excess of the different ionic components of the diffuse double layer for representative solution mixtures and the results of the

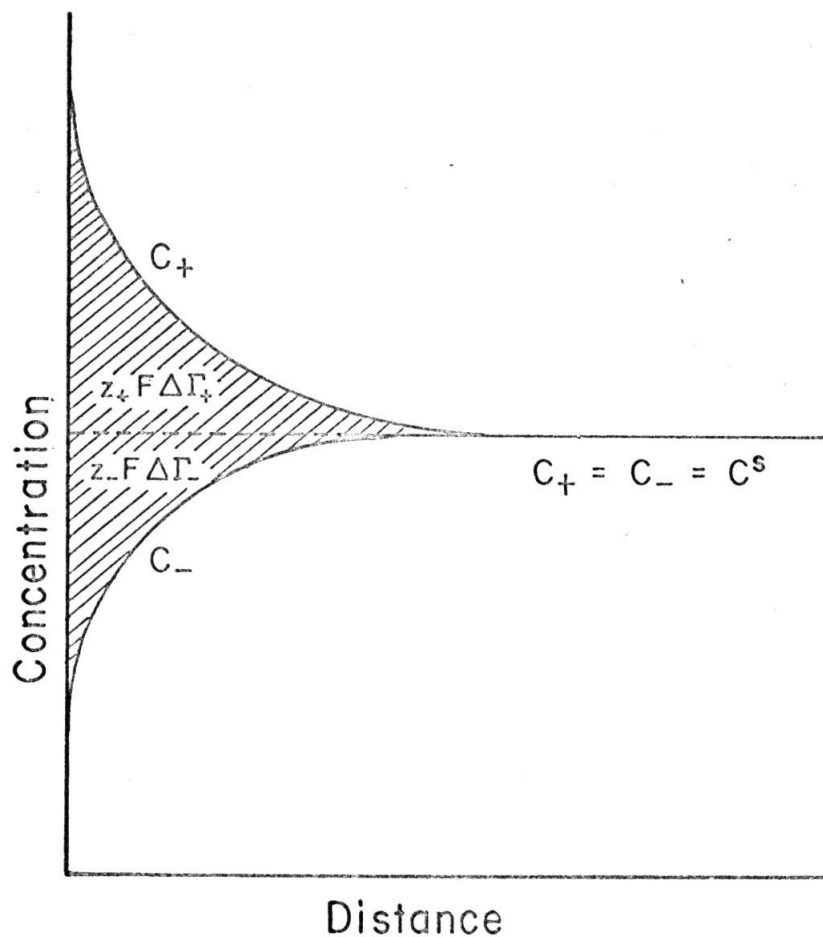


Figure 16. Schematic representation of the initial change in the composition of the diffuse layer following an abrupt shift in the potential of the electrode from E_0 to $E_1 < E_0$. For pictorial convenience, E_0 was chosen to be the potential of zero charge and the solution was assumed to contain only a single symmetrical electrolyte of concentration C^S .

application of the chronopotentiometric and potential step chronocoulometric techniques to the attempted "faradaic integration" of the diffuse double layer.

CHAPTER 7.

The Relative Population Densities in the
Diffuse Double Layer for Mixtures of Ions

In the absence of specific adsorption, the psi potential and the excess charge in the diffuse double layer can be related by the Gouy-Chapman Theory (72). This relationship can be expressed as follows for an infinite planar electrode,

$$-\sigma = \sum z_j F \Gamma_j = \pm \left[\frac{RT}{2\pi} \frac{\epsilon}{\sum_j C_j^S} (e^{-z_j F \psi_2 / RT} - 1) \right]^{\frac{1}{2}} \quad (1)$$

where $-\sigma$ is the excess surface charge in the diffuse layer in C/cm², Γ_j is the surface excess of the j^{th} ionic species in moles/cm², ϵ is the dielectric constant in the nonrationalized, MKS system ($78.5 \times 1.11 \times 10^{-12}$ C/volt-cm in water at 25°C), C_j^S is the bulk concentration of the j^{th} ionic species in moles/cm³, z_j is the charge, with sign, of the j^{th} ionic species, ψ_2 is the psi potential measured at the outer Helmholtz plane ($x = x_2$), and the summation is taken over all of the ions in the solution. The notation is that of Delahay (72).

The contribution of individual ions to the excess surface charge in the diffuse double layer can be calculated as follows,

$$q_j^{2-S} = z_j F \Gamma_j = \int_{x_2}^{\infty} (\rho_j - z_j F C_j^S) dx' \quad (2)$$

(72) P. Delahay, "Double Layer and Electrode Kinetics," Interscience, Inc., N. Y., 1965, Chapter 3.

where ρ_j is the charge density of the j^{th} ionic species in C/cm^3 at a distance x' from the electrode surface and $z_j F C_j^S$ is the uniform charge density of the j^{th} ionic species in the bulk of the solution. The integration is carried out over that region of the solution where the psi potential is non-zero. Since

$$\rho_j(x) = z_j F C_j^S \exp[-z_j F \psi(x)/RT] \quad (3)$$

$$\nabla \psi \cdot \nabla \psi = \frac{8\pi RT}{\epsilon} \sum_j C_j^S \{ \exp - z_j F \psi / RT - 1 \} \quad (4)$$

Equation (2) becomes (69)

$$q_j^2 - s = \pm z_j F C_j^S \int_{x_2}^{\infty} \left[\frac{8\pi RT}{\epsilon} \sum C_j^S (e^{-z_j F \psi / RT} - 1) \right]^{\frac{1}{2}} (e^{-z_j F \psi / RT} - 1) \nabla \psi \cdot dx \quad (5)$$

$$= \pm z_j F C_j^S \int_{u(\psi_2)}^1 \frac{u^{z_j} - 1}{[\sum C_j^S (u^{z_j} - 1)]^{\frac{1}{2}}} \frac{du}{u} \quad (6)$$

$$u = \exp(-F\psi(x)/RT)$$

For solutions of salts of the same charge type, *i.e.*, $z_1 = z_2 = -z_3$, Eqns. (1) and (6) reduce to their more familiar forms,

$$-\sigma = 2 \left(\frac{RT\epsilon C^S}{2\pi} \right)^{\frac{1}{2}} \sinh \left(\frac{|z| F \psi_2}{2RT} \right) \quad (7)$$

$$q_j^2 - s = \pm \left(\frac{RT\epsilon C^S}{2\pi} \right)^{\frac{1}{2}} \left[e^{\pm |z| F\psi_2 / 2RT} - 1 \right] \quad (8)$$

where C^S is the sum of the concentrations of the cations in the bulk of the solution and where the \pm signs in (8) refer to cations and anions respectively.

We have evaluated Eqn. (6) for three component salt mixtures containing a +2 pilot ion, a singly charged indifferent cation, and a singly charged counter ion. The composition of the mixtures were chosen to include solutions comparable to those employed in this research program. We repeated the original calculations of Joshi and Parsons (69) in the course of debugging the method of calculation and agreement was obtained.

The numerical integration of Eqn. (6) was performed by the application of Simpson's rule. The integration interval was subdivided until the error in the integral was less than about 0.1 per cent. Some difficulty was experienced in the calculation of the integrand for $u \sim 1$ under conditions where both the numerator and the denominator are tending to zero. Therefore the integrand was set equal to zero for $|1 - u| < 10^{-6}$.

Unfortunately, Eqns. (1) and (6) cannot be combined to obtain the total charge density in the diffuse layer as the dependent variable. Therefore the results of these calculations are presented in Table I as a function of the psi potential. This table is directly applicable to either solutions of doubly charged electroactive cations or electroactive anions. When the table is applied to anions, ψ_2 is replaced by $-\psi_2$. This feature

Table I

Charge composition of the diffuse double layer for a solution composed of a mixture of 0.5 mF doubly charged cations and varying amounts of a singly charged supporting electrolyte with a common counter-ion. Calculated from Gouy-Chapman theory in the absence of specific adsorption.

A. 0.5 mF supporting electrolyte

ψ , mv	Q_e , $\mu\text{C}/\text{cm}^2$	$-2F\Gamma_1/Q_e$	$2F\Gamma_1$, $\mu\text{C}/\text{cm}^2$	$F\Gamma_2$, $\mu\text{C}/\text{cm}^2$	$-F\Gamma_3$, $\mu\text{C}/\text{cm}^2$
-130	-20.746	0.980	20.326	0.278	C.126
-128	-19.196	0.978	18.782	0.273	C.126
-126	-17.763	0.977	17.355	0.268	C.126
-124	-16.437	0.976	16.035	0.263	C.126
-122	-15.210	0.974	14.814	0.258	C.127
-120	-14.075	0.972	13.685	0.253	C.127
-118	-13.025	0.970	12.641	0.248	C.127
-116	-12.054	0.969	11.675	0.243	C.127
-114	-11.156	0.967	10.782	0.238	C.127
-112	-10.324	0.964	9.956	0.233	C.127
-110	-9.555	0.962	9.193	0.228	C.127
-108	-8.844	0.960	8.487	0.223	C.127
-106	-8.185	0.957	7.834	0.218	C.126
-104	-7.576	0.954	7.231	0.213	C.126
-102	-7.013	0.952	6.673	0.209	C.126
-100	-6.491	0.948	6.157	0.204	C.126
-95	-5.352	0.940	5.031	0.191	C.125
-90	-4.414	0.930	4.107	0.179	C.125
-85	-3.641	0.919	3.348	0.167	C.123
-80	-3.004	0.907	2.725	0.155	C.122
-75	-2.479	0.893	2.213	0.143	C.120
-70	-2.045	0.877	1.794	0.131	C.118
-65	-1.687	0.859	1.450	0.120	C.116
-60	-1.391	0.840	1.168	0.109	C.113
-55	-1.145	0.819	0.937	0.097	C.110
-50	-0.941	0.795	0.748	0.087	C.105
-40	-0.627	0.743	0.467	0.066	C.095
-30	-0.404	0.686	0.277	0.047	C.080
-20	-0.238	0.624	0.149	0.029	C.060
-10	-0.109	0.562	0.061	0.014	C.034
0	0.	0.	0.	0.	-C.
10	C.099	0.441	-0.043	-0.012	-C.043
20	C.195	0.385	-0.075	-0.022	-C.098
30	C.295	0.334	-0.099	-0.030	-C.165
40	C.404	0.289	-0.117	-0.038	-C.249
50	C.527	0.248	-0.131	-0.044	-C.353
60	C.670	0.212	-0.142	-0.049	-C.479
70	C.838	0.180	-0.151	-0.053	-C.634
80	1.038	0.152	-0.158	-0.056	-C.823
90	1.276	0.128	-0.164	-0.059	-1.053
100	1.564	0.108	-0.168	-0.061	-1.333
110	1.910	0.090	-0.172	-0.063	-1.674
120	2.330	0.075	-0.175	-0.065	-2.089
130	2.837	0.063	-0.178	-0.066	-2.592
135	3.130	0.057	-0.179	-0.067	-2.884
140	3.453	0.052	-0.180	-0.067	-3.205
145	3.808	0.048	-0.181	-0.068	-3.559
150	4.200	0.043	-0.182	-0.068	-3.950
155	4.631	0.039	-0.183	-0.068	-4.381
160	5.106	0.036	-0.183	-0.069	-4.857
165	5.630	0.033	-0.184	-0.069	-5.383
170	6.207	0.030	-0.185	-0.069	-5.967
175	6.843	0.027	-0.185	-0.069	-6.617
180	7.543	0.025	-0.186	-0.070	-7.346
185	8.315	0.022	-0.186	-0.070	-8.172
190	9.166	0.020	-0.186	-0.070	-9.119
195	10.104	0.018	-0.187	-0.070	-10.222
200	11.138	0.017	-0.187	-0.070	-11.532

B. 1.0 mF supporting electrolyte

ψ , mv	Q_e , $\mu\text{C}/\text{cm}^2$	$-2F\Gamma_1/Q_e$	$2F\Gamma_1$, $\mu\text{C}/\text{cm}^2$	$F\Gamma_2$, $\mu\text{C}/\text{cm}^2$	$-F\Gamma_3$, $\mu\text{C}/\text{cm}^2$
-130	-20.810	0.965	20.092	0.537	C.156
-128	-19.261	0.963	18.554	0.527	C.156
-126	-17.827	0.961	17.132	0.517	C.156
-124	-16.501	0.959	15.817	0.507	C.156
-122	-15.274	0.956	14.602	0.497	C.156
-120	-14.139	0.953	13.478	0.487	C.156
-118	-13.089	0.950	12.439	0.477	C.156
-116	-12.118	0.947	11.479	0.467	C.156
-114	-11.219	0.944	10.591	0.458	C.156
-112	-10.388	0.941	9.771	0.448	C.156
-110	-9.618	0.937	9.012	0.438	C.156
-108	-8.907	0.933	8.311	0.428	C.156
-106	-8.248	0.929	7.664	0.418	C.156
-104	-7.639	0.925	7.065	0.408	C.156
-102	-7.075	0.920	6.512	0.399	C.156
-100	-6.553	0.916	6.001	0.389	C.155
-98	-6.071	0.911	5.529	0.379	C.155
-96	-5.624	0.906	5.093	0.369	C.155
-94	-5.211	0.900	4.691	0.360	C.154
-92	-4.828	0.894	4.319	0.350	C.154
-90	-4.474	0.888	3.975	0.340	C.153
-85	-3.700	0.872	3.228	0.316	C.152
-80	-3.062	0.855	2.617	0.293	C.150
-75	-2.535	0.835	2.116	0.270	C.148
-70	-2.100	0.813	1.707	0.247	C.145
-65	-1.740	0.789	1.373	0.224	C.142
-60	-1.442	0.763	1.100	0.202	C.139
-55	-1.194	0.736	0.878	0.181	C.134
-50	-0.987	0.707	0.697	0.160	C.129
-40	-0.667	0.645	0.430	0.121	C.115
-30	-0.435	0.581	0.253	0.085	C.097
-20	-0.260	0.518	0.135	0.053	C.072
-10	-0.120	0.457	0.055	0.025	C.041
0	C.	0.	-0.	-0.	-C.
10	0.111	0.348	-0.039	-0.021	-C.051
20	C.221	0.301	-0.067	-0.039	-C.115
30	C.336	0.260	-0.087	-0.054	-C.195
40	C.463	0.223	-0.103	-0.066	-C.293
50	C.605	0.190	-0.115	-0.077	-C.413
60	C.771	0.162	-0.125	-0.086	-C.560
70	C.965	0.137	-0.133	-0.093	-C.739
80	1.196	0.116	-0.139	-0.099	-C.957
90	1.472	0.098	-0.144	-0.103	-1.224
100	1.804	0.082	-0.148	-0.107	-1.547
110	2.205	0.069	-0.151	-0.111	-1.941
120	2.689	0.057	-0.154	-0.113	-2.420
130	3.275	0.048	-0.156	-0.116	-3.002
135	3.614	0.044	-0.157	-0.117	-3.339
140	3.986	0.040	-0.158	-0.118	-3.710
145	4.397	0.036	-0.159	-0.118	-4.119
150	4.849	0.033	-0.160	-0.119	-4.570
155	5.347	0.030	-0.160	-0.120	-5.067
160	5.896	0.027	-0.161	-0.120	-5.617
165	6.500	0.025	-0.162	-0.121	-6.225
170	7.167	0.023	-0.162	-0.121	-6.899
175	7.901	0.021	-0.163	-0.122	-7.650
180	8.710	0.019	-0.163	-0.122	-8.492
185	9.601	0.017	-0.163	-0.123	-9.446
190	10.584	0.015	-0.164	-0.123	-10.539
195	11.667	0.014	-0.164	-0.123	-11.813
200	12.861	0.013	-0.164	-0.123	-13.325

C. 2.0 mF supporting electrolyte

ψ , mv	Q_e , $\mu\text{C}/\text{cm}^2$	$-2F\Gamma_1/Q_e$	$2F\Gamma_1$, $\mu\text{C}/\text{cm}^2$	$F\Gamma_2$, $\mu\text{C}/\text{cm}^2$	$-F\Gamma_3$, $\mu\text{C}/\text{cm}^2$
-130	-20.938	0.940	19.692	1.013	C.207
-128	-19.389	0.937	18.163	0.993	C.208
-126	-17.955	0.933	16.751	0.974	C.208
-124	-16.629	0.929	15.446	0.954	C.208
-122	-15.402	0.925	14.240	0.934	C.208
-120	-14.266	0.920	13.126	0.915	C.208
-118	-13.216	0.915	12.096	0.895	C.208
-116	-12.244	0.910	11.145	0.875	C.208
-114	-11.345	0.905	10.267	0.856	C.208
-112	-10.513	0.899	9.456	0.836	C.208
-110	-9.743	0.894	8.707	0.817	C.208
-108	-9.031	0.888	8.015	0.797	C.208
-106	-8.372	0.881	7.377	0.778	C.207
-104	-7.762	0.874	6.787	0.759	C.207
-102	-7.198	0.867	6.243	0.739	C.207
-100	-6.676	0.860	5.741	0.720	C.206
-98	-6.192	0.852	5.278	0.701	C.206
-96	-5.745	0.844	4.851	0.682	C.205
-94	-5.331	0.836	4.457	0.663	C.205
-92	-4.948	0.827	4.094	0.644	C.204
-90	-4.593	0.818	3.759	0.625	C.203
-85	-3.817	0.794	3.032	0.579	C.201
-80	-3.176	0.768	2.440	0.533	C.199
-75	-2.646	0.740	1.959	0.488	C.195
-70	-2.207	0.711	1.568	0.445	C.192
-65	-1.843	0.679	1.251	0.402	C.187
-60	-1.539	0.646	0.995	0.361	C.182
-55	-1.286	0.613	0.788	0.321	C.175
-50	-1.073	0.579	0.621	0.283	C.168
-40	-0.739	0.511	0.378	0.211	C.149
-30	-0.492	0.446	0.219	0.147	C.125
-20	-0.299	0.386	0.116	0.091	C.093
-10	-0.140	0.332	0.047	0.042	C.052
C	C.	0.	-0.	-0.	-C.
10	C.133	0.245	-0.033	-0.035	-C.065
20	C.266	0.210	-0.056	-0.065	-C.145
30	C.407	0.179	-0.073	-0.090	-C.244
40	C.562	0.153	-0.086	-0.111	-C.365
50	C.737	0.130	-0.096	-0.128	-C.513
60	0.940	0.111	-0.104	-0.142	-C.694
70	1.179	0.094	-0.110	-0.154	-C.914
80	1.462	0.079	-0.115	-0.163	-1.182
90	1.801	0.066	-0.120	-0.171	-1.508
100	2.208	0.056	-0.123	-0.178	-1.905
110	2.698	0.047	-0.126	-0.183	-2.388
120	3.292	0.039	-0.128	-0.188	-2.975
130	4.010	0.032	-0.130	-0.191	-3.688
135	4.425	0.029	-0.130	-0.193	-4.100
140	4.881	0.027	-0.131	-0.194	-4.555
145	5.384	0.024	-0.132	-0.196	-5.056
150	5.938	0.022	-0.132	-0.197	-5.608
155	6.548	0.020	-0.133	-0.198	-6.218
160	7.220	0.018	-0.133	-0.199	-6.891
165	7.961	0.017	-0.134	-0.200	-7.636
170	8.777	0.015	-0.134	-0.201	-8.461
175	9.676	0.014	-0.135	-0.201	-9.381
180	10.667	0.013	-0.135	-0.202	-10.413
185	11.759	0.012	-0.135	-0.203	-11.580
190	12.962	0.010	-0.136	-0.203	-12.919
195	14.289	0.010	-0.136	-0.204	-14.479
200	15.751	0.009	-0.136	-0.204	-16.332

D. 5.0 mF supporting electrolyte

ψ , mv	Q_e , $\mu\text{C}/\text{cm}^2$	$-2F\Gamma_1/Q_e$	$2F\Gamma_1$, $\mu\text{C}/\text{cm}^2$	$F\Gamma_2$, $\mu\text{C}/\text{cm}^2$	$-F\Gamma_3$, $\mu\text{C}/\text{cm}^2$
-130	-21.319	0.878	18.721	2.241	C.328
-128	-19.768	0.871	17.221	2.193	C.328
-126	-18.333	0.864	15.837	2.144	C.328
-124	-17.006	0.856	14.559	2.096	C.328
-122	-15.777	0.848	13.381	2.048	C.329
-120	-14.641	0.840	12.294	1.999	C.328
-118	-13.589	0.831	11.291	1.952	C.328
-116	-12.615	0.822	10.367	1.904	C.328
-114	-11.715	0.812	9.515	1.856	C.328
-112	-10.881	0.802	8.731	1.809	C.328
-110	-10.109	0.792	8.008	1.762	C.327
-108	-9.395	0.781	7.342	1.715	C.327
-106	-8.734	0.770	6.729	1.668	C.326
-104	-8.122	0.759	6.164	1.622	C.325
-102	-7.555	0.747	5.645	1.576	C.325
-100	-7.030	0.735	5.168	1.530	C.324
-98	-6.544	0.723	4.729	1.485	C.323
-96	-6.094	0.710	4.325	1.440	C.322
-94	-5.677	0.697	3.954	1.395	C.321
-92	-5.290	0.683	3.614	1.351	C.319
-90	-4.932	0.669	3.301	1.307	C.318
-88	-4.146	0.634	2.628	1.199	C.314
-86	-3.494	0.597	2.086	1.095	C.309
-84	-2.951	0.559	1.651	0.994	C.303
-82	-2.499	0.522	1.303	0.896	C.297
-80	-2.120	0.484	1.026	0.803	C.289
-78	-1.800	0.447	0.805	0.714	C.280
-76	-1.529	0.411	0.629	0.630	C.269
-74	-1.297	0.377	0.490	0.550	C.256
-72	-1.092	0.316	0.291	0.404	C.226
-70	-0.832	0.263	0.166	0.278	C.187
-68	-0.594	0.219	0.086	0.169	C.138
-66	-0.389	0.183	0.035	0.077	C.077
-64	0.	0.	0.	0.	0.
-62	0.183	0.130	-0.024	-0.065	-0.094
-60	0.370	0.110	-0.041	-0.119	-0.210
-58	0.568	0.093	-0.053	-0.163	-0.352
-56	0.788	0.079	-0.062	-0.200	-0.525
-54	1.037	0.067	-0.069	-0.231	-0.736
-52	1.325	0.057	-0.075	-0.256	-0.993
-50	1.663	0.048	-0.079	-0.276	-1.306
-48	2.064	0.040	-0.083	-0.294	-1.686
-46	2.543	0.034	-0.086	-0.308	-2.148
-44	3.119	0.028	-0.088	-0.319	-2.710
-42	3.814	0.024	-0.090	-0.329	-3.393
-40	4.654	0.020	-0.092	-0.337	-4.223
-38	5.670	0.016	-0.093	-0.343	-5.232
-36	6.256	0.015	-0.094	-0.346	-5.815
-34	6.902	0.014	-0.094	-0.348	-6.458
-32	7.613	0.012	-0.095	-0.351	-7.166
-30	8.396	0.011	-0.095	-0.353	-7.948
-28	9.259	0.010	-0.096	-0.355	-8.810
-26	10.210	0.009	-0.096	-0.356	-9.762
-24	11.257	0.009	-0.096	-0.358	-10.815
-22	12.411	0.008	-0.096	-0.359	-11.983
-20	13.683	0.007	-0.097	-0.361	-13.284
-18	15.085	0.006	-0.097	-0.362	-14.743
-16	16.629	0.006	-0.097	-0.363	-16.394
-14	18.331	0.005	-0.097	-0.364	-18.288
-12	20.207	0.005	-0.098	-0.365	-20.494
-10	22.275	0.004	-0.098	-0.366	-23.114

E. 10 mF supporting electrolyte

ψ , mv	Q_e , $\mu\text{C}/\text{cm}^2$	$-2F\Gamma_1/Q_e$	$2F\Gamma_1$, $\mu\text{C}/\text{cm}^2$	$F\Gamma_2$, $\mu\text{C}/\text{cm}^2$	$-F\Gamma_3$, $\mu\text{C}/\text{cm}^2$
-130	-21.938	0.798	17.498	3.922	C.477
-128	-20.384	0.787	16.050	3.827	C.477
-126	-18.947	0.776	14.709	3.733	C.477
-124	-17.616	0.765	13.474	3.639	C.477
-122	-16.384	0.753	12.338	3.546	C.477
-120	-15.244	0.741	11.292	3.453	C.477
-118	-14.188	0.728	10.331	3.361	C.476
-116	-13.211	0.715	9.447	3.270	C.476
-114	-12.306	0.702	8.635	3.179	C.475
-112	-11.468	0.688	7.889	3.089	C.474
-110	-10.691	0.674	7.204	3.000	C.474
-108	-9.972	0.659	6.575	2.911	C.473
-106	-9.306	0.645	5.998	2.823	C.471
-104	-8.688	0.630	5.470	2.736	C.470
-102	-8.115	0.614	4.985	2.650	C.469
-100	-7.584	0.599	4.542	2.565	C.467
-98	-7.091	0.583	4.136	2.481	C.466
-96	-6.634	0.567	3.764	2.398	C.464
-94	-6.210	0.551	3.424	2.316	C.462
-92	-5.816	0.535	3.114	2.235	C.460
-90	-5.450	0.519	2.830	2.156	C.457
-88	-5.110	0.503	2.570	2.078	C.454
-86	-4.794	0.487	2.334	1.999	C.451
-84	-4.500	0.471	2.120	1.922	C.448
-82	-4.228	0.455	1.926	1.847	C.443
-80	-3.978	0.439	1.744	1.777	C.443
-78	-3.748	0.423	1.574	1.707	C.443
-76	-3.538	0.407	1.416	1.637	C.443
-74	-3.348	0.391	1.270	1.567	C.443
-72	-3.178	0.375	1.136	1.497	C.443
-70	-3.028	0.359	1.014	1.427	C.443
-68	-2.898	0.343	0.904	1.357	C.443
-66	-2.788	0.327	0.806	1.287	C.443
-64	-2.698	0.311	0.720	1.217	C.443
-62	-2.628	0.295	0.646	1.147	C.443
-60	-2.578	0.279	0.584	1.077	C.443
-58	-2.538	0.263	0.534	1.007	C.443
-56	-2.508	0.247	0.494	0.937	C.443
-54	-2.488	0.231	0.464	0.867	C.443
-52	-2.478	0.215	0.434	0.797	C.443
-50	-2.478	0.199	0.414	0.727	C.443
-48	-2.488	0.183	0.394	0.657	C.443
-46	-2.508	0.167	0.374	0.587	C.443
-44	-2.538	0.151	0.354	0.517	C.443
-42	-2.578	0.135	0.334	0.447	C.443
-40	-2.628	0.119	0.314	0.377	C.443
-38	-2.688	0.103	0.294	0.307	C.443
-36	-2.748	0.087	0.274	0.237	C.443
-34	-2.818	0.071	0.254	0.167	C.443
-32	-2.898	0.055	0.234	0.097	C.443
-30	-2.988	0.039	0.214	0.027	C.443
-28	-3.088	0.023	0.194	-0.043	C.443
-26	-3.198	0.007	0.174	-0.113	C.443
-24	-3.318	-0.009	0.154	-0.183	C.443
-22	-3.448	-0.025	0.134	-0.253	C.443
-20	-3.588	-0.041	0.114	-0.323	C.443
-18	-3.738	-0.057	0.094	-0.393	C.443
-16	-3.898	-0.073	0.074	-0.463	C.443
-14	-4.068	-0.089	0.054	-0.533	C.443
-12	-4.248	-0.105	0.034	-0.603	C.443
-10	-4.438	-0.121	0.014	-0.673	C.443
-8	-4.638	-0.137	0.004	-0.743	C.443
-6	-4.848	-0.153	-0.016	-0.813	C.443
-4	-5.068	-0.169	-0.036	-0.883	C.443
-2	-5.298	-0.185	-0.056	-0.953	C.443
0	C.	0.	-0.	-0.	-C.
2	C.245	0.073	-0.018	-0.097	-C.130
4	C.496	0.061	-0.030	-0.177	-C.288
6	C.765	0.052	-0.040	-0.244	-C.481
8	1.063	0.044	-0.046	-0.298	-C.717
10	1.400	0.037	-0.052	-0.344	-1.004
12	1.790	0.031	-0.056	-0.381	-1.352
14	2.248	0.026	-0.059	-0.412	-1.776
16	2.792	0.022	-0.062	-0.437	-2.292
18	3.442	0.019	-0.064	-0.458	-2.917
20	4.222	0.016	-0.066	-0.475	-3.679
22	5.163	0.013	-0.067	-0.489	-4.604
24	6.300	0.011	-0.068	-0.501	-5.728
26	7.676	0.009	-0.069	-0.510	-7.094
28	8.470	0.008	-0.070	-0.514	-7.884
30	9.345	0.008	-0.070	-0.518	-8.754
32	10.308	0.007	-0.071	-0.522	-9.714
34	11.368	0.006	-0.071	-0.525	-10.772
36	12.537	0.006	-0.071	-0.527	-11.940
38	13.824	0.005	-0.071	-0.530	-13.229
40	15.242	0.005	-0.072	-0.532	-14.655
42	16.805	0.004	-0.072	-0.534	-16.236
44	18.527	0.004	-0.072	-0.536	-17.998
46	20.424	0.004	-0.072	-0.538	-19.973
48	22.516	0.003	-0.072	-0.539	-22.209
50	24.820	0.003	-0.072	-0.541	-24.773
52	27.360	0.003	-0.073	-0.542	-27.760
54	30.160	0.002	-0.073	-0.543	-31.307

of the results is due to the fact that only the product $z_j \psi_2$ appears in these calculations.

The charge fraction of the diffuse layer which is composed of electroactive material is presented as a function of the total charge in the diffuse double layer in Fig. 17. It is evident that the doubly charged ions compose over fifty per cent of the diffuse layer in the presence of a twenty-fold molar excess of supporting electrolyte if the total diffuse layer charge is greater than about $5 \mu\text{C}/\text{cm}^2$. Thus, if we were willing to confine our interest to the potential region cathodic to about $-700 \text{ mv. vs. S.C.E.}$ for electroactive cations and anodic to about $-300 \text{ mv. vs. S.C.E.}$ for electroactive anions, the diffuse layer would be composed principally of electroactive material even in the presence of an "excess" of supporting electrolyte.

The electronic charge/electrode potential data used in the preparation of Figs. 17 and 27 was that obtained for the charge density on the surface of a mercury electrode in 10 mF sodium perchlorate solutions (68). Although these data do not correspond exactly to the solution compositions described either in this chapter or in Chapters 8 and 9, it should be emphasized that this approximation does not alter the qualitative features and conclusions of any of the results presented in these chapters.

Inspection of the charge data presented in Table II reveals that the electronic charge on the surface of the electrode is insensitive to the solution concentration at fixed potential. From this information

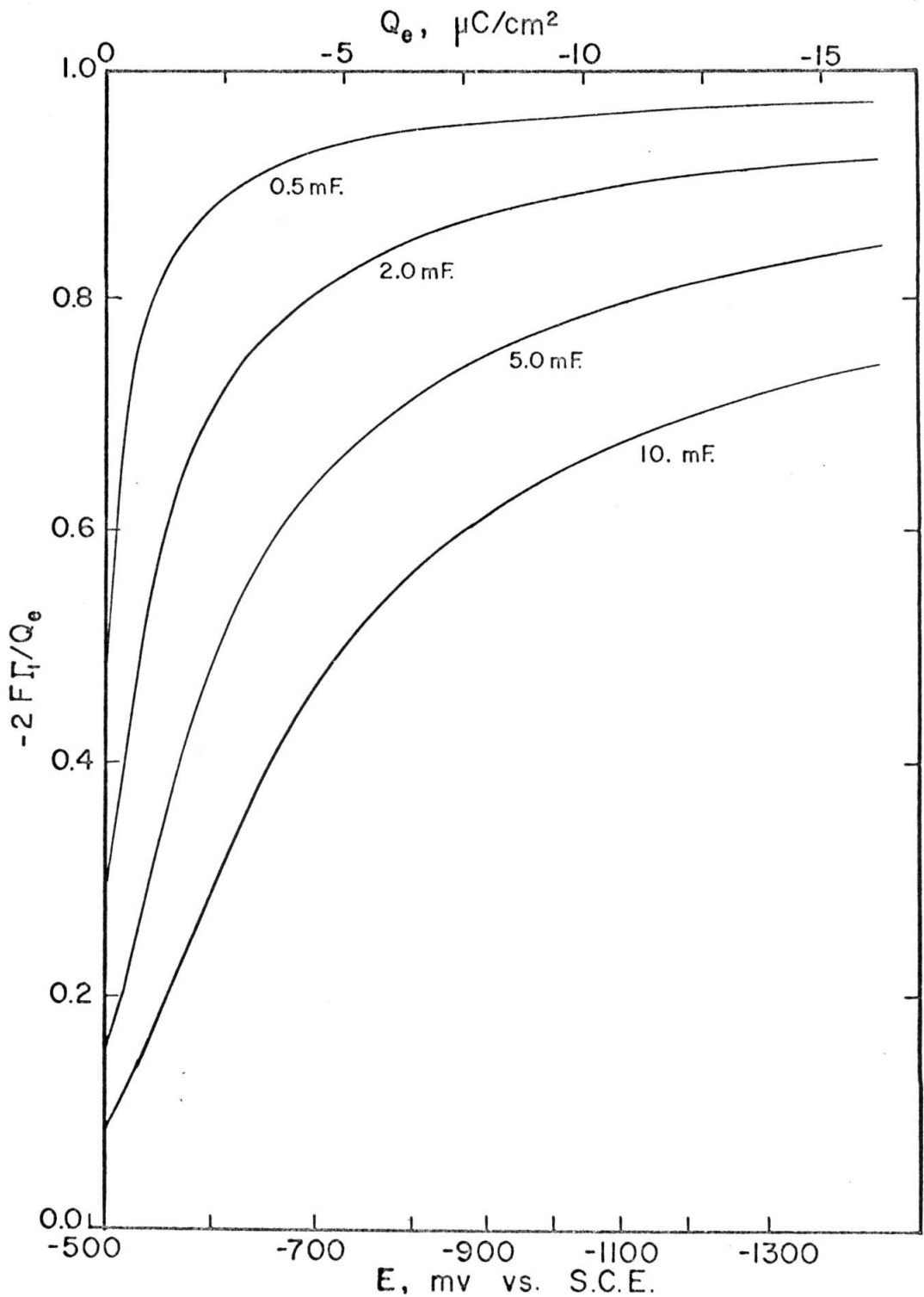


Figure 17. The fraction of the diffuse double-layer charge provided by a +2 ion whose bulk concentration is 0.5 mF as a function of the potential of the electrode and of the concentration of the singly charged indifferent electrolyte.

Table II

The Surface Excess of a 0.5 mF +2 Cation in the Presence of a 2.0 mF Singly Charged Supporting Electrolyte and Experimental Values of the Charge on the Electrode Surface as a Function of the Potential of the Electrode

E, mv. vs. S. C. E.	$2F\Gamma$, $\mu\text{C}/\text{cm}^2$	Q_e , $\mu\text{C}/\text{cm}^2$	
		0.01 mF*	0.03 mF*
-1300		-13.9	
1250		13.0	-14.3
1200		12.2	13.5
1150		11.5	12.8
1100	+9.7	10.8	12.0
1050	8.9	10.1	11.2
1000	8.4	9.4	10.4
950	7.7	8.7	9.6
900	7.0	8.0	8.8
850	6.2	7.2	7.9
800	5.4	6.4	7.0
750	4.5	5.4	6.2
700	3.6	4.4	5.1
650	2.5	3.3	4.1
600	1.6	2.2	3.1
550	0.55	1.0	1.9
500	-0.07	+ 0.35	0.5
450	.12	1.6	+ .9
400	.13	2.9	
350	.13	4.15	
300		5.5	
250		6.8	
200		8.1	
150		9.3	
100		10.5	

* Data for NaClO_4 . (68)

we estimate that the theoretical curves presented in Figs. 17 and 27 are accurate at the most anodic potentials but need to be shifted by perhaps 100 mv. at the most cathodic potentials.

CHAPTER 8.

Chronopotentiometric Results

It is impossible to measure the absolute potential difference between the indicator electrode and the reference electrode in solutions of low conductivity because of the large and position-sensitive voltage developed across the "uncompensated" resistance between the tip of even a Luggin capillary and the surface of the indicator electrode when current is passing through the cell. The measured potential is also in error by a liquid junction due to the electrolysis of the material in the vicinity of the electrode. Fortunately, under conditions of constant current, the presence of these error voltages does not render the chronopotentiometric technique inapplicable as long as the sum of these voltages remains approximately constant during the course of the experiment since only a knowledge of the change in the potential of the indicator electrode is necessary for the determination of the transition time.

Constancy of V

We can determine the magnitude of these voltages by integrating the expression given above for $\nabla\phi$ (p. 107).

$$V(t) = \int \nabla\phi \cdot \vec{dx} = \frac{RT}{F(z_1D_1 - z_3D_3)} \left[\frac{i_0}{z_1F} \int \frac{dx}{C_1} - (D_1 - D_3) \int \frac{\nabla C_1}{C_1} \cdot \vec{dx} \right] \quad (1)$$

The change in this voltage is given by

$$\Delta V(t) = V(t) - V(0) \quad (2)$$

$$= \frac{RT}{F(z_1 D_1 - z_3 D_3)} \left[\frac{i_0}{z_1 F} \int \frac{C_1^S - C_1}{C_1 C_1^S} dx - (D_1 - D_3) \ln \frac{C_1^S}{C_1(0,t)} \right] \quad (3)$$

where C_1^S is the bulk concentration of the electroactive species.

At a distance greater than the thickness of the diffusion layer from the surface of the electrode, $C_1 \sim C_1^S$. Thus the integrand in Eqn. (3) is essentially zero for $x \gg 20\sqrt{D_S t}$ and only a negligible error results if this value of the distance coordinate is introduced as the upper limit of integration.

$$\Delta V(t) = \frac{RT}{F(z_1 D_1 - z_3 D_3)} \left[\frac{i_0}{z_1 F} \int_0^{20\sqrt{D_S t}} \frac{C_1^S - C_1}{C_1 C_1^S} dx - (D_1 - D_3) \ln \frac{C_1^S}{C_1(0,t)} \right] \quad (4)$$

$C_1(x,t)$ is given by

$$C_1(x,t) = C_1^S - 2\lambda \sqrt{\frac{D_S t}{\pi}} \exp \frac{-x^2}{4D_S t} + \lambda \operatorname{erfc} \frac{x}{2\sqrt{D_S t}} \quad (5)$$

where

$$i_0 = \frac{z_1 F C_1^S D_1}{2} \frac{z_3 - z_1}{z_3} \sqrt{\frac{\pi}{D_S \tau}} \quad (6)$$

and

$$\lambda = \frac{i_0}{z_1 F D_1} \frac{z_3}{z_3 - z_1} = \frac{C_1^S}{2} \sqrt{\frac{\pi}{D_3 \tau}} \quad (7)$$

Therefore,

$$C_1(x,t) = C_1^S \left[1 - \sqrt{\frac{t}{\tau}} e^{-y^2} + \sqrt{\frac{\pi t}{\tau}} y \operatorname{erfc} y \right] \quad (8)$$

where

$$y = x/2\sqrt{D_s t}$$

Thus

$$\Delta V(t/\tau) = \frac{RT}{F(z_1 D_1 - z_3 D_3)} \left[D_1 \frac{z_3 - z_1}{z_3} \sqrt{\frac{\pi t}{\tau}} \psi + (D_1 - D_3) \ln \left\{ 1 - \sqrt{\frac{t}{\tau}} \right\} \right] \quad (9)$$

where

$$\psi = \int_0^{1.0} \frac{e^{-y^2} - \pi^{\frac{1}{2}} y \operatorname{erfc} y}{\sqrt{\frac{\tau}{t}} - e^{-y^2} + \pi^{\frac{1}{2}} y \operatorname{erfc} y} dy \quad (10)$$

Since the change in the sum of the voltage developed across the uncompensated resistance and the liquid junction potential is a function only of the ratio t/τ , the distortion of the chronopotentiometric E-t curves by changes in this voltage is independent of the current density and the solution concentration.

Values of ψ and of $\Delta V(t/\tau)$ are listed in Table I for solutions of zinc perchlorate and perchloric acid. The " iR_u " term and the "liquid junction" term add in the case of zinc perchlorate ($D_{\text{ClO}_4^-} > D_{\text{Zn}^{++}}$) but have opposite signs for perchloric acid ($D_{\text{ClO}_4^-} < D_{\text{H}^+}$). The values of ΔV become similar for these solutions for large values of t/τ . This treatment results in the interesting prediction that the sign of ΔV changes during the experiment for the reduction of perchloric acid.

The distortion of the chronopotentiograms for the reversible and irreversible reduction of zinc perchlorate are illustrated in Fig. 18.

In the presence of some supporting electrolyte, the variation of the sum of the liquid junction potential and the voltage developed across the uncompensated resistance cannot be calculated analytically.

Table I

The Function ψ and the Net Distortion of the Chronopotentiometric Wave in the Absence of Supporting Electrolyte

t/τ	ψ	HClO_4		$\text{Zn}(\text{ClO}_4)_2$	
		Liquid Junction, mv	ΔV , mv	Liquid Junction, mv	ΔV , mv
0.050	0.114	-4.40	-2.46	2.17	2.94
.100	.172	-6.61	-2.46	3.25	4.90
.150	.223	-8.52	-1.94	4.19	6.81
.200	.271	-10.31	-1.07	5.08	8.75
.250	.318	-12.05	0.08	5.94	10.76
.300	.366	-13.80	1.49	6.79	12.87
.350	.415	-15.57	3.15	7.67	15.11
.400	.466	-17.40	5.08	8.57	17.51
.450	.519	-19.32	7.28	9.51	20.09
.500	.577	-21.35	9.79	10.51	22.89
.550	.639	-23.53	12.65	11.59	25.97
.600	.707	-25.90	15.93	12.76	29.39
.650	.784	-28.53	19.71	14.05	33.23
.700	.871	-31.50	24.13	15.51	37.63
.750	.973	-34.95	29.39	17.21	42.79
.800	1.10	-39.09	35.84	19.25	49.04
.850	1.26	-44.34	44.13	21.84	57.01
.900	1.48	-51.63	55.65	25.43	68.08
.950	1.87	-63.91	74.90	31.48	86.67
.960	1.99	-67.84	81.00	33.41	92.58
.970	2.15	-72.89	88.77	35.89	100.16
.980	2.38	-79.98	99.62	39.39	110.79
.990	2.76	-92.07	117.93	45.35	128.84
.995	3.15	-104.15	136.11	51.29	146.81
.999	4.15	-132.15	184.84	65.08	191.11

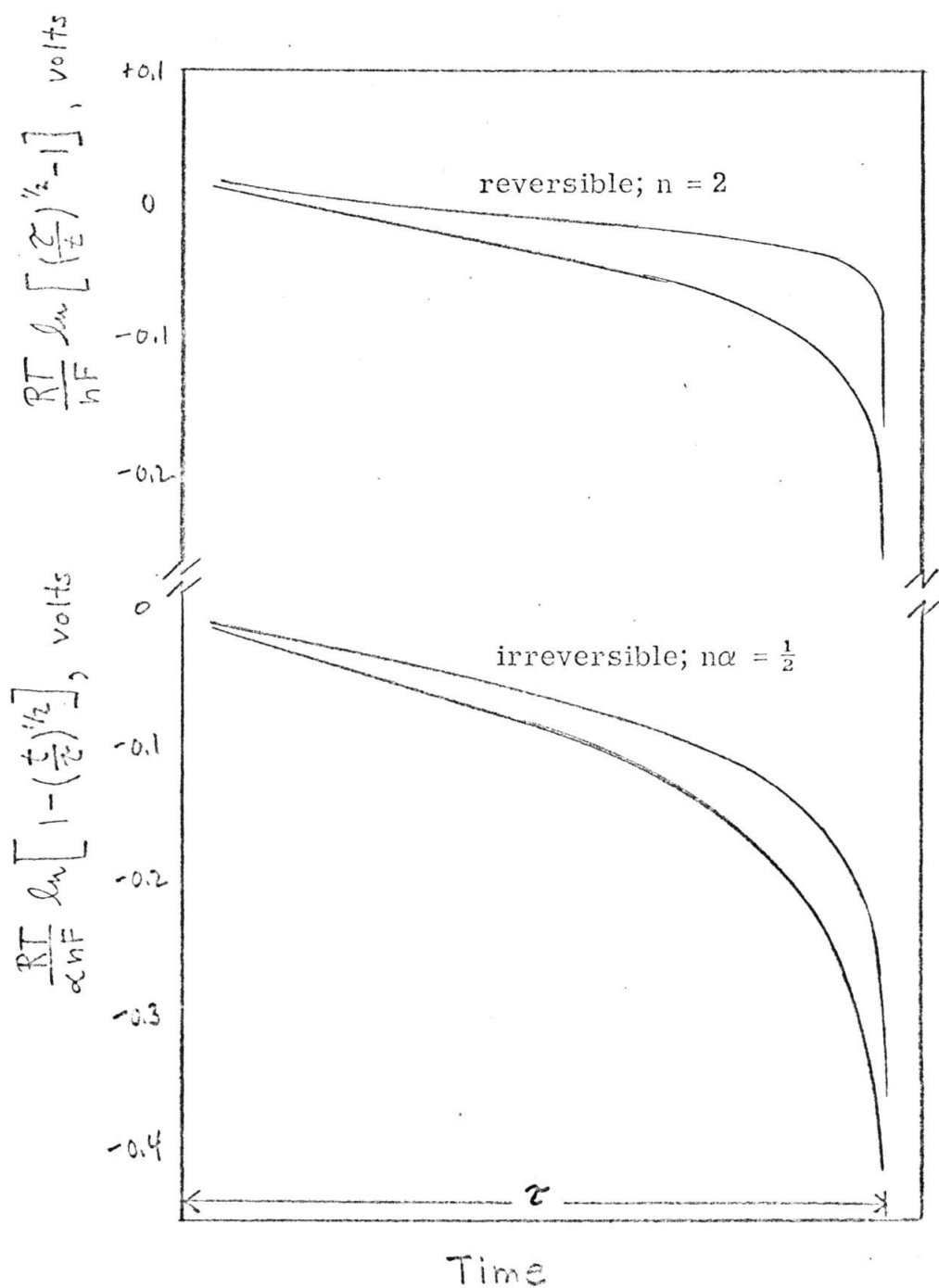


Figure 18. Schematic chronopotentiograms for the reversible and irreversible reduction of $\text{Zn}(\text{ClO}_4)_2$. The lower curve in each case is the theoretical E-t curve observed in the absence of supporting electrolyte.

However, the effects should be much less pronounced and probably totally negligible in the presence of even small amounts of supporting electrolyte.

Morphology of the Chronopotentiometric Wave

In the absence of sufficient supporting electrolyte, the chronopotentiometric reduction of solutions of chromate, cobalt(II), copper(II), thallium(I), and zinc(II) result in doublet chronopotentiometric waves while the reduction of hydrogen ion produces only a singlet chronopotentiometric wave. Morris and Lingane (59) had investigated the chronopotentiometric reduction of both copper(II) and thallium(I) in the absence of supporting electrolyte and they observed only singlet chronopotentiometric waves. Their experiments were conducted at somewhat lower current densities than those employed here and we have confirmed the fact that only singlet waves are observed under their conditions.

The morphology of the chronopotentiometric wave observed for the reduction of zinc(II) was investigated in some detail. Figure 19 illustrates the effect of increasing current density on the morphology of the chronopotentiometric wave observed for the reduction of zinc chloride; the doublet character of the wave seems to disappear with increasing current density. These effects disappear completely in the presence of a ten-fold excess of supporting electrolyte.

These doublet waves might be interpreted as indicating a slow equilibrium between the aquo zinc ion and one of the zinc hydroxy complexes; this hypothesis is rendered unlikely by the fact that the doublet

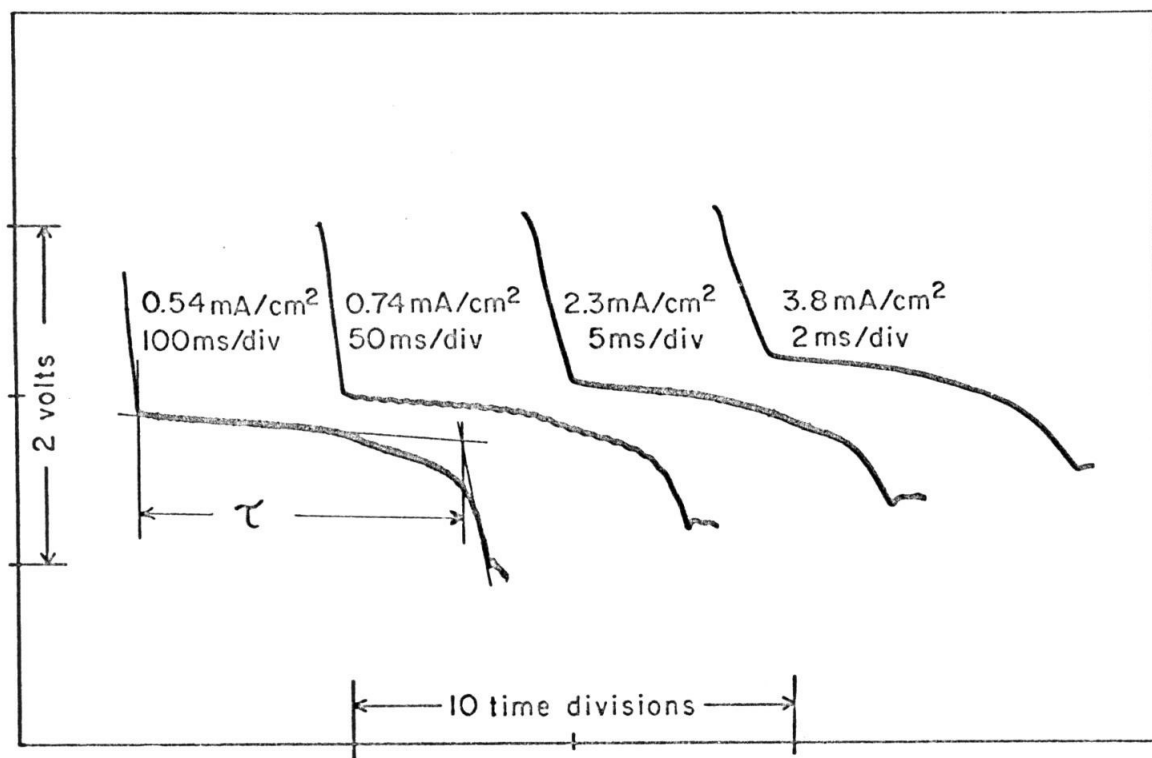


Figure 19. Experimental chronopotentiograms observed for the reduction of 0.4 mM ZnCl_2 , $\text{pH} = 3.7$, in the absence of supporting electrolyte. The absolute potential scale is unknown and the curves were shifted upwards one from another with increasing current density solely to aid in the clarity of the presentation.

waves are observed over a pH range of at least three to seven.

Chronopotentiograms for the reduction of zinc perchlorate and for the reduction of zinc chloride in the absence of supporting electrolyte are indistinguishable. This fact renders unlikely an ion pairing hypothesis whereby the doublet wave would correspond to the stepwise reduction of the simple aquo ion and an ion pair, e.g., ZnCl^+ , since such a hypothesis would require the ion pairing constants for ZnCl^+ and for ZnClO_4^+ to be similar in order to explain the similarity in the observed chronopotentiometric waves for these systems. The ion pairing constants appropriate to these systems are not known but they are probably very dissimilar.

Although we have attempted to discover the cause of the doublet character of these waves in terms of these and other models, a satisfactory explanation has eluded us.

The Chronopotentiometric Constant as a Function of Current Density

The transition times appropriate to the singlet chronopotentiometric waves were measured by the method of Reinmuth (73). The transition time appropriate to two successive chronopotentiometric waves is normally taken to be the sum of the transition times of the individual waves. The two chronopotentiometric waves observed in these experiments are not sufficiently separated on the voltage axis to allow this procedure to be employed in the present case. We have

(73) W. H. Reinmuth, Anal. Chem., 33, 485 (1961).

therefore approximated the transition times appropriate to the total doublet waves by the modification of the method of Reinmuth (73) illustrated in Fig. 19. We are encouraged that this approach is adequate since the chronopotentiometric constants observed for the reduction of the transition metal cations evince the same qualitative characteristics as that observed for the reduction of hydrogen ion.

The experimental values of the chronopotentiometric constant observed for the reduction of cobalt(II), thallium(I), zinc(II), and hydrogen ion are presented in Figs 20-24 as functions of the square roots of the observed transition times. Since the experimental determination of chronopotentiometric transition times, even at moderate current densities, in the presence of excess supporting electrolyte, and in the absence of multiple waves, is at best a consistent art, the data presented in these figures are open to ready criticism. The possibly controversial aspects of the procedures employed in these experiments have been constantly and carefully considered during the analysis of this data and it is our opinion that the qualitative aspects of these figures would be retained even if another procedure were adopted for the determination of the values of the transition time but that the absolute magnitudes of the chronopotentiometric constant obtained in the high current density regions might be substantially different from those reported here. For example, several of the other accepted methods (20) for the determination of the transition time were applied to portions of this data and although these procedures yielded values for the transition time varying by as

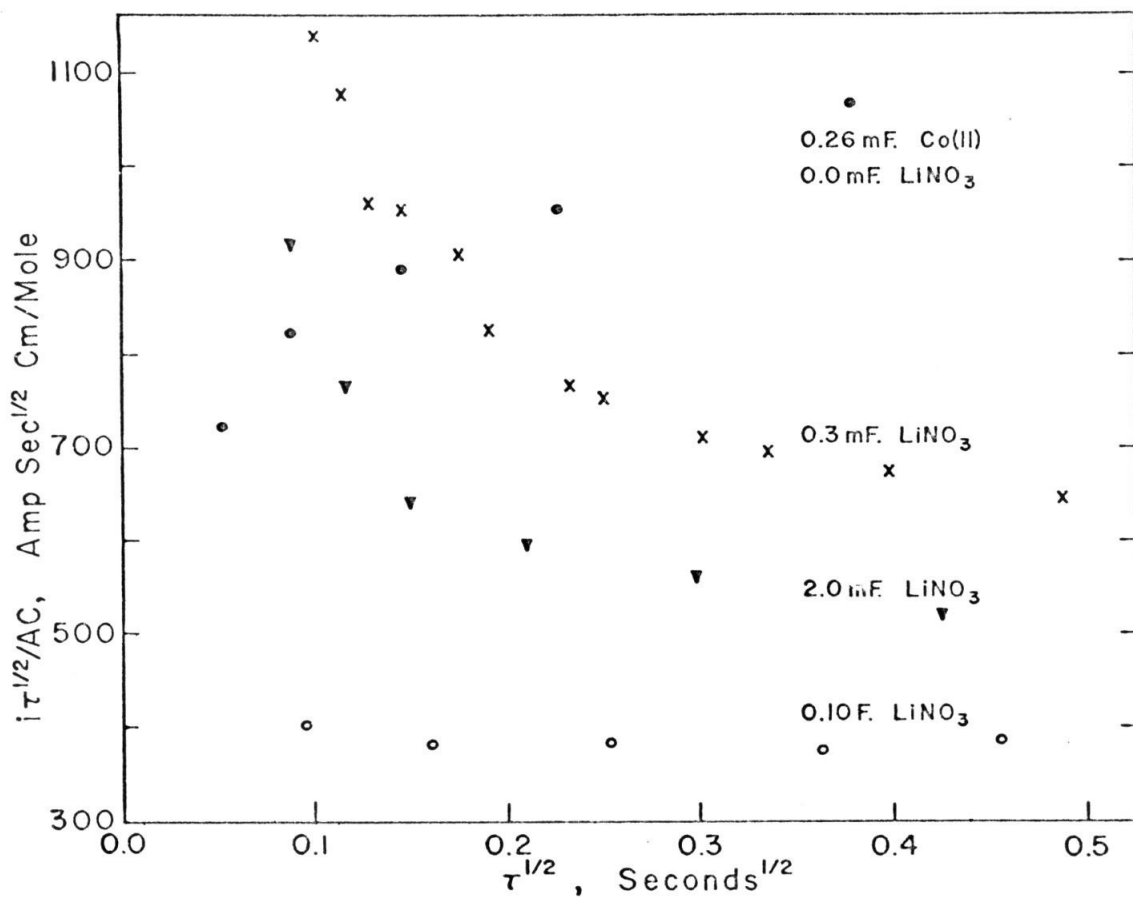


Figure 20. Plot of the chronopotentiometric constant as a function of the square root of the observed transition time for the reduction of Co(II) in the presence of increasing amounts of LiNO₃, pH ~ 6., Cu(Hg) reference electrode. Data was obtained using the circuit of Fig. 25 and the indicator electrode was prebiased at ~ -0.9 v. vs. S.C.E.

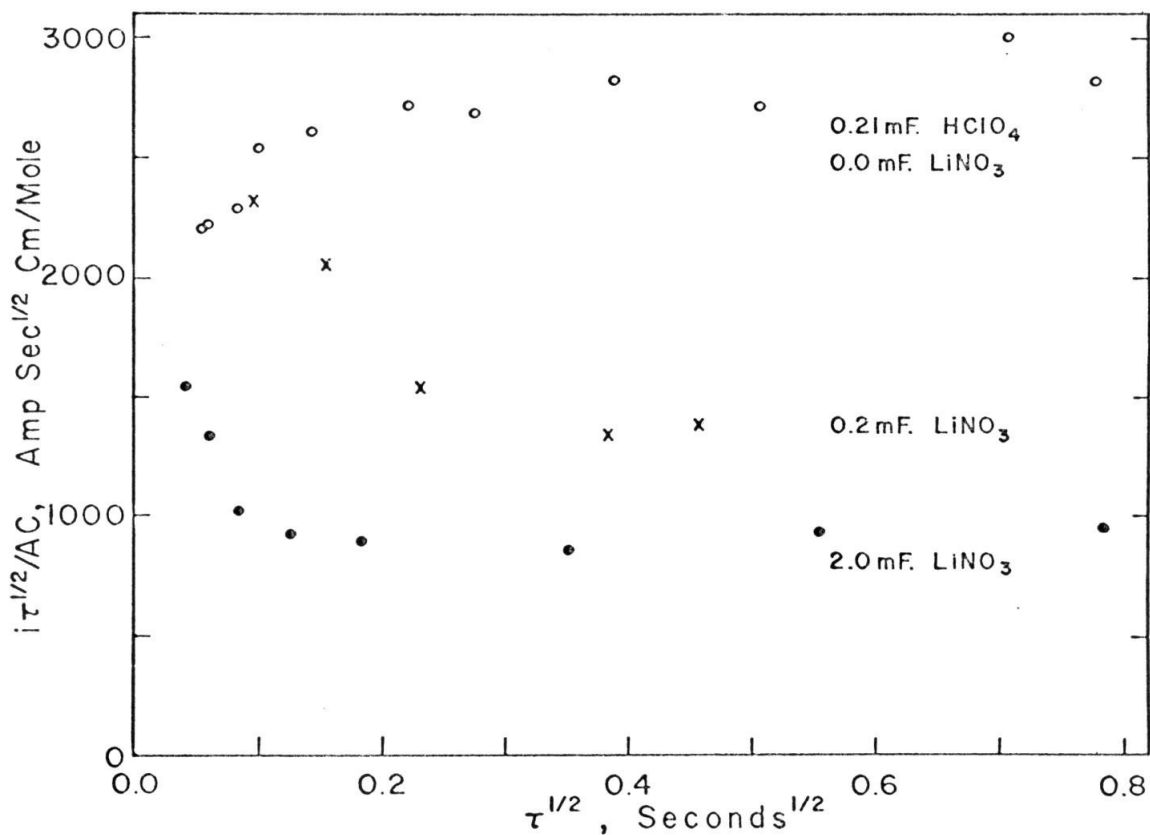


Figure 21. Plot of the chronopotentiometric constant as a function of the square root of the observed transition time for the reduction of hydrogen ion in the presence of increasing amounts of LiNO₃. Zn(Hg) reference electrode. Data was obtained using the circuit of Fig. 25 and the indicator electrode was prebiased at -1.3 v. vs. S.C.E.

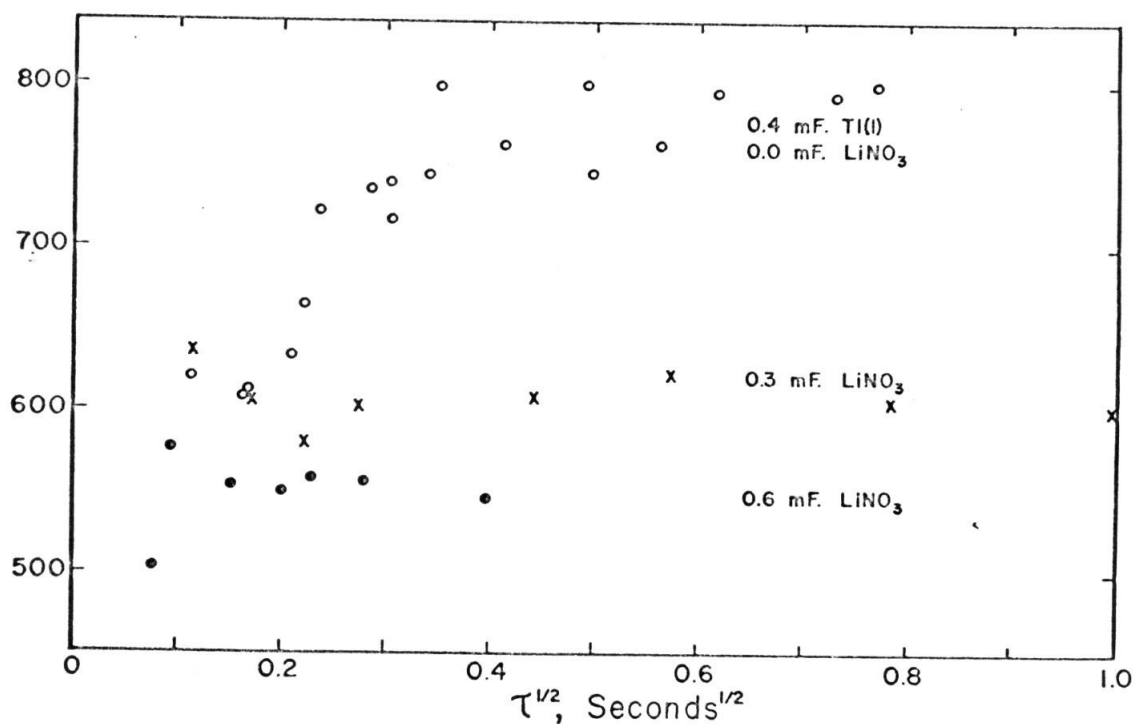


Figure 22. Plot of the chronopotentiometric constant as a function of the square root of the observed transition time for the reduction of Tl(I) in the presence of increasing amounts of LiNO₃, pH ~ 5. Tl(Hg) reference electrode. Data was obtained using a battery and dropping resistors as the constant current source and the indicator electrode was not prebiased.

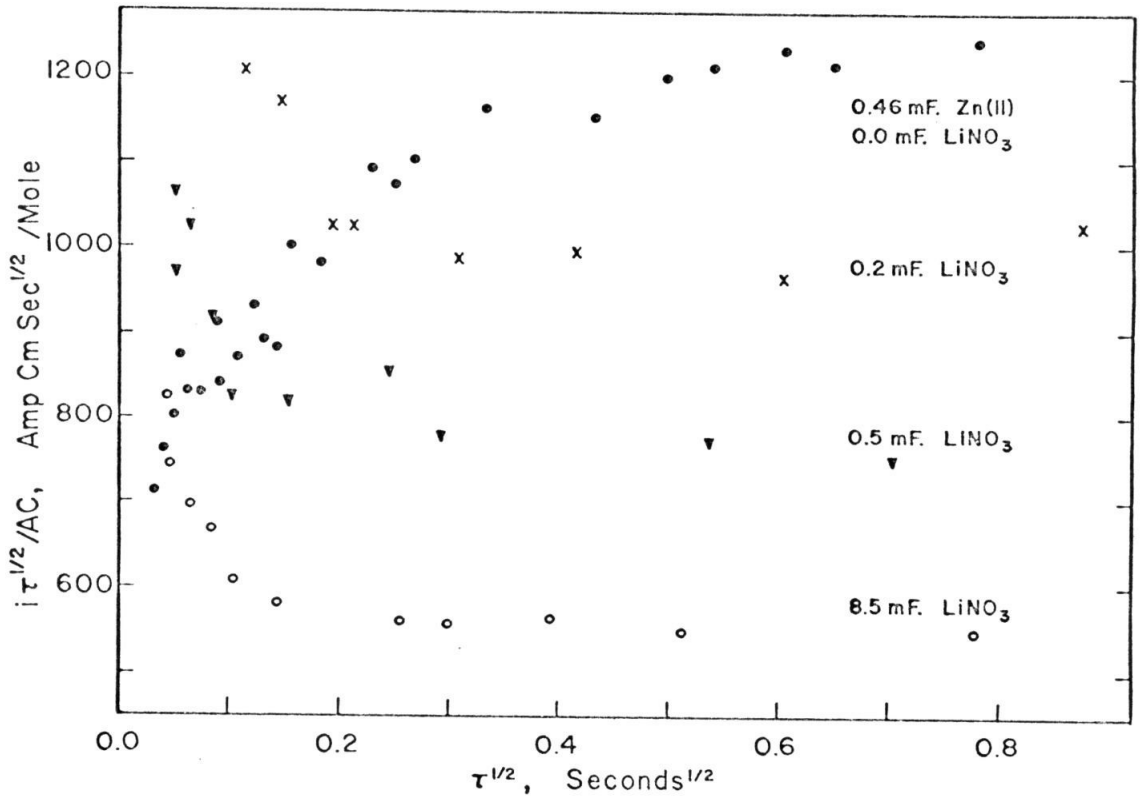


Figure 23. Plot of the chronopotentiometric constant as a function of the square root of the observed transition time for the reduction of Zn(II) in the presence of increasing amounts of LiNO₃, pH ~ 5.5. Zn(Hg) reference electrode. Most of the data was obtained using the circuit of Fig. 25.

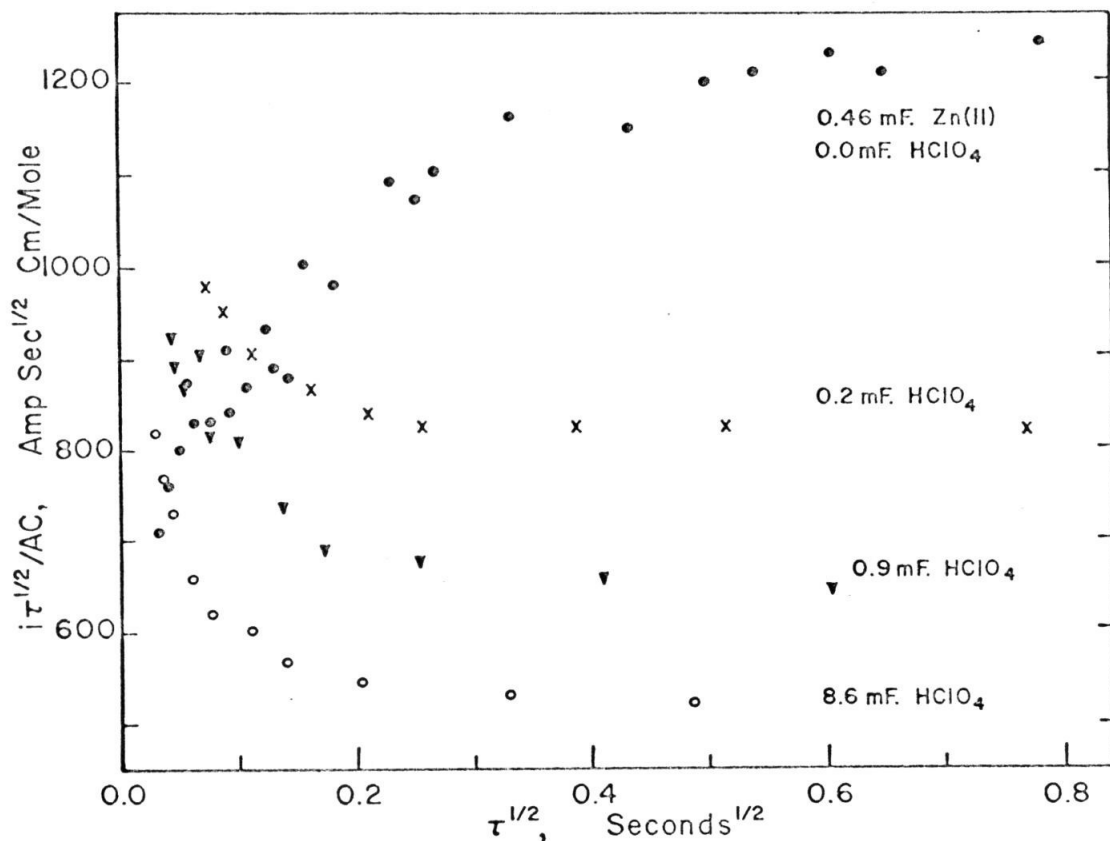


Figure 24. Plot of the chronopotentiometric constant as a function of the square root of the observed transition time for the reduction of Zn(II) in the presence of increasing amounts of HClO₄. Zn(Hg) reference electrode. Most of the data was obtained using the circuit of Fig. 25.

much as 20 per cent from the values reported here, the qualitative features of Figs. 20-24 were retained.

We hypothesize that the ions from the supporting electrolyte gradually replace the electroactive material electrostatically bound in the diffuse layer once electrolysis has appreciably lowered the concentration of the electroactive species in the vicinity of the electrode. Since this electroactive material is "released" at the surface of the electrode, its electrolysis should be characterizable as "adsorption" phenomenon. Thus we interpret the increase in the chronopotentiometric constant observed at high current densities in the presence of small amounts of supporting electrolyte as resulting from the reaction of the electroactive material in the diffuse layer. In the next section, we will make estimates of the amount of material so released.

Some credence is lent to this point by the fact that the experiments with thallium(I) do not indicate the reaction of material from the diffuse layer. Cf. Fig. 22. Tl^+ is reduced in the vicinity of the point of zero charge on mercury, i.e., in the potential region where the diffuse layer is very small, and thus we would expect the enhancement of the measured transition times to be too small to be detected.

The apparent "negative adsorption" indicated by the decrease in the observed values of the chronopotentiometric constant at high current densities in the absence of supporting electrolyte could be interpreted as the "trapping" of electroactive material in the diffuse layer due to a positive change in the diffuse layer charge. As we have

postulated on p. 115 ff, an increase in the positive charge in the diffuse layer is effected by the uniform movement of cations towards the electrode and the uniform movement of anions away from the electrode. Such a process would decrease the concentration of the "reactive" material in the vicinity of the electrode by an amount equal to that portion of the change in the double layer charge which is effected by the expulsion of the counter ions. Therefore, an increase in the positive charge in the diffuse layer would cause a decrease in the value of the chronopotentiometric constant observed at high current densities.

One would anticipate that the change in double layer charge during a chronopotentiometric experiment would be no more than perhaps $5 \mu\text{C}/\text{cm}^2$; this would correspond to an expulsion of perhaps $2-3 \mu\text{C}/\text{cm}^2$ of counter ions from the vicinity of the electrode. Thus the observed decrease in the chronopotentiometric constant should correspond to a "trapping" of no more than perhaps $2-3 \mu\text{C}/\text{cm}^2$. The quantitative calculations discussed in the next section and presented in Table II suggest, however, that the observed effect is many times too large to be explained in this fashion. An alternative explanation which is more consonant with the facts will be presented shortly.

Quantitative Adsorption Estimates

In order to make quantitative estimates of adsorption phenomena from data obtained with a constant current technique, it is necessary to make assumptions about the relative current efficiencies for the various electrode processes during the course of the experiment. There

are at least three principal models which one can assume for the manner in which non-diffusing material is electrolyzed (74,75).

The non-diffusing material could react first. According to this model

$$\begin{aligned}\tau_{\text{obs}} &= \tau + nF\Gamma/i_0 \\ i_0(\tau_{\text{obs}} - nF\Gamma/i_0)^{\frac{1}{2}} &= \frac{nFC}{2} (\pi D)^{\frac{1}{2}} = b \\ nF\Gamma &= i_0\tau_{\text{obs}} - b^2/i_0\end{aligned}\quad (11)$$

Alternatively, the non-diffusing material could react at a constant rate during the experiment.

$$\begin{aligned}i_{\text{obs}} &= i_0 + nF\Gamma/\tau \\ (i_{\text{obs}} - \frac{nF\Gamma}{\tau})\tau^{\frac{1}{2}} &= b \\ nF\Gamma &= i_{\text{obs}}\tau - b\tau^{\frac{1}{2}}\end{aligned}\quad (12)$$

Finally, the non-diffusing material might react after the concentration of the diffusing material is reduced to zero at the electrode surface. This situation is somewhat more complicated and only the final result will be given here.

$$\pi nF\Gamma = i_0\tau \cos^{-1} \left(\frac{2b^2}{i_0^2\tau} - 1 \right) - \frac{2}{i_0} [b^2(i_0^2\tau - b^2)]^{\frac{1}{2}} \quad (13)$$

(74) S. V. Tatwawadi and A. J. Bard, Anal. Chem., 36, 2 (1964).

(75) H. A. Laitinen and L. M. Chambers, Anal. Chem., 36, 5 (1964).

The chronopotentiometric data illustrated in Figs. 20-24 were analyzed according to these three models by a weighted least squares technique very similar to that employed in Chapter 5. The details of the calculations are given in the appendix to this chapter and the results of these calculations are summarized in Table II. Incidentally, this is the correct least squares analysis of chronopotentiometric data. Cf. Proposition I.

Our intuition suggests that the actual physical description of the diffusion of supporting electrolyte into the region of the diffuse double layer and the release and subsequent reaction of the electroactive material electrostatically bound in the diffuse double layer lies intermediate between the "constant rate" and "reacts last" models. The "reacts first" model would require the diffuse layer to be electrolyzed before the diffusing material and would appear to be the poorest description of the actual physical situation.

The values of $nF\Gamma$ estimated for the data in the presence of supporting electrolyte according to the "constant rate" and "reacts last" models are of the magnitude of the charge in the diffuse layer at potentials corresponding, very roughly, to the reduction potential of the particular electroactive species. The magnitudes of the estimated values of $nF\Gamma$ and the qualitative dependence of the estimated values of $nF\Gamma$ and of D on the concentration of the supporting electrolyte are not inconsistent with the conclusion that the chronopotentiometric experiments conducted in the presence of small quantities of supporting

Table II

The Extent of "Positive" and "Negative" Adsorption
Calculated According to Three Chronopotentiometric Models.

$$\sigma_T^2 = (\tau/20)^2.$$

	"Reacts First"			"Constant Rate"			"Reacts Last"		
	$nF \times 10^4$ coulombs/cm ²	$D \times 10^4$ cm ² /sec	$X^2/N-3$	$nF \times 10^4$ coulombs/cm ²	$D \times 10^4$ cm ² /sec	$X^2/N-3$	$nF \times 10^4$ coulombs/cm ²	$D \times 10^4$ cm ² /sec	$X^2/N-3$
1. 0.462 mF Zn(II)									
a. no supporting electrolyte	-17.4 ± 0.65	4.16 ± 0.06 ^a	13.3	-5.9 ± 0.2	3.85 ± 0.05	15.8	12.4 ± 7.4	no results	
b. 0.2 mF LiNO ₃	23.4 ± 3.3	2.95 ± 2.24	2.24	12.7 ± 2.1	2.93 ± 0.12	2.36	5.5 ± 1.9	2.39 ± 0.16	3.32
8.3	11.4 ± 0.9	1.87 ± 0.06	2.63	6.5 ± 0.6	1.85 ± 0.05	2.69	4.7 ± 1.12	1.58 ± 0.07	3.38
8.3	9.2 ± 0.5	0.92 ± 0.02	1.43	5.5 ± 0.3	0.91 ± 0.03	1.91		0.77 ± 0.03	3.03
c. 0.2 mF HClO ₄	11.2 ± 1.6	2.12 ± 0.07	0.285	6.2 ± 0.96	2.10 ± 0.07	0.333	4.1 ± 2.7	1.92 ± 0.09	0.595
0.9	10.7 ± 0.7	1.36 ± 0.04	1.98	6.4 ± 0.5	1.33 ± 0.04	1.53	5.1 ± 1.46	1.15 ± 0.05	1.43
8.6	7.3 ± 0.4	0.87 ± 0.03	0.273	4.5 ± 0.3	0.84 ± 0.03	0.137	3.5 ± 0.85	0.73 ± 0.03	0.235
2. 0.260 mF Co(II)									
a. 0.34 mF LiNO ₃	23.3 ± 1.1	1.02 ± 0.05	0.390	16.2 ± 0.96	0.90 ± 0.05	0.405	15.2 ± 3.3	0.67 ± 3.3	0.467
2.0	14.7 ± 1.0	0.68 ± 0.05	1.63	9.74 ± 0.87	0.62 ± 0.05	2.56	9.58 ± 3.0	0.44 ± 0.05	3.23
102.	1.07 ± 0.73	0.48 ± 0.02	0.591	0.54 ± 0.39	0.48 ± 0.02	0.588	0.43 ± 1.11	0.44 ± 0.04	1.04
3. 0.266 mF H ⁺									
a. no supporting electrolyte	-20.5 ± 1.6	113 ± 2.6 ^b	1.57	-8.97 ± 0.56	111. ± 2.4	1.69	24.5 ± 7.4	no results	
b. 0.2 mF LiNO ₃	36. ± 2.4	17.9 ± 1.2	4.39	24.9 ± 2.1	16.0 ± 1.3	4.17	5.9 ± 1.6	11.5 ± 1.2	4.45
2.0	8.1 ± 0.53	8.9 ± 0.3	10.9	4.6 ± 0.4	8.9 ± 0.3	12.8		6.1 ± 0.4	19.0

^aD_S = 0.37 × 10⁻³ cm²/sec

^bD_S = 1.6 × 10⁻³ cm²/sec

electrolyte are sensitive to that portion of the diffuse double layer composed of the electroactive material.

Origin of the "Negative Adsorption"

In an earlier portion of this chapter, we saw that the sum of the voltage developed across the uncompensated resistance plus the liquid junction potential should distort the observed chronopotentiometric wave. A comparison of Figs. 18 and 19 demonstrates that the idealized form of the chronopotentiometric waves illustrated in Fig. 18 is not, in fact, obtained at high current densities in the absence of supporting electrolyte. These waves are additionally distorted at high current densities by the capacitive charging of the diffuse double layer which serves to limit the rate of change of the potential of the indicator electrode.

When the additional distortion caused by the uncompensated resistance is superimposed upon the substantial distortion due to double layer charging, it is expected that the effect of the uncompensated resistance would be to substantially reduce the measured transition time. More importantly, the effect would not be independent of the magnitude of the current density but the high current density data would be affected most strongly since double layer charging distorts this data to the largest extent.

The downward trend observed for the chronopotentiometric constant in the absence of supporting electrolyte would be completely explained if the net distortion of the chronopotentiometric wave were to

result in a shortening of the observed transition time of fifty per cent at the highest current densities employed. The strong likelihood that the effect is of this magnitude leads us to the conclusion that the "negative adsorption" observed in the absence of supporting electrolyte is, in all probability, spurious.

Some significance might be attached to the fact that the observed constant fails to increase in the absence of supporting electrolyte. This could be interpreted as indicating that normally electroactive material is rendered non-electroactive by its inclusion in the diffuse layer in the absence of supporting electrolyte because it must be replaced by material from the supporting electrolyte in order to react. This hypothesis is reasonable, independent of experiment, since the reaction of the material in the diffuse layer would, in the absence of supporting electrolyte, be equivalent to the elimination of the diffuse layer. These experiments alone, however, are insufficient to justify such a conclusion.

Experimental

A 450 v. battery bank in series with a large variable resistor or a Wenking "R" potentiostat were employed as constant current sources. Since the potentiostat, when employed as in Fig. 25, is in operation before as well as during the chronopotentiometric experiment, the resistance "R" was taken to be sufficiently large that the minimum current of approximately $\pm \frac{1}{R}$ mA flowing prior to the current step was always less than one per cent of the final chronopotentiometric current. In

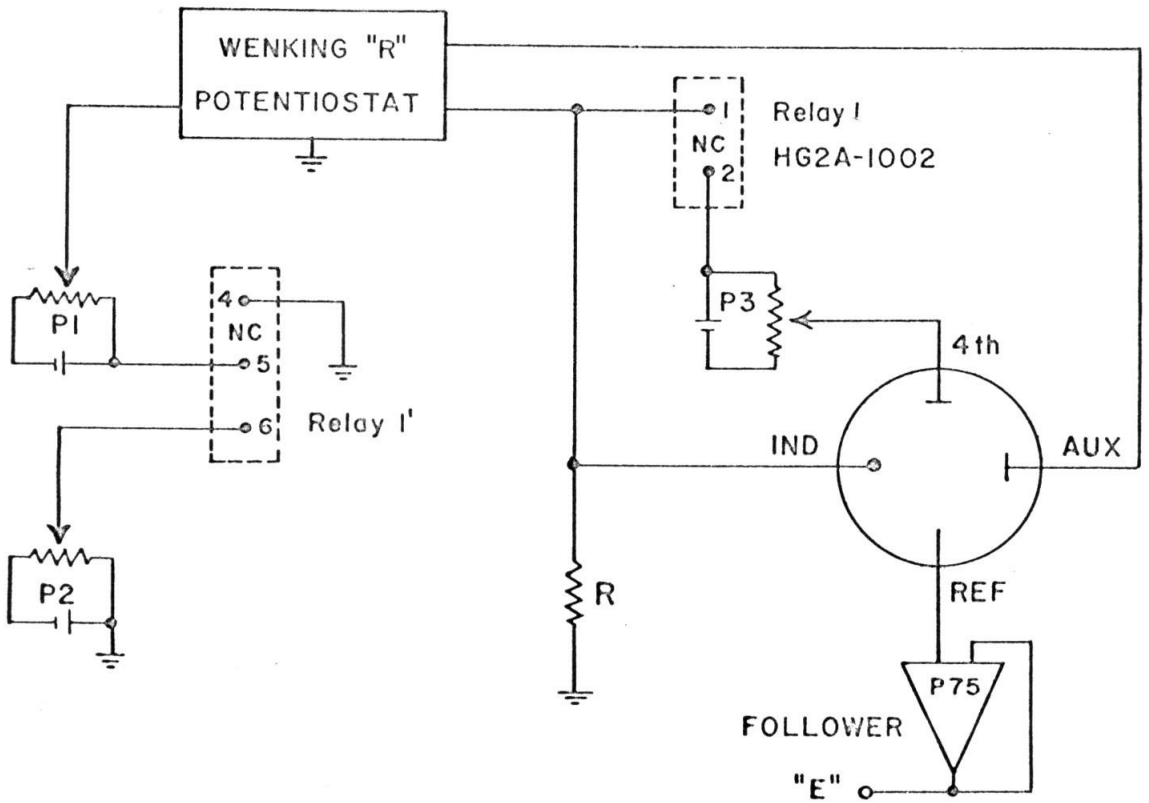


Figure 25. Block diagram of the apparatus for the constant current chronopotentiometric experiments. P1 is used to adjust the current flowing prior the the current step to zero and P2 controls the height of the current step. These circuits employ a G. A. Philbrick Researches, Inc. solid state operational amplifier and a DPDT C.P. Clare & Co. mercury-wetted relay.

this way, effects due to electrolysis before the experiment were effectively minimized. No differences were observed between chronopotentiograms obtained with either current source.

Certain of the experiments employed a fourth electrode as illustrated in Fig. 25 to adjust the initial potential of the indicator electrode to some prechosen value. The pre-biasing circuit illustrated in Fig. 25 is interrupted about $1 \mu\text{s}$. before the current step by one-half of relay 1. No qualitative influence of the potential at which the indicator electrode was prebiased was observed.

The indicator electrode was of the Kemula hanging mercury drop variety. The drop area was about 0.041 cm^2 and was calculated by weighing a series of drops and assuming spherical geometry.

The reference electrode was a dilute zinc or copper amalgam separated from the test solution by a thin glass wool plug. A sintered glass frit cannot be employed under these conditions because the resulting high resistance, in the presence of small amounts or less of supporting electrolyte, raises the impedance of the reference electrode to a point where large amounts of AC noise appear at the output of the voltage follower. The potential of the reference electrode was checked frequently against a large S.C.E. in a separate sample of the test solution.

All experiments were conducted at room temperature.

Cobaltous perchlorate. -- A 0.26 F stock solution, $\text{pH} = 2.5$, was prepared from B&A $\text{CoSO}_4 \cdot 7\text{H}_2\text{O}$. The cobalt was twice precipitated as the carbonate and redissolved in perchloric acid to remove the sulfate.

The final solution was assayed for total cation with an ion exchange column (Amberlite IRA-120, Mallinckrodt).

Cupric nitrate. -- A 0.113 F stock solution was prepared from B&A $\text{Cu}(\text{NO}_3)_2 \cdot 3\text{H}_2\text{O}$ and assayed iodometrically.

Lithium nitrate. -- A 0.85 F stock solution, $\text{pH} = 3.3$, was prepared by oxidizing B&A LiCl with boiling, concentrated nitric acid. The resulting salt was recrystallized from boiling nitric acid and then from water. The final solution tested free of chloride; the lithium content was assayed gravimetrically as the sulfate.

The salt was prepared from LiCl in order to eliminate most of the sodium and sulfate impurities in commercial LiNO_3 . $\text{SO}_4^{-2} < 0.01\%$; $\text{Na}^+ < 0.2\%$ (est.).

Mercury. -- Mallinckrodt "AR" mercury was employed exclusively.

Perchloric acid. -- A 0.862 F stock solution was prepared by reducing, by boiling, a 110 ml volume of Mallinckrodt 60% perchloric acid plus 5 ml Baker 70% nitric acid to a volume of about 70 ml. The solution was tested free of chloride and assayed vs. Na_2CO_3 after dilution.

Sodium perchlorate. -- Cf. p. 102.

Thallosulfate. -- A hot saturated solution of Fisher "purified" Tl_2SO_4 was filtered and precipitated. The salt was reprecipitated from ~ 0.01 F H_2SO_4 . After drying at 100°C , a stock solution of approximately

known composition was prepared by dissolving a weighed portion of this salt in water.

Zinc perchlorate. -- A 0.1024 F stock solution, pH = 4.5, was prepared by equilibrating an excess of Mallinckrodt "AR" ZnO with a portion of perchloric acid. The solution was filtered, boiled, diluted and then assayed vs. EDTA using Erio Black T indicator in an ammoniacal buffer solution for the end point detection.

All test solutions were prepared by the dilution of these stock solutions with triply distilled water. All solutions were deaerated in the cell with Matheson's "prepurified nitrogen," < 8 ppm oxygen, which was passed through a V(II) solution and distilled water in separate gas washing towers, prior to entry into the cell.

Appendix. Least Squares Estimation of the Chronopotentiometric Adsorption Statistics

The analysis proceeds in a fashion identical to that employed in Chapter 5 and therefore only the highlights will be touched upon here.

The measured parameters in chronopotentiometry are the time-independent current density i_0 and the corresponding transition time τ . Since the current density is generally known to a much higher degree of precision than the measured values of τ , it is reasonable to weight the data as if the measured values of i_0 were free of error. Under these conditions, the weighting function becomes

$$L_j = (F_{\tau}^j)^2 \sigma_{\tau_j}^2$$

The relative precision for the individual transition time measurements is frequently remarkably constant--often varying by less than a factor of two over a thousand-fold transition time range. Under these conditions, it is satisfactory to treat the measured values of τ as if they were associated with a fixed relative error. This procedure was adopted in obtaining the results presented in Table II. Therefore, the weighting function employed here is

$$L_j = (F_{\tau}^j)^2 E^2 \tau_j^2$$

"Reacts first" model. -- For this model, we choose $a = nF\Gamma$ and $b = (nFC/2)^2 \pi D$; if we let a_0 and b_0 be zero we obtain

$$f^j = i_0 \tau$$

where the appropriate derivatives are

$$\frac{\partial f}{\partial a} = -1; \quad \frac{\partial f}{\partial b} = -1/i_0; \quad \frac{\partial f}{\partial \tau} = i_0$$

"Constant rate" model. -- We let $a = nF\Gamma$ and $b = nF\pi^{1/2}D^{1/2}C$. Under these conditions,

$$f^j = i_0 \tau_j - a_0 - b_0 \tau_j^{1/2}$$

and the appropriate derivatives are

$$\frac{\partial f}{\partial a} = -1; \quad \frac{\partial f}{\partial b} = -\tau^{1/2}; \quad \frac{\partial f}{\partial \tau} = i_0 - b_0/2\tau^{1/2}$$

We can choose initial values of zero for a_0 and b_0 and calculate approximate values of a and b . If the calculations are now repeated, we will obtain an improved value for the weighting function. One continues to "cycle on the weights" in this fashion until stable solutions are obtained. Three iterations are generally satisfactory.

"Reacts last" model. -- We let $a = nF\pi\Gamma$ and $b = (nFC/2)^2\pi D$. Under these conditions,

$$f^j = a_0 - i_0 \tau \cos^{-1} \left[\frac{2b_0}{i_0^2 \tau} - 1 \right] + \frac{2}{i_0} [b_0(i_0^2 \tau - b_0)]^{1/2}$$

where the appropriate derivatives are,

$$\frac{\partial f}{\partial a} = -1; \quad \frac{\partial f}{\partial b} = \frac{2}{i_0} \left(\frac{i_0 \tau - b_0}{b_0} \right)^{1/2}; \quad \frac{\partial f}{\partial \tau} = -i_0 \cos^{-1} \left[\frac{2b_0}{i_0^2 \tau} - 1 \right]$$

When the same data is analyzed according to the "constant rate" and "reacts last" models, essentially identical values are obtained for n_{FT} for both models and a somewhat smaller value of D is obtained according to the "reacts last" model (76). Therefore, it is generally satisfactory to take the final adjusted values of a and b calculated according to the preceding model and to employ these as the preliminary values for analysis according to this model. Thus $a_0 = \pi a'$ and $b_0 = b'^2$ where the primed values correspond to the final values of these parameters estimated according to the "constant rate" model.

As in the "constant rate" model, one must also "cycle on the weights" in this case until stable solutions are obtained.

The Fortran program employed for the estimation of the data is included on the next four pages; its inclusion here is not meant to suggest that this program is particularly unique but rather it is here as an aid to others who might wish to analyze their data in this fashion.

(76) P. J. Lingane, to be submitted to Anal. Chem.


```

$IBFTC CHRONO DECK          PRODUCTION DECK
C   CALCULATES THE ADSORPTION STATISTICS FROM CHRONOPOTENTIOMETRIC
C   DATA ACCORDING TO VARIOUS MODELS.  WEIGHTED LEAST SQUARES ANALYSIS
C   PROGRAMMED BY PETER JAMES LINGANE, FEBRUARY 14, 1966
C   NC   UNITS OF MOLES PER LITER
C   TAU  UNITS OF MILLISECONDS
C   AI   UNITS OF MILLIAMPERES
C   N    NUMBER OF DATA POINTS
C   E    ESTIMATED RELATIVE ERROR IN TAU
C   INTEGR NO. OF ITERATIONS, 5 IS FREQUENTLY SATISFACTORY
COMMON FO(100), FA(100), FB(100), FT(100), ST(100), SA, SB, A, B,
* N, CHISQD, DELTAA, DELTAB, W(100), ALM(100), A0, B0
COMMON RTP1, PI, FARA, NC, D, SD, REST(100), NELEC, INTEGR, AI(100
*), TAU(100)
DIMENSION COMMT(24), AI2T(100), RI(100), AIT(100), SQRTT(100)
REAL NC
PI = 3.1415927
RTP1 = 1.7724539
FARA = 96500.
100 READ(5,3) COMMT
3   FORMAT(12A6)
   READ(5,4) N, NELEC, INTEGR, NC, AREA, E
4   FORMAT(3I5, 3E10.0)
   READ (5,5) (AI(I), TAU(I), I=1,N)
5   FORMAT(2E15.8)
   DO 6 I=1,N
   ST(I) = E*TAU(I)
   AI(I) = AI(I)/AREA
   AI2T(I) = AI(I)**2*TAU(I)
   SQRTT(I) = SQRT(TAU(I))
   AIT(I) = AI(I)*TAU(I)
6   RI(I) = 1./AI(I)
   WRITE(6,1) COMMT
1   FORMAT(1H1, / (10X12A6))
   CALL MD1
   WRITE(6,10) A, SA, D, SD, CHISQD
10  FORMAT(/, 9X15H N*FARA*GAMMA =, 0PF10.3, 20H MICROCOULOMBS/CM**2,
* 10X4H S =, F8.5, / 9X4H D =, E10.3, 10H CM**2/SEC, 10X4H S =,
*E10.3, / 9X9H CHISQD =, E10.3)
   WRITE(6,11)
11  FORMAT(/, 8X3H IT, 10X4H 1/I, 6X7H WEIGHT, 6X5H TIME, 4X11H T R
*ESIDUAL, /)
   WRITE(6,2) (AIT(I), RI(I), W(I), TAU(I), REST(I), I=1,N)
2   FORMAT(2X1P2E13.3, E9.1, 2E13.3)
   WRITE(6,1) COMMT
   CALL MD3
   WRITE(6,10) A, SA, D, SD, CHISQD
   WRITE(6,12)
12  FORMAT(/, 8X3H IT, 7X10H SQRT(TAU), 2X7H WEIGHT, 6X5H TIME, 4X
*11H T RESIDUAL, /)
   WRITE(6,2)(AIT(I), SQRTT(I), W(I), TAU(I), REST(I), I=1,N)
   WRITE(6,1) COMMT
   CALL MD2
   WRITE(6,10) A, SA, D, SD, CHISQD
   WRITE(6,13)
13  FORMAT(/, 6X8H (I**2)T, 8X2H I, 6X7H WEIGHT, 6X5H TIME, 4X11H T R
*ESIDUAL, /)
   WRITE(6,2)(AI2T(I), AI(I), W(I), TAU(I), REST(I), I=1,N)
   GO TO 100
END

```

```

SUBROUTINE MD1
C  CALCULATES ADSORPTION STATISTICS FROM CHRONPOTENTIOMETRIC DATA
C  ACCORDING TO THE ADSORBED SPECIES REACTING FIRST MODEL.
C  PROGRAMMED BY LINGANE, FEBRUARY 14, 1966
COMMON FO(100), FA(100), FB(100), FT(100), ST(100), SA, SB, A, B,
* N, CHISQD, DELTAA, DELTAB, W(100), ALM(100), AO, BO
COMMON RTPI, PI, FARA, NC, D, SD, REST(100), NELEC, INTEGR, AI(100
*), TAU(100)
REAL NC
AO = 0.
BO = 0.
WRITE(6,6)
6  FORMAT(/, 10X13H** MODEL 1 ** )
DO 1 I=1,N
FT(I) = AI(I)
FA(I) = -1.
FO(I) = AI(I)*TAU(I)
1  FB(I) = -1./AI(I)
CALL FT1
DO 2 I=1,N
2  REST(I) = ALM(I)*AI(I)*ST(I)**2
D = 0.004*B/(FARA*NC*RTPI)**2
SD = 0.004*SB/(FARA*NC*RTPI)**2
RETURN
END

```

```

SUBROUTINE MD3
C  CALCULATES ADSORPTION STATISTICS FROM CHRONPOTENTIOMETRIC DATA
C  ACCORDING TO THE ADSORBED SPECIES REACTING AT CONSTANT CURRENT
C  EFFICIENCY MODEL.
C  PROGRAMMED BY LINGANE, FEBRUARY 14, 1966
COMMON FO(100), FA(100), FB(100), FT(100), ST(100), SA, SB, A, B,
* N, CHISQD, DELTAA, DELTAB, W(100), ALM(100), AO, BO
COMMON RTPI, PI, FARA, NC, D, SD, REST(100), NELEC, INTEGR, AI(100
*), TAU(100)
REAL NC
WRITE(6,6)
6  FORMAT(/, 10X13H** MODEL 3 ** )
K = 1
AO = 0.
BO = 0.
3  DO 1 I=1,N
FA(I) = -1.
FB(I) = - SQRT(TAU(I))
FT(I) = AI(I) - BO/(2.*SQRT(TAU(I)))
1  FO(I) = AI(I)*TAU(I) - AO -BO*SQRT(TAU(I))
CALL FT1
K = K + 1
AO = A
BO = B
IF (K.GT.INTEGR) GO TO 4
GO TO 3
4  DO 2 I=1,N
2  REST(I) = ALM(I)*FT(I)*ST(I)**2
D = 0.004*B**2/(FARA*NC*RTPI)**2
SD = 2.*SB*D/B
RETURN
END

```

```

SUBROUTINE MD2
C   CALCULATES ADSORPTION STATISTICS FROM CHRONOPOTENTIOMETRIC DATA
C   ACCORDING TO THE ADSORBED SPECIES REDUCED LAST MODEL.
C   PROGRAMMED BY LINGANE, FEBRUARY 14, 1966
C   CALL TO MD3 MUST JUST PRECEDE CALL TO MD2.
COMMON FO(100), FA(100), FB(100), FT(100), ST(100), SA, SB, A, B,
* N, CHISGD, DELTAA, DELTAB, W(100), ALM(100), AO, BO
COMMON RTPI, PI, FARA, NC, D, SD, REST(100), NELEC, INTEGR, AI(100
*), TAU(100)
DIMENSION AA(100)
REAL NC
WRITE(6,6)
6   FORMAT(/, 10X13H** MODEL 2 ** ,//)
   K = 1
   BO = B**2
   SUM = 0.
   DO 10 I=1,N
     X = AI(I)**2*TAU(I)
     Y = 2.*BO - X
10  AA(I) = (X*ACOS(Y/X) - 2.*SQRT(BO*(X-BO)))/AI(I)
     AO = PI*A
     WRITE(6,11) (AA(I), I=1,N,2)
11  FORMAT(10X3E20.8, /, 10X2E20.8)
     WRITE(6,5) AO, BO
3   DO 1 I=1,N
     X = AI(I)**2*TAU(I)
     Y = 2.*BO - X
     FT(I) = -(AI(I)**2/AO)*ACOS(Y/X)
     FO(I) = AI(I) -X*ACOS(Y/X)/AO + 2.*SQRT(BO*(X-BO))/AO
     FA(I) = (AI(I) - FO(I))/AO
1   FB(I) = 2.*(X-BO)/(AO*SQRT(BO*(X-BO)))
     CALL FT1
     K = K+1
     AO = A
     BO = B
     WRITE(6,5) AO, BO
5   FORMAT(/,2E20.8)
     IF(K.GT.INTEGR) GO TO 4
     GO TO 3
4   DO 2 I=1,N
2   REST(I) = ALM(I)*FT(I)*ST(I)**2
     A = A/PI
     D = 0.004*B/(FARA*NC*RTPI)**2
     SD = 0.004*SB/(FARA*NC*RTPI)**2
RETURN

```

```

SUBROUTINE FT1
C   NON-LINEAR LEAST SQUARES ANALYSIS, 2 PARAMETERS
C   PROGRAMMED BY LINGANE, FEBUARY 14, 1966
COMMON FO(100), FA(100), FB(100), FT(100), ST(100), SA, SB, A, B,
* N, CHISQD, DELTAA, DELTAB, W(100), ALM(100), AO, BO
C11 = 0.
C12 = 0.
C22 = 0.
PHI1 = 0.
PHI2 = 0.
PHI3 = 0.
DO 26 I=1,N
W(I) = 1./(ST(I)*FT(I))**2
C11 = C11 + FA(I)*FA(I)*W(I)
C12 = C12 + FA(I)*FB(I)*W(I)
C22=C22 + FB(I)*FB(I)*W(I)
PHI1 = PHI1 + FA(I)*FO(I)*W(I)
PHI3 = PHI3 + FO(I)*FO(I)*W(I)
26 PHI2 = PHI2 + FB(I)*FO(I)*W(I)
C
DET = C22*C11 -C12**2
DELTAA = (C22*PHI1 - C12*PHI2)/DET
DELTAB = (-C12*PHI1 + C11*PHI2)/DET
A = AO - DELTAA
B = BO - DELTAB
CHISQD = (PHI3 - PHI1*DELTAA - PHI2*DELTAB)/FLOAT(N-3)
SA = SQRT(C22/ABS(DET))
SB = SQRT(C11/ABS(DET))
DO 1 I=1,N
1 ALM(I) = (FO(I) - FA(I)*DELTAA - FB(I)*DELTAB)*W(I)
RETURN
END

```

CHAPTER 9.

Potential Step Chronocoulometric Results

The Cottrell equation applicable in the total absence of supporting electrolyte is

$$i_0 = nFC \frac{z_3 - z_1}{z_3} \sqrt{\frac{D_S}{\pi t}} \quad (1)$$

and the charge-time behavior is

$$Q = 2nFC \frac{z_3 - z_1}{z_3} \sqrt{\frac{D_S t}{\pi}} \quad (2)$$

Thus the charge due to "diffusing material" remains a linear function of $t^{\frac{1}{2}}$ in the absence of supporting electrolyte but the slope of the $Q-t^{\frac{1}{2}}$ curve is altered from that observed in the presence of excess supporting electrolyte by the factor

$$\frac{z_3 - z_1}{z_3} \sqrt{\frac{D_S}{D_1}} = \frac{z_3 - z_1}{z_3} \sqrt{\frac{D_3(z_3 - z_1)}{z_3 D_3 - z_1 D_1}}$$

We shall assume that the charge remains a linear function of $t^{\frac{1}{2}}$ at intermediate concentrations of supporting electrolyte (64, 65).

The assumption explicit in the application of potential step chronocoulometry to the measurement of "adsorbed" reactant is that the reaction of the adsorbed and diffusing material proceed independently of one another and that the reaction of the adsorbed material has proceeded to completion before the first data point is obtained. Under

these conditions, it is possible to obtain the total quantity of adsorbed material which reacted from the intercept of the $Q-t^{\frac{1}{2}}$ plot (25).

$$Q = b t^{\frac{1}{2}} + nFF + Q_{dl} \quad (3)$$

Minimizing the Effects of R_u

As might be imagined, the uncompensated resistance (55,56) encountered in solutions of low concentrations of supporting electrolyte can easily be of the order of several thousand ohms. Therefore it is mandatory to employ an effective method of compensating for the effects of the uncompensated resistance. Both of the experimental arrangements illustrated in Fig. 26 were employed and no differences were observed between them. The arrangement illustrated in Fig. 26B is perhaps slightly to be preferred since it uses one less amplifier and therefore the phase shift in the feedback loop should be decreased and, in theory, a more complete degree of compensation should be possible.

The schematics illustrated in Fig. 26 depict positive feedback situations and thus ones which are inherently unstable. In practice, it is not possible to feed back a voltage corresponding to more than about 60-80 per cent of the total uncompensated resistance because the net phase shift in the signal, caused by the amplifiers in the feedback loop, causes the potentiostat to "loose control" at about this point (56). Our present inability to completely compensate for the effects of uncompensated resistance is of minor importance in the presence of

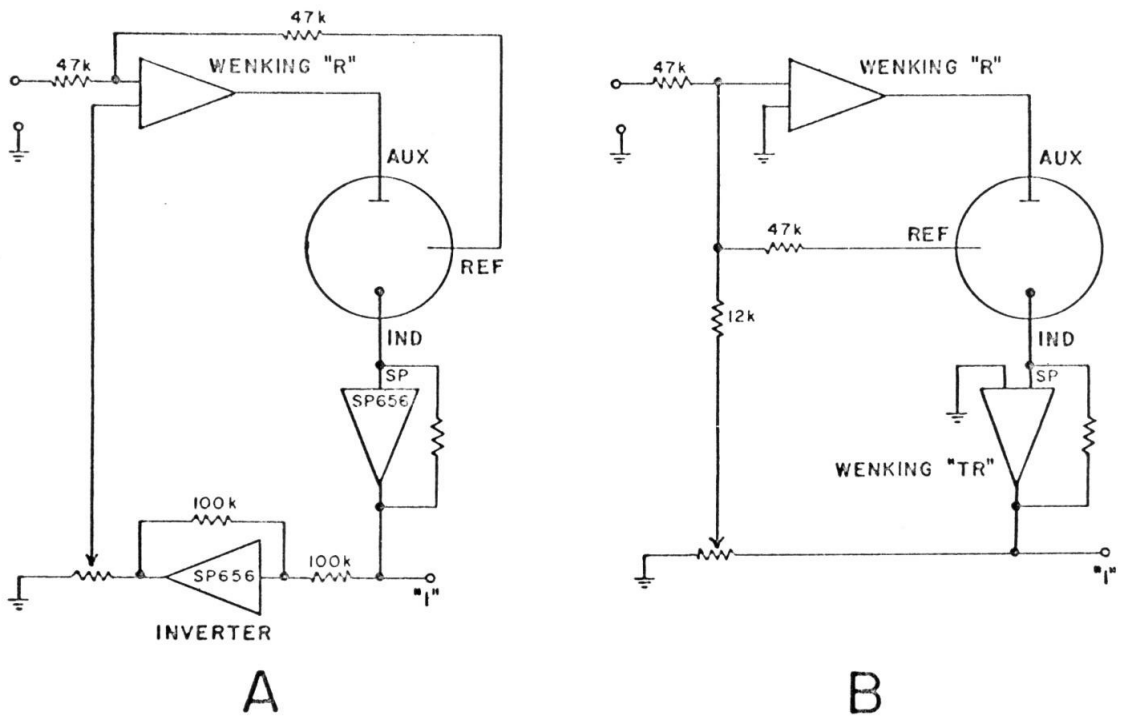


Figure 26. Block diagrams of two possible compensation circuits.

excess supporting electrolyte since the total uncompensated resistance is only of the order of perhaps 20-30 ohms under these conditions. In the presence of small amounts of supporting electrolyte however, the uncompensated resistance is of the order of 5-10 thousand ohms and this factor assumes dominant importance in determining the success or failure of a potential step chronocoulometric experiment.

The method of distinguishing "maximum compensation" and the changes in the qualitative features of I-t traces caused by varying the extent of compensation are discussed in some detail in Ref. (56). Figure 4B of this reference corresponds to the "maximum compensation" condition and is characteristic of all of the data presented in this chapter.

Results and Discussion

Experimental values of the $Q-t^{\frac{1}{2}}$ intercepts and slopes observed for the reduction of zinc in the presence of small amounts of supporting electrolyte are presented in Table I. Unless otherwise noted, these data were obtained with compensation circuit 26-A and a $Zn^{++}/Zn(Hg)$ reference electrode. The total uncompensated resistance is estimated in this table as larger than the measured "maximum compensation" value.

As was discussed above, p. 114 ff, these intercepts should equal

$$a = 2F\Gamma_{Zn}(E_0) + Q_{dl}(E_0, E_1)(1 + T_{Zn}) \quad (4)$$

where $T_{Zn} = 2C_{Zn}\lambda_{Zn}^0 / \sum |z_i| C_i \lambda_i^0$ is the transference number of the zinc ions. In what follows we shall assume $T_{Zn} = 0$; the actual calculated

Table I

The experimental Q, t data were analyzed by an equally-weighted, two parameter, least-squares analysis.

$$Q_0 = a + 2nFC\sqrt{\frac{Dt}{\pi}}$$

The entire experimental error was assumed to be associated with the measured values of the charge.

A. 0.5 mF Zn(II) + 2.0 mF NaClO₄, pH = 5.8, $R_u > 4.3$ kohms. $T_{Zn} = 0.263$

$\frac{E_0/E_1,}{\text{mv. vs. S.C.E.}}$	$a, \mu\text{C}/\text{cm}^2$	$D \times 10^5, \text{cm}^2/\text{sec}$
-300/-1250 2/25	14.0 + 0.8*	1.0 + 0.06*
-500/-1250 1/8 2/25	27.2 + 7.7 12.8 + 0.8*	1.6 + 0.7 1.0 + 0.06*
-700/-1250 2/25	13.0 + 1.0*	0.98 + 0.08*
-800/-1250 1/8 2/25	16.5 + 3.4 13.3 + 0.4*	0.88 + 0.24 0.93 + 0.03*
-850/-1250 2/25	13.4 + 2.5*	1.4 + 0.07*
-900/-1250 1/8 1/9 1/9	15.1 + 0.4 14.1 + 0.4 13.7 + 0.4	1.0 + 0.03 1.0 + 0.03 1.0 + 0.02

* Ag/AgCl reference electrode. $\text{Cl}^- = 0.001$. $R_u > 6.3$ kohm; compensation circuit 26-B.

B. 0.5 mF Zn^{++} + 2.0 mF HClO_4 , pH = 2.7, $R_u > 2$. kohms

Chronopotentiometric $D = 0.87 \pm 0.06 \times 10^{-5} \text{ cm}^2/\text{sec}$;

cf. also Table II, Chapter 8. $T_{\text{Zn}} = 0.107$

-200/-1250		
12/2	22.5 ± 0.8	0.83 ± 0.06
12/5	23.2 ± 1.1	0.99 ± 0.09
-470/-1250		
11/27	$24.9 \pm 1.5^*$	$2.0 \pm 0.2^*$
-500/-1250		
12/1	28.3 ± 0.7	0.96 ± 0.05
12/2	13.5 ± 1.6	0.87 ± 0.12
12/5	14.4 ± 1.1	0.79 ± 0.08
-600/-1250		
12/9	20.7 ± 4.3	0.91 ± 0.3
-700/-1250		
12/9	16.0 ± 0.9	0.88 ± 0.07
-800/-1200		
11/27	$10.5 \pm 1.3^*$	$1.1 \pm 0.1^*$
12/1	12.1 ± 0.5	0.77 ± 0.03
-800/-1250		
11/27	$10.3 \pm 3.5^*$	$1.3 \pm 0.3^*$
12/1	14.1 ± 1.1	0.89 ± 0.09
12/2	10.5 ± 0.6	0.92 ± 0.05
12/5	11.5 ± 1.6	1.0 ± 0.13
-900/-1250		
12/5	10.6 ± 1.3	0.94 ± 0.11
12/9	11.6 ± 3.0	0.98 ± 0.24

* Hanging mercury drop electrode: 0.0407 cm^2 in area.

C. 0.5 mF Zn^{++} + 1.0 mF $\text{Ba}(\text{ClO}_4)_2$, pH = 5.7, $R_u > 4.6$ kohms
 Chronopotentiometric $D = 1.06 \pm 0.06 \times 10^{-5} \text{ cm}^2/\text{sec}$. $T_{\text{Zn}} = 0.247$

-500/-1250 12/19	10.2 ± 0.9	1.1 ± 0.07
-800/-1250 12/19	6.2 ± 0.8	0.93 ± 0.06

D. 0.5 mF Zn^{++} + 2.0 mF $\text{Ba}(\text{ClO}_4)_2$, $R_u > 3.0$ kohms. $T_{\text{Zn}} = 0.157$

-300/-1250 1/13	28.2 ± 0.7	0.95 ± 0.05
-500/-1250 1/13	21.2 ± 1.1	0.94 ± 0.08
-800/-1250 1/13	11.5 ± 0.6	0.84 ± 0.04
-900/-1250 1/13	7.9 ± 0.6	0.85 ± 0.04

values are given in the table. The error thus introduced is small compared to the other uncertainties in the data.

Some of the data in this table appears to be dramatically larger than the rest of the data with respect to both intercept and slope. The immediately suggested explanation for this effect, that the charge axis is improperly calibrated, appears to be untenable since a change in calibration sufficient to increase the intercept by the necessary amount would have caused the measured values of D to be much larger than observed. The cause of this effect is not known and the divergent data were eliminated from further consideration.

Figure 27 presents the plot of $Q_{dl}(E_0, -1250) + 2FT_{Zn}(E_0)$ given by Eqn. (4) and of selected values of the $Q-t^{\frac{1}{2}}$ intercepts as a function of E_0 . Qualitative agreement is obtained.

The experiments dealing with the reduction of zinc in the presence of barium were performed in the hope of demonstrating that the preferential electrostatic attraction of zinc into the diffuse layer disappears in the presence of a doubly charged indifferent cation. The intercepts observed for the reduction of zinc in the presence of milliformal barium are somewhat smaller than the values anticipated for double-layer charging alone while the values observed in 2. mF barium are substantially, and inexplicably, larger.

Values of $Q_{dl}(E_0, E_1)$ were determined by repeating the potential step experiments in the 2. mF barium solution but in the absence of zinc (57). The results are presented in Table II. Note that nearly

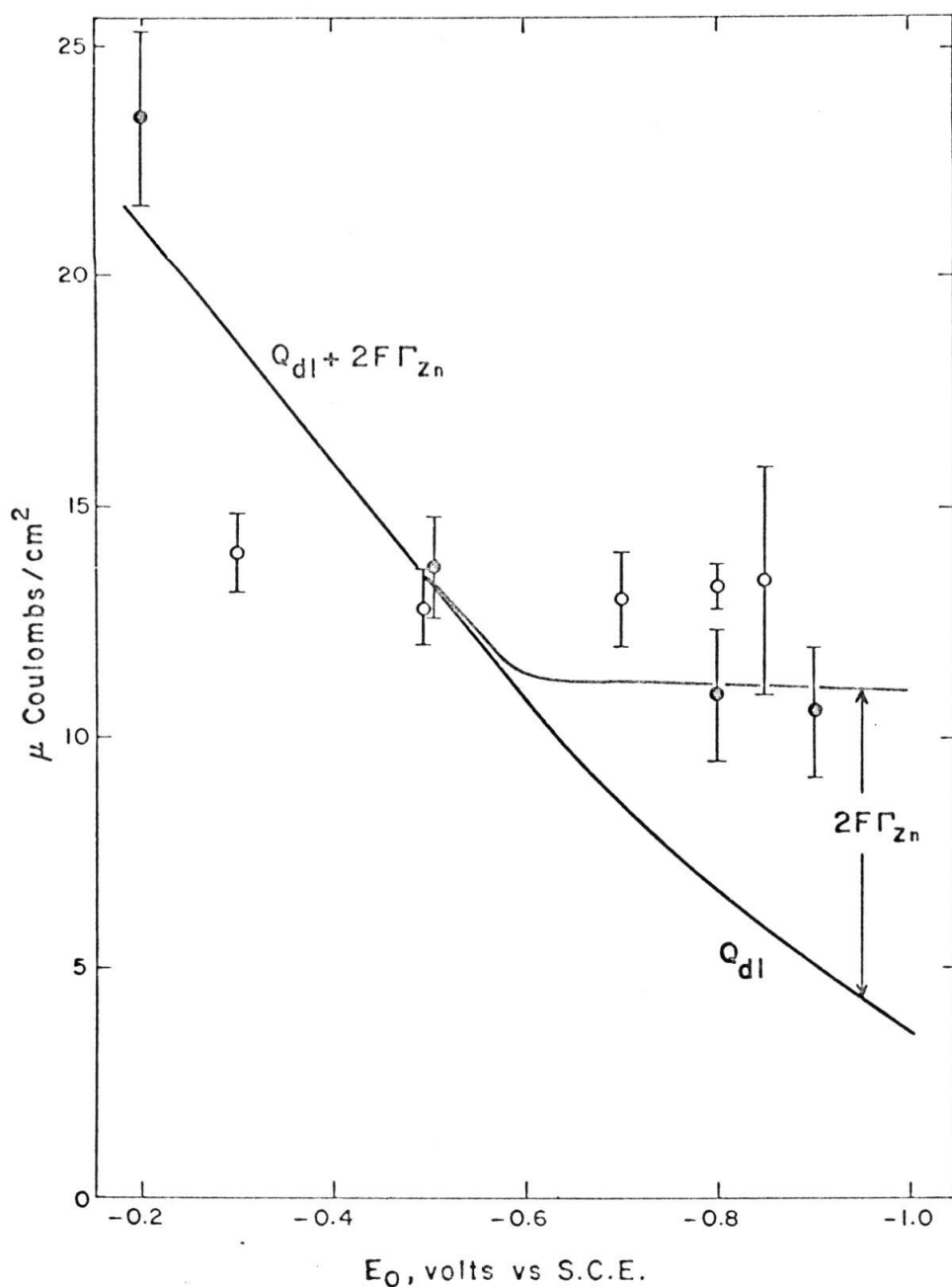


Figure 27. Selected experimental $Q-t^{\frac{1}{2}}$ intercepts observed for the reduction of zinc in the presence of small amounts of supporting electrolyte. The potential step is from E_0 to -1.25 v. vs. S.C.E.

- 0.5 mF $\text{Zn}(\text{ClO}_4)_2$ + 2.0 mF HClO_4
- 0.5 mF ZnCl_2 + 2.0 mF NaClO_4

Table II

Q_{dl} , measured from E_0 to -1.25 v. vs. S.C.E.

E_0 mv. vs. S.C.E.	Q_{dl} , $\mu\text{C}/\text{cm}^2$			
	I	II	III	IV
-200	35.		15.4	21.1
-300		29.0	13.5	18.5
-400		24.8	11.9	15.9
-500	24.1	21.3	12.0	13.4
-600		17.4	9.3	10.8
-700		14.7	8.6	8.6
-800	12.2	11.8	6.7	6.6
-850			6.0	5.8
-900	8.2	8.6		

I: 2. $\text{m}\underline{\text{F}}$ HClO_4 + 0.5 $\text{m}\underline{\text{F}}$ $\text{Ba}(\text{ClO}_4)_2$, 1/16

II: 2.0 $\text{m}\underline{\text{F}}$ $\text{Ba}(\text{ClO}_4)_2$; 1/16

III: 1.0 $\text{m}\underline{\text{F}}$ NaCl + 1.0 $\text{m}\underline{\text{F}}$ NaClO_4 , 2/26

IV: 10. $\text{m}\underline{\text{F}}$ NaClO_4 ; data of Wroblowa, Kovac, and Bockris (68)

identical values are obtained for the measured values of Q_{dl} and for the observed $Q-t^{\frac{1}{2}}$ intercepts for solutions with 2. mF barium supporting electrolyte, the hoped-for result, but that these values are a factor of two larger than anticipated. Similarly, the measured values of Q_{dl} for the 2 mF perchloric acid solutions appear to be too large. We conclude that neither the $Q-t^{\frac{1}{2}}$ intercepts observed for the barium solutions, nor the Q_{dl} data observed for either the barium perchlorate or perchloric acid solutions are trustworthy.

A much more important and far reaching criticism of all of these data is the fact that the observed $Q-t^{\frac{1}{2}}$ intercepts are probably substantially too small because of incomplete compensation for the effects of the uncompensated resistance.

In general, the time required for the "charging of the double layer," the rise time of the voltage developed across the faradaic resistance R_f of Fig. 15, is limited by one of two factors (56): namely, by the inherent maximum rise-time of the potentiostat and the current measuring amplifier or by the double-layer time-constant, $R_u C_{dl}$. The instrumental rise time of this system is less than 20 μ sec; the double-layer time-constant, in the presence of insufficient supporting electrolyte, is substantially larger than this and limits the rise-time of the system.

The net uncompensated resistance remaining at maximum compensation can be estimated by considering that the total uncompensated resistance is about five thousand ohms in these solutions. If the net uncompensated resistance were to correspond to only 20 per cent of

this figure, approximately one thousand ohms would remain uncompensated. If we assume a double layer capacity of about $25 \mu\text{F}/\text{cm}^2$ and an electrode area of about 0.02 cm^2 , a double-layer time-constant of $500 \mu\text{sec}$ results.

One way of understanding the effect of such a large value of the double-layer time-constant is to consider it as shifting the zero on the time axis. Therefore, the values of the intercepts presented in Table I are too small since they were obtained, in effect, by extrapolating past the "true" zero time. We can estimate the magnitude of this effect by considering the magnitude of the change in the intercept which would result if the time axis were shifted by $500 \mu\text{sec}$. Assuming $D = 1 \times 10^{-5} \text{ cm}^2/\text{sec}$, the observed intercepts should be increased by $7.7 \mu\text{C}/\text{cm}^2$.

This effect is of such a magnitude as to completely invalidate the potential step chronocoulometric technique in the absence of a more complete compensation technique.

On the basis of these experiments we conclude that the "true" $Q-t^{\frac{1}{2}}$ intercepts are probably at least as large as the change in the electronic charge on the electrode plus the quantity of electroactive charge in the diffuse layer; quantitative statements are not possible because the uncertainty introduced into the $Q-t^{\frac{1}{2}}$ intercepts is at least as large as the quantity of electroactive charge in the diffuse layer.

Experimental

The stock solutions were identical with those employed in the preceding chapter.

The electronic circuitry and supporting equipment were essentially as described in Chapter 4 except for the presence of one of the compensation circuits illustrated in Fig. 26.

The comments made in the last chapter about the need for low impedance reference electrodes are especially germane here because the potentiostat as well as the voltage follower require a low impedance reference potential for satisfactory operation. Dilute zinc amalgam electrodes, whose potentials were known by comparison with a large S.C.E., were initially employed; these were later discarded in favor of a Ag/AgCl reference electrode because the potential of the latter is more stable and reproducible than a $Zn^{++}/Zn(Hg)$ electrode and the use of a Ag/AgCl reference electrode eliminates the liquid junction potential inherent in the use of an S.C.E. as the ultimate potential standard. The potential of the Ag/AgCl ($Cl^- = 0.001$) electrode is 160 mv. anodic to that of an S.C.E.

It is thought that the presence of milliformal chloride will not lead to significant complexation of the 0.5 mF zinc(II). pK_{ZnCl^+} appears to be in the range of -1 to +1 (77); therefore $ZnCl^+/Zn^{++} < 0.01$ in milliformal chloride. The principal effect of complexation

(77) "Stability Constants of Metal-Ion Complexes," L. G. Sillen and A. E. Martell, Eds., Special Pub. No. 17, The Chemical Society, London, 2nd Ed., 1964.

would be to lower the charge on the zinc species and thereby reduce its preferential attraction into the diffuse layer.

The data given above in Table II indicate that the charge in the diffuse layer is independent of the presence of chloride, at least at potentials cathodic to the zero charge potential. The calculation of the surface excesses of various ions would not be applicable in the presence of significant specific adsorption of chloride.

A dropping mercury electrode was employed rather than a Kemula-type hanging mercury drop electrode because it was found that the former resulted in far more reproducible values for the uncompensated resistance. A 12 second capillary yielded a mercury flow rate of about 0.6 mg/sec; a variable time-delay circuit was used in conjunction with a drop rapper so that the potential step was applied about 8-10 seconds into the drop life. In this way, highly reproducible drops of known area of about 0.02 cm² were obtained.

The use of a DME in this fashion places a restriction on the maximum times which can be employed if area changes are to be neglected. Since the area of a mercury electrode is proportional to $m^{\frac{2}{3}}t^{\frac{2}{3}}$,

$$\frac{\Delta A}{A} = \frac{1}{A} \frac{dA}{dt} \Delta t = \frac{2}{3} \frac{\Delta t}{t}$$

Thus for a drop time of about 10 sec., t must be less than about 70 msec. if the change in area is to be less than one per cent.

The time scale is further restricted by the requirement that diffusion to the spherical mercury electrode be adequately approximated

by a linear model. This requirement is satisfied to within 1 per cent if $t < 10^{-4} \rho_0^2 / \pi D \sim 6$ msec. under our experimental conditions.

It is advantageous to employ as short a time scale as possible because such a scheme maximizes the absolute precision with which the magnitude of the $Q-t^{\frac{1}{2}}$ intercept can be determined. The minimum time cannot be chosen arbitrarily close to zero however because of the requirement that the minimum time values be long compared to the "rise-time" of the system.

The instrumental rise-time is of the order of $20 \mu\text{sec.}$; the system rise-time, even with maximum compensation, is about 1 msec. The current plateau observed in the I-t traces (27, 56) causes the $Q-t^{\frac{1}{2}}$ plots to be nonlinear until $t > 2-3$ msec.

The combination of these effects restricts the usable time range to about 2-10 msec. This time range is convenient because the absolute error associated with each measurement of Q is the same, thereby permitting an unweighted least-squares analysis of the $Q-t^{\frac{1}{2}}$ plots, since this time range can be conveniently covered with a single oscilloscopic picture.

The computer program, written in Fortran IV, is included on the next two pages; its presence here is not meant to suggest that the program contains any unique features but it is included here simply as an aid to others who might like to analyze their data in this fashion.

```

$IBFTC QRTT   DECK
C   POTENTIAL STEP CHRONOCOULOMETRY. Q-SQRT(T) PLOTS.
C
C   PROGRAMMED BY PETER JAMES LINGANE, JANUARY 15, 1966
C
C   COMMT CARD FORMAT 'BMM/DD/YY-NN.....'
C   NC      NO OF ELEC*CONC, MEQUIV/LITER
C   N       NUMBER OF DATA CARDS
C   AREA    ELECTRODE AREA, CM**2
C   S       RAW Q DATA FROM 'SCOPE, DIVISIONS
C   T       RAW TIME DATA, MILLISECONDS
C   SCALE   CONVERSION FACTOR, MICROCOULOMBS/DIVISION
C
C   DIMENSION COMMT(12), DT(300), T(300), TT(300), S(300), Q(300)
C   REAL NC
C   RTPI = 1.772454
C   FARA = 96500.
100  READ(5,1) COMMT
1    FORMAT(12A6)
    WRITE(6,2) COMMT
2    FORMAT(1H1, //, 10X12A6)
    READ(5,3) N, NC, SCALE, AREA
3    FORMAT(15, 3F10.0)
    N = 3*N
    READ(5,4)(DT(I), S(I), I=1,N)
4    FORMAT(6F10.0)
C
C   THIS SECTION IS TO ELIMINATE ZERO VALUED DATA PAIRS
C   NN = 0
C   K = 0
201  K = K+1
    IF (K-N)200,202,202
200  IF (DT(K).EQ.0.) GO TO 201
    NN = NN + 1
    T(NN) = DT(K)
    Q(NN) = SCALE*S(K)/AREA
    GO TO 201
202  WRITE(6,8)NN
8    FORMAT(/,10X15, 11H DATA PAIRS )
C
    DO 10 I=1,NN
    T(I) = T(I)/1000.
10   TT(I) = SQRT(T(I))
    WRITE(6,5) (Q(I), T(I), TT(I), I=1,NN)
5    FORMAT(//, 10X20H MICROCOULOMBS/CM**2, 7X 14H TIME, SECONDS, 14X,
1    11H SQRT(TIME),/(1P3E25.3))
    CALL FITY(NN,TT , Q, A, B, ALPHA, BETA)
C
    D = (B*RTPI/(2.*NC*FARA))**2
    SIGMAD = 2.*(BETA/B)*D
    WRITE(6,6) D, SIGMAD
6    FORMAT(//, 10X4H D =, E10.2, 5X9H CI(95) =, E10.2)
    PUNCH 7, (COMMT(I), I=1,2), A,ALPHA,D,SIGMAD
7    FORMAT(2A6, 0P4E11.4)
    GO TO 100
    END

```

```

SUBROUTINE FITY(N,X,Y,A,B,ALPHA,BETA)
C
C 2 PARAMETER LINEAR LEAST SQUARES ANALYSIS. X COORDINATE FREE OF
C ERROR, Y COORDINATE ASSOCIATED WITH SAME ABSOLUTE PRECISION.
C PROGRAMMED BY PETER JAMES LINGANE, 4/16/64
C
C DIMENSION X(300),Y(300),STUDT(31)
C
C TABLE OF STUDENT T, 95 PERCENT CONFIDENCE LEVEL
C M DEGREES OF FREEDOM = N - 2
C
C DATA (STUDT(M), M=1,30)/12.706,4.303,3.182,2.776,2.571,2.447,2.365
*,2.306,2.262,2.228,2.201,2.179,2.160,2.145,2.131,2.120,2.110,
*,2.101,2.093,2.086,2.080,2.074,2.069,2.064,2.060,2.056,2.052,2.048,
*,2.045,2.042/
C
SUMY=0
SUMX=0
SUMXY=0
SUMX2=0
SUMSQX=0
DO 43 I=1,N
SUMY=SUMY+Y(I)
SUMX=SUMX+X(I)
SUMXY=SUMXY+X(I)*Y(I)
SUMX2=SUMX2+X(I)*X(I)
43 CONTINUE
XAVG=SUMX/FLOAT(N)
YAVG=SUMY/FLOAT(N)
DO45 I=1,N
SUMSQX=SUMSQX+(X(I)-XAVG)**2
45 CONTINUE
DET=FLOAT(N)*SUMX2-SUMX*SUMX
A=(SUMY*SUMX2-SUMX*SUMXY)/DET
B=(FLOAT(N)*SUMXY-SUMX*SUMY)/DET
C PROGRAM SKIPS ERROR CALCULATION IF N.LT.3.
IF(N-2) 202,202,49
49 VAR=0
DO 44 I=1,N
44 VAR=VAR+((Y(I)-A-B*X(I))**2)/(FLOAT(N)-2.0)
IF(N-32) 51,51,52
52 SIGMA = 1.96*SQRT(VAR)
ALPHA = 1.96*(SQRT(VAR*(1.0/FLOAT(N)+(XAVG**2)/SUMSQX)))
BETA = 1.96*SQRT(VAR/SUMSQX)
GO TO 204
51 CONTINUE
SIGMA = STUDT(N-2)*SQRT(VAR)
ALPHA = STUDT(N-2)*SQRT(VAR*(1.0/FLOAT(N)+(XAVG**2)/SUMSQX))
BETA = STUDT(N-2)*SQRT(VAR/SUMSQX)
204 WRITE(6,200) A, ALPHA, B, BETA
200 FORMAT(//,10X13H INTERCEPT = , 1PE15.8, 11X, 10H CI(95) = , E15.8,
1 / 10X9H SLOPE = , E15.8, 15X10H CI(95) = , E15.8)
GO TO 201
202 BETA = 1.
ALPHA = 1.
WRITE(6,203) A,B
203 FORMAT(///,24H LESS THAN 3 DATA PAIRS.,///, 12H INTERCEPT = ,
*E15.8,//,8H SLOPE = , E15.8,// 29H ALPHA AND BETA ARE NONSENSE.)
201 RETURN
END

```

Proposition I:

The calculations of Tatwawadi and Bard (4) for the extent of electroactive adsorption of riboflavin on mercury electrodes are incorrect because the particular least-squares analysis employed by these authors is not applicable to the models they employed; their observation that mathematical reformulations of the models leads to apparently different values for the parameters D and $nF\Gamma$ is a direct consequence of this error.

The assumption implicit in their analysis is that the values of $i\tau$ are free of error but that the values of $\tau^{\frac{1}{2}}$ are associated with equal absolute errors and that the values of $i\tau^{\frac{1}{2}}$ are free of error but that the values of $1/\tau^{\frac{1}{2}}$ are associated with equal absolute errors; these criteria are obviously totally incompatible since all of the quantities are different functions of the same measured variable, the transition time. Therefore, the analysis employed by these authors does not apply in the present case.

It is a quite general conclusion that the parameters estimated according to a correctly formulated least-squares analysis are insensitive to mathematical reformulations of the model (2). We can illustrate that this is indeed so in the present case by considering the correct solutions for $nF\Gamma$ and for the chronopotentiometric constant $nF\pi^{\frac{1}{2}}D^{\frac{1}{2}}C/2$, hereafter denoted by the symbol "b". The correct solutions for their

$$\text{model 3: } i\tau - nF\Gamma - b\tau^{\frac{1}{2}} = 0$$

$$\text{model 3*: } i\tau^{\frac{1}{2}} - nF\Gamma/\tau^{\frac{1}{2}} - b = 0$$

models 3 and 3* are (1,3)

model 3:

$$\begin{pmatrix} \sum 1/w_j & \sum \tau_j^{\frac{1}{2}}/w_j \\ \sum \tau_j^{\frac{1}{2}}/w_j & \sum \tau_j/w_j \end{pmatrix} \begin{pmatrix} nF\Gamma \\ b \end{pmatrix} = \begin{pmatrix} \sum i_j \tau_j / w_j \\ \sum i_j \tau_j^{\frac{3}{2}} / w_j \end{pmatrix}$$

model 3*:

$$\begin{pmatrix} \sum 1/\tau_j w_j^* & \sum 1/\tau_j^{\frac{1}{2}} w_j^* \\ \sum 1/\tau_j^{\frac{1}{2}} w_j^* & \sum 1/w_j^* \end{pmatrix} \begin{pmatrix} nF\Gamma \\ b \end{pmatrix} = \begin{pmatrix} \sum i_j / w_j^* \\ \sum i_j \tau_j^{\frac{1}{2}} / w_j^* \end{pmatrix}$$

The appropriate weighting functions are

$$\text{model 3: } w_j = (i_j - b/2\tau_j^{\frac{1}{2}})^2 \sigma_{\tau_j}^2$$

$$\text{model 3*: } w_j^* = 1/\tau_j (i_j/2 + nF\Gamma/2\tau_j)^2 \sigma_{\tau_j}^2$$

We have asserted that the values of the current density i are known much more precisely than the values of the transition time τ and hence that $\sigma_i^2 \sim 0$ in formulating these weighting functions.

If we now define

$$\epsilon_j \equiv i_j \tau_j - nF\Gamma - b\tau_j^{\frac{1}{2}}$$

it follows directly that

$$w_j = \tau_j w_j^* + \epsilon_j / \tau_j (i_j - b/2\tau_j^{\frac{1}{2}}) + O(\epsilon_j^2)$$

Thus in the limit of low experimental errors, w_j may be set equal to $\tau_j w_j^*$ and the matrix solutions become identical for both models 3 and 3*. A similar analysis may be made for the models 1 and 1* of Tatwawadi and Bard;

$$\text{model 1: } i\tau - nF\Gamma - b^2/i = 0$$

$$\text{model 1*}: i^2\tau - nF\Gamma i - b^2 = 0$$

in this case, the result is that w_j is identically $i_j^2 w_j^*$.

To convince the pragmatically inclined, the data of Tatwawadi and Bard were analyzed in the correct fashion, as outlined in the Appendix to Chapter 8 of the dissertation, and the results are presented in the accompanying table for comparison with the incorrect results of Tatwawadi and Bard. It is evident that the correctly calculated estimates of D and of Γ are indeed insensitive to these particular reformulations of models 1 and 3.

References

- (1) W. E. Deming, "The Statistical Adjustment of Data," John Wiley and Sons, New York, 1943. Republished by Dover, New York, 1964, Chap. X.
- (2) *ibid.*, p. 156.
- (3) W. C. Hamilton, "Statistics in Physical Science," Ronald Press, New York, 1964, Chap. 4.
- (4) S. V. Tatwawadi and A. J. Bard, Anal. Chem., 36, 2 (1964).

Least-Squares Analysis of Chronopotentiometric Adsorption Data
 Reduction of Riboflavin in 0.5 M NaHSO₄ plus 1 M Na₂SO₄

	Correct Analysis				T & B's Analysis	
	$\Gamma \times 10^6$ moles/cm ²	$S \Gamma$ cm ² /sec	$S D$ cm ² /sec	$\chi^2/N-3^\dagger$	$\Gamma \times 10^6$ moles/cm ²	$D \times 10^5$ cm ² /sec
Model 1						
0.8 mF Riboflavin	0.96	0.13	0.55	0.81	0.72	0.63
0.4 mF	.60	.04	.70	0.35	.53	.71
0.2 mF	.43	.03	.84	1.72	.43	.85
Model 1*						
0.8 mF	0.96	0.13	0.55	0.81	1.09	0.52
0.4 mF	.60	.04	.70	0.35	.65	.63
0.2 mF	.43	.03	.84	1.72	.55	.38
Model 2						
0.8 mF	0.61	0.47	0.39	1.45		
0.4 mF	.36	.16	.49	.78		
0.2 mF	.34	.14	.47	3.15		
Model 3						
0.8 mF	0.58	0.11	0.54	1.05	0.43	0.62
0.4 mF	.38	.04	.64	0.54	.33	.69
0.2 mF	.31	.03	.74	2.55	.31	.79
Model 3*						
0.8 mF	0.59	0.11	0.54	1.10	0.69	0.49
0.4 mF	.38	.04	.64	0.55	.42	.59
0.2 mF	.32	.03	.73	2.65	.41	.46

[†] Calculated on the basis of $\sigma_T^2 = (\tau/10)^2$.

Proposition II:

Decay to the Steady State in Twin Electrode, Thin Layer Electrochemistry

Recent interest in twin electrode, thin layer electrochemistry has demonstrated that steady state measurements are of considerable value for the determination of a variety of electrochemical parameters (1,2). In this proposition, we present the time dependent solutions for Dirichlet, Neumann, and Cauchy boundary conditions and show that the values of the "time to steady state" parameter obtained for these conditions are in the ratio 1:4:16. In addition, it is shown that the steady state current observed in the total absence of supporting electrolyte for Dirichlet boundary conditions is larger by the factor " $(z_3 - z_1)/z_3$ " than the steady state current observed in the presence of excess supporting electrolyte.

1. Dirichlet Conditions

We seek a solution to Fick's second law

$$\frac{\partial C}{\partial t} = D \frac{\partial^2 C}{\partial x^2} \quad (1-1)$$

such that the following boundary and initial conditions are satisfied.

$$\nabla C|_{x=0} = \nabla C|_{x=l} \quad (1-2)$$

$$C(x,0) = {}^*C_0; \quad 0 \leq x \leq l \quad (1-3)$$

$$C(0,t) = 0; \quad t > 0$$

This solution can be obtained by either the Fourier or Laplace transform techniques. The results are

$$C(x,t) = {}^*C_o \left\{ \frac{2x}{\ell} + \frac{2}{\pi} \sum_{m=1}^{\infty} \frac{1}{m} \sin \frac{2m\pi x}{\ell} \exp \left[-\left(\frac{2m\pi}{\ell} \right)^2 D t \right] \right\} \quad (1-4)$$

$$= {}^*C_o \left[1 - \sum_{m=0}^{\infty} \left(\operatorname{erfc} \frac{m\ell + x}{2\sqrt{Dt}} - \operatorname{erfc} \frac{(m+1)\ell - x}{2\sqrt{Dt}} \right) \right] \quad (1-5)$$

The steady state concentration profile can be obtained most conveniently from (1-4).

$$C_{SS}(x) = \lim_{t \rightarrow \infty} C(x,t) = \frac{2^* C_o x}{\ell} \quad (1-6)$$

The time required to achieve steady state conditions can be estimated as the time required for the exponential terms in (1-4) to decay to less than 1% of their initial values. Thus

$$t_{SS} \equiv 4.6 / \left(\frac{2\pi}{\ell} \right)^2 D = 0.117 \ell^2 / D \quad (1-7)$$

Anderson and Reilley (1) report that steady state conditions are achieved experimentally within 2-3 seconds for $\ell \sim 100-200 \mu$ and $D \sim 10^{-5} \text{ cm}^2/\text{sec}$. Under these same experimental conditions, (1-7) predicts that t_{SS} should be 1-4 seconds. The agreement is very good.

The current density-time behavior can be obtained by evaluating the gradient of the concentration of the electroactive species at the electrode surface.

$$i_0 = nFD \nabla C \Big|_{x=0, \ell} \quad (1-8)$$

$$i_0 = \frac{2nFD^* C_0}{\ell} \left\{ 1 + 2 \sum_{m=1}^{\infty} \exp \left[- \left(\frac{2m\pi}{\ell} \right)^2 Dt \right] \right\} \quad (1-9)$$

$$= nF^* C_0 \sqrt{\frac{D}{\pi t}} \sum_{m=0}^{\infty} \left\{ \exp \left[- \left(\frac{m\ell}{2} \right)^2 / Dt \right] + \exp \left[- \left(\frac{m\ell + \ell}{2} \right)^2 / Dt \right] \right\} \quad (1-10)$$

The steady state current density is most conveniently obtained from (1-9).

$$i_{SS} = 2nFD^* C_0 / \ell \quad (1-11)$$

This expression is equivalent to those obtained by Anderson and Reilley (1).

The short time limit of the current density is most conveniently obtained from (1-10).

$$\lim_{\frac{t}{\ell^2} \rightarrow 0} i_0 = nF^* C_0 \sqrt{\frac{D}{\pi t}} \quad (1-12)$$

This is the Cottrell equation (3).

2. Neumann Conditions

The boundary conditions appropriate to this section are

$$\nabla C \Big|_{x=0, \ell} = \frac{i_0}{nFD} = \text{const} \quad (2-1)$$

Note that the controlled current must be less than the diffusion limited

steady state value given by (1-11) or secondary electrode reactions, such as the decomposition of the solvent, will occur. The concentration profiles are

$$C(x,t) = {}^*C_o - \frac{i_o \ell}{nFD} \left[\frac{1}{2} - \frac{x}{\ell} - \frac{4}{\pi^2} \sum_{m=0}^{\infty} \frac{\cos \frac{(2m+1)\pi x}{\ell}}{(2m+1)^2} \exp \left[- \left(\frac{(2m+1)\pi}{\ell} \right)^2 Dt \right] \right] \quad (2-2)$$

$$= {}^*C_o - \frac{2i_o}{nF} \sqrt{\frac{t}{D}} \sum_{m=0}^{\infty} (-1)^m \left[\operatorname{ierfc} \frac{m\ell + x}{2\sqrt{Dt}} - \operatorname{ierfc} \frac{(m+1)\ell - x}{2\sqrt{Dt}} \right] \quad (2-3)$$

If we let the separation between the electrodes become large,

$$\lim_{\frac{\ell^2}{t} \rightarrow \infty} C(x,t) = {}^*C_o - \frac{2i_o}{nF} \sqrt{\frac{t}{D}} \operatorname{ierfc} \frac{x}{2\sqrt{Dt}} \quad (2-4)$$

This expression is identical with the concentration profile derived under conditions of semi-infinite linear diffusion (4).

The time needed to achieve steady state conditions is given by

$$t_{ss} = 4.6 / \left(\frac{\pi}{\ell} \right)^2 D = 0.468 \ell^2 / D \quad (2-5)$$

3. Cauchy Conditions

The boundary conditions appropriate to this section are

$$\nabla C \Big|_{x=\ell} = i_o/nFD = \text{const} \quad (3-1)$$

$$C(0,t) = 0; t > 0 \quad (3-2)$$

It is evident that the steady state current density must equal i_0 and that, in general, a net electrolysis of the electroactive species will occur in the thin layer of solution before the steady state is achieved. The Fourier solution is

$$C(x,t) = \frac{i_0 x}{nFD} + \frac{2}{\ell} \sum_{m=0}^{\infty} \left\{ C^* - (-1)^m \left[\frac{2\ell}{(2m+1)\pi} \right]^2 \frac{i_0}{nFD} \right\} \sin \frac{(2m+1)\pi x}{\ell} \exp \left[- \left(\frac{2m+1}{2\ell} \pi \right)^2 Dt \right] \quad (3-3)$$

The Laplace transform solution to this problem is given by Carslaw and Jaeger (5)

$$C(x,t) = {}^*C_0 - \frac{2i_0}{nF} \sqrt{\frac{t}{D}} \sum_{m=0}^{\infty} (-1)^m \left\{ \text{ierfc} \frac{(2m+1)\ell - x}{2\sqrt{Dt}} - \text{ierfc} \frac{(2m+1)\ell + x}{2\sqrt{Dt}} \right\} \quad (3-4)$$

$$\lim_{\frac{\ell^2}{t} \rightarrow \infty} C(x,t) = {}^*C_0 \quad (3-5)$$

The current passing through the potentiostated electrode is not initially time-independent and is given by

$$i_0|_{x=0} = nFD\nabla C|_{x=0} = i_0|_{x=\ell} \sum_{m=0}^{\infty} (-1)^m \left\{ \operatorname{erfc} \frac{(2m+1)\ell - x}{2\sqrt{Dt}} + \operatorname{erfc} \frac{(2m+1)\ell + x}{2\sqrt{Dt}} \right\} \quad (3-6)$$

$$= i_0|_{x=\ell} \left\{ 1 + \frac{8}{\pi} \sum_{m=0}^{\infty} \frac{(-1)^m}{2m+1} \exp \left[- \left(\frac{2m+1}{2\ell} \pi \right)^2 Dt \right] \right\} \quad (3-7)$$

The time needed to achieve steady state is given by

$$t_{SS} = 4.6 / \left(\frac{\pi}{2\ell} \right)^2 D = 1.87 \ell^2 / D \quad (3-8)$$

4. Absence of Supporting Electrolyte

The modifications of the diffusion equations needed in order to account for the transport of ionic material in the absence of supporting electrolyte have been reviewed on p. 104 ff of this dissertation. The only soluble problem is the case where $n = z_1$, i. e., only when there are two ionic components present in the solution. Under this condition, the solutions (1-4), (1-5), (1-6), and (1-7) are directly applicable with D_S substituted for D .

$$D_S = D_1 D_3 (z_3 - z_1) / (z_3 D_3 - z_1 D_1) \quad (4-1)$$

Equations (1-9) and (1-10) become

$$\frac{i_0}{z_1 F D_1} = \frac{2^* C_1}{\ell} \frac{z_3 - z_1}{z_3} \left(1 + \sum_{n=1}^{\infty} \exp \left[- \left(\frac{2n\pi}{\ell} \right)^2 D_S t \right] \right) \quad (4-2)$$

$$= \frac{1}{(\pi D_S t)^{\frac{1}{2}}} \frac{z_3 - z_1}{z_3} \sum_{n=0}^{\infty} \left\{ \exp \left[- (n\ell)^2 / 4D_S t \right] + \exp \left[- (n\ell + \ell)^2 / 4D_S t \right] \right\} \quad (4-3)$$

The steady state current density is

$$\frac{i_{SS}}{z_1 F D_1} = \frac{z_3 - z_1}{z_3} \frac{2^* C_1}{\ell} \quad (4-4)$$

Note that this limiting current is larger by the factor " $(z_3 - z_1)/z_3$ " than the value observed in the presence of excess supporting electrolyte, Eqn. (1-11).

In a similar fashion, Eqns. (2-2) and (2-3) become

$$C(x, t) = {}^* C_1 - \frac{i_0 \ell}{z_1 F D_1} \frac{z_3 - z_1}{z_3 - z_1} \left[\frac{1}{2} - \frac{x}{\ell} - \frac{4}{\pi^2} \sum_{n=1}^{\infty} \frac{\cos \frac{(2n+1)\pi x}{\ell}}{(2n+1)^2} \exp \left[- \left(\frac{(2n+1)\pi}{\ell} \right)^2 D_S t \right] \right] \quad (4-5)$$

$$= \frac{2i_0}{z_1 F D_1} \sqrt{D_S t} \sum_{n=0}^{\infty} (-1)^n \left\{ \text{ierfc} \frac{(n+1)\ell - x}{2\sqrt{D_S t}} - \text{ierfc} \frac{n\ell + x}{2\sqrt{D_S t}} \right\} \quad (4-6)$$

The gradient of the electrical field in the solution can be expressed as

$$\nabla\phi(x,t) = \frac{RT}{FC_1(z_1D_1 - z_3D_3)} \left[\frac{i_0}{z_1F} - (D_1 - D_3)\nabla C_1 \right] \quad (4-7)$$

This gradient can be evaluated explicitly for particular values of i_0 and C_1 . Note that it is, in general, a nonlinear function of the distance x . At the steady state, the total voltage drop across the thin layer cell becomes

$$V_{SS} = \int_0^{\ell} \nabla\phi_{SS} \cdot dx = -\frac{RT}{z_3F} \ln \frac{C_3(\ell)}{C_3(0)} = -\frac{0.059}{z_3} \log \frac{C_1(\ell)}{C_1(0)} \quad (4-8)$$

It is clear that it is simply not possible to achieve, experimentally, the condition that $C_1(0, t_{SS})$ be arbitrarily small since V_{SS} is unbounded under these conditions.

Literature Cited

- (1) L. Anderson and C. N. Reilley, J. Electroanal. Chem., 10, 295 (1965).
- (2) L. Anderson and C. N. Reilley, J. Electroanal. Chem., 10, 538 (1965).
- (3) P. Delahay, "New Instrumental Methods in Electrochemistry," Interscience, N.Y., 1954, p. 180.
- (4) P. Delahay, "New Instrumental Methods in Electrochemistry," Interscience, N.Y., 1954, p. 51.
- (5) H. S. Carslaw and J. C. Jaeger, "Conduction of Heat in Solids," 2nd Ed., Oxford at the Clarendon Press, 1959, p. 113.

Proposition III:

Determination of Ruthenium in a Ten Thousand-Fold Excess
of Zinc by Pulse Polarography

Kesser, Meyer, and Larsen (1) describe a spectrophotometric method for the determination of ruthenium in the presence of a ten thousand-fold excess of zinc and/or magnesium. Their method involves a distillation/oxidation separation of the ruthenium as RuO_4 and a final empirical color development scheme with α -nitroso, β -naphthol. This method is plagued by incomplete oxidation of the ruthenium, by traces of reducing impurities, and by the instability of the reagents used in the final colorometric assay. An additional drawback is that a long elapsed time, ~ 2 days, is required in order to complete the assay. A relative precision of about 2 per cent is obtained.

It is proposed that this assay can be completed within an hour, without prior separation of the ruthenium, and with equal precision using pulse polarography (2). A 300 mg. sample of the alloy ($< 50\%$ Mg, $> 50\%$ Zn, $\sim 0.01\%$ Ru) could be dissolved in about 50 mls of nitric acid; the resulting solution would be about $14 \mu\text{M}$ in ruthenium and about 0.2 M in zinc and magnesium salts. Since ruthenium(III) undergoes a reversible one-electron reduction well before the reduction of zinc or magnesium (the potential of the Ru(III)-Ru(II) aquo-couple is about $+0.2 \text{ v. vs. NHE}$ (3)), the ruthenium could be determined by a variety of electrochemical techniques using the zinc and magnesium salts as indifferent electrolytes. Pulse polarography was selected because of

its high sensitivity in the micromolar concentration range.

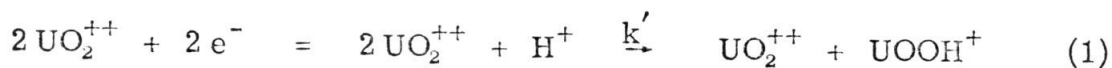
Literature Cited

- (1) G. Kesser, R. J. Meyer, and R. P. Larsen, Anal. Chem., 38, 221 (1966).
- (2) E. P. Parry and R. A. Osteryoung, Anal. Chem., 37, 1634 (1965) and references contained therein.
- (3) E. E. Mercer and R. R. Buckley, Inorg. Chem., 4, 1692 (1965).

Proposition IV:

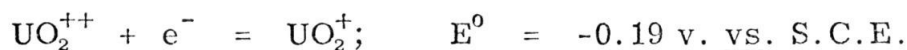
Although the theoretical expressions describing the polarographic characteristics of a second-order disproportionation reaction clearly indicate that the measured half-wave potential is a function of the rate of the disproportionation reaction, this feature of the wave appears to have escaped notice as a characteristic of such a reaction (1) and has not been investigated in experimental studies (2-4). It is proposed to verify the existence of this effect through pH, ionic strength, and temperature studies of the uranium(V) disproportionation reaction. The existence of this effect will require a re-evaluation of the origin of the shift of $E_{\frac{1}{2}}$ in chloride media (2).

Although the standard potential for the reduction of uranium(V) is anodic to the reduction potential for uranium(VI), the polarographic wave observed in the vicinity of -0.2 v. vs. S.C.E. corresponds only to the reduction to uranium(V) because the further reduction of uranium proceeds very irreversibly at the D.M.E. Since the one-electron reduction product is thermodynamically unstable, it disproportionates in acidic aqueous solutions. The principal scheme for this disproportionation reaction may be formalized as (2,3,5)

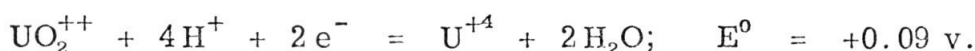


It is clear that the position of the uranium(VI) reduction wave on the potential axis will be a function of the rate of this disproportionation reaction. As the rate approaches zero, $E_{\frac{1}{2}}$ will approximate the

standard potential of the $\text{UO}_2^{++}/\text{UO}_2^+$ couple.



As the rate becomes very large, the wave will shift anodic to the potential of the $\text{UO}_2^{++}/\text{U}^{+4}$ couple.



Koutecky and Koryta (6) have obtained a solution applicable to the polarographic reduction of uranium(VI) followed by a pseudo-second order ($k = \text{H}^+k'$) disproportionation reaction. The instantaneous polarographic current observed at a particular value of λ ,

$$\lambda = \exp \left[- \frac{F}{RT} (E - E^0_{\text{U(VI)}, \text{U(V)}}) \right] \quad (2)$$

is given by

$$i(\lambda) = i_d(\lambda) \left[\frac{1}{1+\lambda} + F \right] \left[1 + H \right]^{-1} \quad (3)$$

where i_d is the instantaneous current observed on the diffusion plateau and F and H are given by

$$F(\lambda, \beta) = \sum_{n=1}^{\infty} A_n(\lambda) \beta^n \quad (4)$$

$$H(\beta) = \sum_{n=1}^{\infty} C_n \beta^n \quad (5)$$

where $\beta = 2U^*kt$; U^* is the bulk concentration of U(VI) , and t is the drop

time. (The coefficients C_n are tabulated (6) for $n \leq 7$ and it appears that H converges rapidly for $\beta < 5$. Unfortunately, Koutecky and Koryta do not evaluate the coefficients A_n although they derive the expressions from which they may be evaluated. The coefficients were not evaluated here since to do so requires a high degree of algebraic complexity.)

Since the coefficients A_n are functions of λ , it is not possible to rearrange Eqn. (3) to obtain an explicit solution for the polarographic I-E wave. It is clear, none-the-less, that λ is an implicit function of β at fixed values of the ratio i/i_d . Thus the half-wave potential must shift with increasing values of the rate of the disproportionation reaction.

The uranium(V) disproportionation reaction provides an ideal model system for the verification of this effect because the electrochemical step proceeds reversibly at the D.M.E. (3) and because the value of β can be easily increased by a factor of several thousand from the smallest value detectable polarographically by changing the pH, the ionic strength, the drop time, the bulk concentration of uranium, and the temperature.

The pseudo-second order rate constant for the disproportionation reaction is proportional to the hydrogen ion activity over at least a hundred-fold range from 0.02 to 2. M (2-5). In addition, the rate constant increases sharply in solutions of high ionic strength, probably because the activity coefficients of the reacting species become greater than unity in these solutions. The Arrhenius energy for the disproportionation reaction is about 10 kcal/mole (5) and the rate increases

by about a factor of two per 10° change in the temperature.

Chloride appears to catalyze the disproportionation reaction (2,4) although there is some disagreement as to the magnitude of the effect (5). Imai (2) has investigated the possibility of a difference between the number of chloride ligands complexed to the uranium(V) and (VI) species by plotting $\log [\text{Cl}^-]$ versus $E_{\frac{1}{2}}$ (7); a value of 0.83 was obtained. Such a treatment assumes that $E_{\frac{1}{2}}$ is insensitive to changes in the rate constant of the disproportionation reaction (the pseudo-second order rate constant increases by more than an order of magnitude over the chloride concentration range studied). Since the total measured shift in $E_{\frac{1}{2}}$ is only 25 mv, it is probable that the shift of $E_{\frac{1}{2}}$ with the increased rate of the reaction is significant and that the results of Imai require reinterpretation.

Literature Cited

- (1) A. A. Vlcek, in "Progress in Inorganic Chemistry," Vol. 5, F. A. Cotton, Ed., Interscience, N. Y., 1963, p. 331.
- (2) H. Imai, Bull. Chem. Soc. Japan, 30, 873 (1957).
- (3) D.M.H. Kern and E. F. Orlemann, J. Am. Chem. Soc., 71, 2102 (1949).
- (4) E. F. Orlemann and D.M.H. Kern, J. Am. Chem. Soc., 75, 3058 (1953).
- (5) T. W. Newton and F. B. Baker, Inorg. Chem., 4, 1166 (1965).
- (6) J. Koutecky and J. Koryta, Coll. Czech. Chem. Comm., 19, 845 (1954).
- (7) I. M. Kolthoff and J. J. Lingane, "Polarography," Interscience, N. Y., 2nd Ed., 1952, Chapter XII.

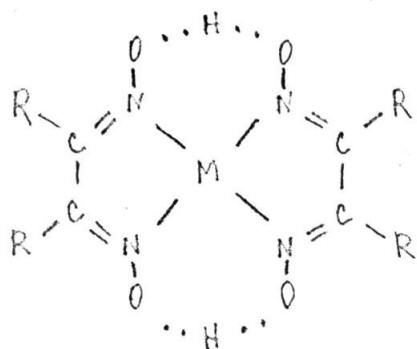
Proposition V:

It is proposed that iron, cobalt, and nickel complexes with dimethylglyoxime, α -benzildioxime, 4-methyl-1,2-cyclohexanedione-dioxime, and similar oximes should form series of salts interrelated by one-electron transfer reactions in analogy with the behavior of the complexes formed with the dinegative anions of o-phenylenediamine, maleonitriledithiol, cis-disubstituted ethylene 1,2-dithiols, and other ligands (1-6).

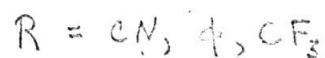
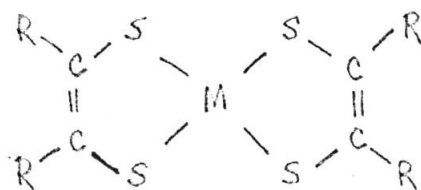
This proposal is based in large part on the strikingly similar structures and π -systems of the bis complexes, cf. the accompanying figure.

In addition, there is some evidence for the d^7 member of the bis α -benzildioximato nickel series (7,8). In both of the laboratories where it was reported, this "Ni(III)" salt was obtained by oxidizing the Ni(II) salt with solid iodine or bromine in carbon tetrachloride solution. The solid Ni(III) salts were characterized by elemental analyses and by molecular and equivalent weight determinations.

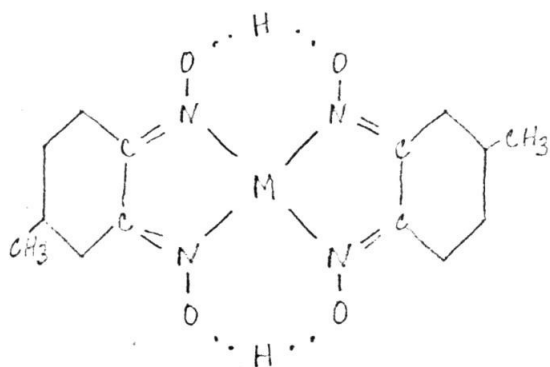
The bright red oxidation product of nickel dimethylglyoxime in strongly basic solutions has long been known. The oxidized species appears to be $\text{Ni}(\text{DMG})_3^-$ (8). Recent electrochemical evidence demonstrates that the bright red species is a two-electron oxidation product (9). This salt appears to be analagous to the tris cis-disubstituted 1,2-dithiolato complexes of vanadium, chromium, molybdenum, and tungsten (10,11). All of these latter salts form series of four complexes which



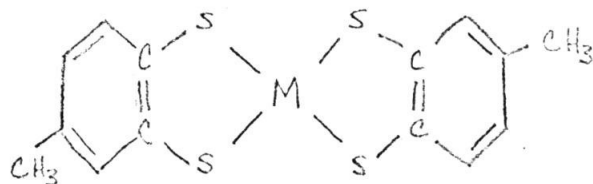
$R = \text{CH}_3, \phi$
disubstituted glyoximate
complexes



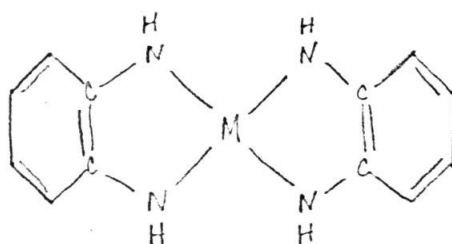
disubstituted ethylenedithiolato
complexes



4-methylnioximate
complexes



toluene 3,4-dithiolato
complexes



o-phenylenediamine complexes

are interrelated by one-electron transfer reactions and whose electronic configurations are normally d^0 , d^1 , d^2 , and d^3 . Neutral tris complexes of toluene 3,4-dithio| have been reported (12) for cobalt and nickel (nominally d^3 and d^4 systems) and thus it would appear that $\text{Ni}(\text{DMG})_3^-$ is the nominally d^6 member of the tris dimethylglyoximate series and that it should be further oxidizable in appropriate media.

Literature Cited

- (1) A. Davison, N. Edelstein, R. H. Holm, and A. H. Maki, Inorg. Chem., 2, 1227 (1963).
- (2) A. Davison, N. Edelstein, R. H. Holm, and A. H. Maki, Inorg. Chem., 3, 814 (1964).
- (3) S. I. Shupack, E. Billig, R. J. H. Clark, R. Williams, and H. B. Gray, J. Am. Chem. Soc., 86, 4594 (1964).
- (4) E. I. Stiefel, J. H. Waters, E. Billig, and H. B. Gray, J. Am. Chem. Soc., 87, 3016 (1964).
- (5) R. Williams, E. Billig, J. H. Waters, and H. B. Gray, J. Am. Chem. Soc., 88, 43 (1966).
- (6) A. H. Maki, T. E. Berry, A. Davison, R. H. Holm, and A. L. Balch, J. Am. Chem. Soc., 88, 1080 (1966).
- (7) L. E. Edelman, J. Am. Chem. Soc., 72, 5765 (1950).
- (8) A. Okac and M. Simek, Coll. Czech. Chem. Comm., 24, 2699 (1959).
- (9) D. G. Davis and E. A. Boudreaux, J. Electroanal. Chem., 8, 434 (1964).
- (10) A. Davison, N. Edelstein, R. H. Holm, and A. H. Maki, J. Am. Chem. Soc., 86, 2799 (1964).
- (11) A. Davison, N. Edelstein, R. H. Holm, and A. H. Maki, Inorg. Chem., 4, 55 (1965).
- (12) R. Williams, unpublished results. Quoted in Ref. (3).

Proposition VI:

A knowledge of where metal complexes of EDTA are protonated is important because of its bearing on the mechanism of ligand exchange between transition metal complexes(1). The nuclear magnetic resonance spectra of many metal complexes of EDTA have been studied(2,3,4) and the chemical shift-pH behavior of the ethylenic and acetate protons has been interpreted(4) as indicating that the initial protonation is at the nitrogens. The ethylenic and acetate proton resonances are shifted parallel to each other as a function of pH; this requires that protonation be occurring at the nitrogens because protonation of the carboxyl groups would result in a larger chemical shift of the acetate protons than of the ethylenic protons. New resonance lines corresponding to the acid protons have not been reported, presumably because the quadrupole moment of the ^{14}N and chemical exchange broadens these lines to the point where no distinct resonances are observed.

It is proposed that observation of the shift of the nitrogen resonances as a function of pH would provide additional evidence for the protonation site. The ^{14}N spectra should be shifted if protonation does indeed occur at the nitrogens and should be essentially unaffected if protonation occurs at the carboxyl groups. Studies of ^{15}N enriched EDTA complexes should be helpful because

the ^{15}N spectra will be shifted substantially downfield upon protonation of the nitrogen(5) and because a distinct resonance should be observed for the acid protons ($I = \frac{1}{2}$ for ^{15}N).

Literature Cited

- (1) D. W. Margerum, D. L. Janes, and H. M. Rosen, J. Am. Chem. Soc. 87, 4463 (1965).
- (2) J. Day and C. N. Reilley, Anal. Chem. 36, 1073 (1964).
- (3) R. J. Kula, Anal. Chem. 37, 989 (1965).
- (4) R. J. Kula, D. T. Sawyer, S. I. Chan, and C. M. Finley, J. Am. Chem. Soc. 85, 2930 (1963).
- (5) J. B. Lambert, PhD Thesis, California Institute of Technology, Pasadena, 1965. Part II.